Chapter Four

Description and Theories of Bioreactors

In this chapter we shall discuss different types of bioreactors and their conception also we will see the basic theories and principles that occur inside the bioreactors.

SOME PHENOMENON INSIDE BIOREACTORS

Fed-Batch

A fed-batch is a biotechnological batch process which is based on feeding of a growth limiting nutrient substrate to a culture. The fed-batch strategy is typically used in bio-industrial processes to reach a high cell density in the bioreactor. Mostly the feed solution is highly concentrated to avoid dilution of the bioreactor. The controlled addition of the nutrient directly affects the growth rate of the culture and helps to avoid overflow metabolism (formation of side metabolites, such as acetate for *Escherichia coli*, lactic acid in cell cultures, ethanol in *Saccharomyces cerevisiae*), oxygen limitation (anaerobiosis). Substrate limitation offers the possibility to control the reaction rates to avoid technological limitations connected to the cooling of the reactor and oxygen

transfer. Substrate limitation also allows the metabolic control, to avoid osmotic effects, catabolite repression and overflow metabolism of side products.

Different strategies can be used to control the growth in a fed-batch process:

Control Parameter	Control Principle
DOT (pO_2)	DOstat (DOT= constant), F~DOT
Oxygen uptake rate (OUR)	OUR=constant, F~OUR
Glucose	on-line measurement of glucose (FIA), glucose=constant
Acetate	on-line measurement of acetate (FIA), acetate=constant
pH (pHstat)	F~pH (acidification is connected to high glucose)
Ammonia	on-line measurement of ammonia (FIA), ammonia=constant
Temperature	T adapted according to OUR or pO_2

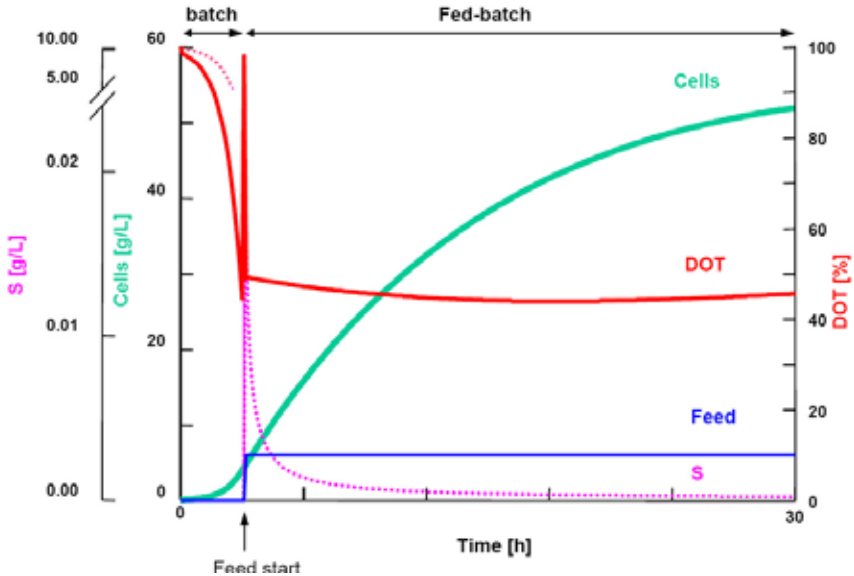

Fig. 15: The graph shows the principle of a substrate limited fed-batch cultivation with an initial batch phase. After consumption of the initial substrate a continuous feed of this substrate is started.

Gas Analysis in Bioreactors

The desire to reduce development times for drug manufacture drives companies to look for reliable technologies to improve fermentation and cell culture production. Companies have invested millions of dollars in production plant and R&D facilities, and they want their expensive assets to be used as efficiently as possible. The shortfall of worldwide production capacity adds to their urgency: Even small yield increases at existing bioreactor facilities can forestall production shortages until new facilities come on-line. Standard bioreactor design has changed little during the past 20 years, but the electronics and sensors available now are radically improved, and production efficiencies have increased greatly. The trend toward better instrumentation and data collection continues. Extracting and analyzing more information from each bioreactor run is now a priority for process development teams. The many off-line measurement techniques currently available provide useful data, but what is needed for even more efficient control of bioreactors and the bioprocesses within them is on-line, real-time measurement information.

An Alternative to Mass Spectroscopy

Mass spectrometers have traditionally been used to analyze the exhaust gas from a bioreactor to increase understanding of a bioprocess. These analyzers are, unfortunately, expensive tools, and they are often multiplexed to several bioreactors, with the result that detailed information about each individual unit may be lost. Furthermore, servicing a multiplexed analyzer means that a significant number of a facility's bioreactors are idle at one time, costing money and causing scheduling uncertainty. Should the multiplexer or analyzer fail, all information on all the bioreactors is lost, possibly at the cost of an entire batch. The best solution would be a dedicated gas sensor on each bioreactor that can be reliably used for automatic measurement and control of the bioreactor's exhaust gas mixture, just as a dissolved oxygen probe is used inside the bioreactor.

DSM Biologics (Groningen, The Netherlands, www.dsm.com/en_US/html/biologics/home_biologics.htm) had laboratory and pilot bioreactors already installed and wanted to buy a flexible gas monitoring system. One of its manufacturing customers had developed a laboratory-scale process for the production of a recombinant subunit vaccine in *Escherichia coli*, for which off-gas analysis data were required not only to prove a successful technology

transfer and scale up (similar exit gas profiles), but also to support claims for process consistency and reproducibility. It chose the Tandem off-gas analyzer. The system was installed by DSM personnel without help from the vendor's engineers. Furthermore, DSM found that its personnel could easily transfer the analyzer among its many bioreactors. Scale-up demands and process reproducibility are two of the parameters that best demonstrate the value of bioprocess off-gas analysis in process development. The use of gas sensors for metabolic analysis requirements and fed-batch control is also increasingly common. Although microbial fermenters still dominate the gas analysis market, changing market pressures are moving gas analysis into cell culture bioreactors also. For example, the worldwide shortage of cell culture production capacity is leading production and development managers to consider off-gas analysis to increase yields with existing bioreactors. However, many companies cannot afford to install expensive off-gas analysis systems, especially when such systems may require complex interfaces to work with existing instrumentation and software controls. The Tandem analyzer provides continuous and accurate measurements of O^2 and CO^2 (± 0.01% partial pressure) and transmits these data by means of 4–20 mA or 0–10 V signals back to the control system. The Tandem scales up well with a bioprocess because of its relatively low per-unit cost, which allows individual installation on each bioreactor. The pitfalls of multiplexing a single expensive analyzer are thus avoided. Furthermore, the precision and accuracy of the Tandem competes well with other on-line analytical methods.

Applications

The process run at DSM required induction of recombinant protein expression at a predetermined optical density value. Using off-gas analysis with off-the-shelf data-logging software, DSM scientists could correlate that point accurately with a specific carbon dioxide concentration in the exit gas. In subsequent batches, a combination of the optical density data and the gas analysis data was used to pinpoint the moment to initiate recombinant protein expression. As a result, DSM was able to generate highly consistent and reproducible data for subsequent consistency batches. That success led to the introduction of the Tandem at DSM's GMP manufacturing plant in Canada. By attaching the Tandem to its existing system, the company increased the flexibility of its GMP plant. In addition, it now has a reliable system on which

to base new control strategies. Other companies are also taking advantage of the technology. David Anderson, research director at Chem Gen Corporation (Gaithersburg, MD, www.chemgen.com), says "We use Tandems for analysis of laboratory fermentations. Using the instrument is a very easy and cost effective way to determine O_2 and CO_2 concentration in the off gas." Paul Milner, of Micro science Ltd (Reading, UK, www.microscience.com), explains, "We have found the system to be both reliable and consistent. The information on CO2 evolution directly correlates with product formation, and so we now use it to monitor the physiological state of our cultures." Researchers in development laboratories are becoming more clever in their analysis of gas data from

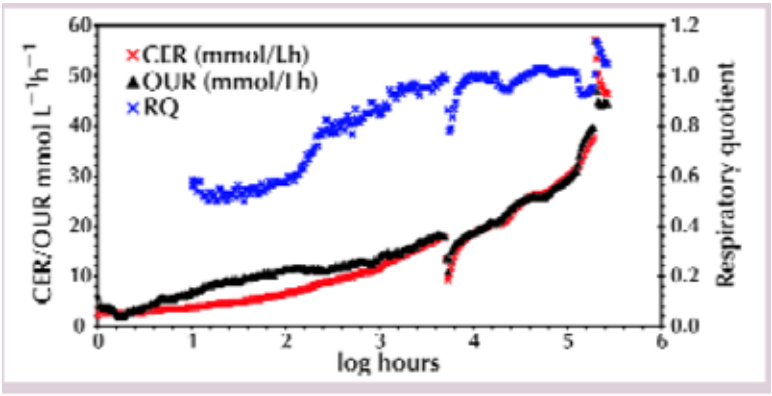

Fig. 16: Growth of Escherichia coli on a succession of substrates; CER = Carbon dioxide evolution rate; OUR = oxygen utilization rate (left); RQ = respiratory quotient (right)

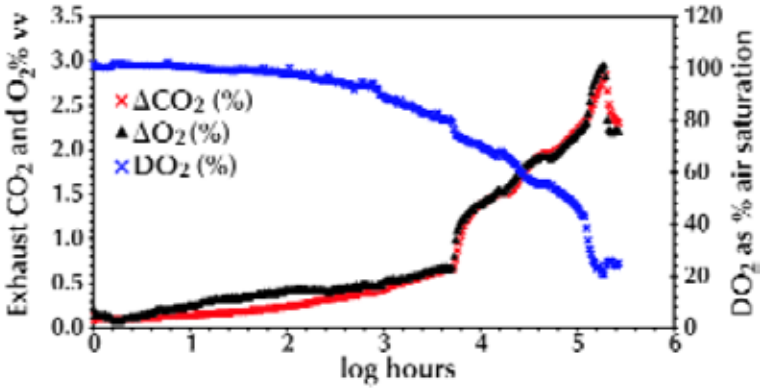

Fig. 17: Growth of Escherichia coli on a succession of substrates; Raw CO_2 and O_2 profiles (difference of inlet minus outlet, left) and dissolved oxygen (DO_2) profile (right)

bioreactors. Common derived variables such as the carbon dioxide evolution rate (CER) and respiratory quotient (RQ) are now frequently used for scale-up calculations and understanding metabolism for feeding control. Less used, but still important, are derived variables for growth rates and dissolved oxygen and carbon dioxide in the media. For example, engineers at production sites find that using gas analysis to produce estimated dissolved oxygen (DO_2) level in large tanks helps them troubleshoot DO_2 probe readings.

AIRLIFT BIOREACTORS

General Introdcution

The term *airlift reactor* (ALR) covers a wide range of gas– liquid or gas–liquid–solid pneumatic contacting devices that are characterized by fluid circulation in a defined cyclic pattern through channels built specifically for this purpose. In ALRs, the content is pneumatically agitated by a stream of air or sometimes by other gases. In those cases, the name *gas lift reactors* have been used. In addition to agitation, the gas stream has the important function of facilitating exchange of material between the gas phase and the medium; oxygen is usually transferred to the liquid, and in some cases reaction products are removed through exchange with the gas phase. The main difference between ALRs and bubble columns (which are also pneumatically agitated) lies in the type of fluid flow, which depends on the geometry of the system. The bubble column is a simple vessel into which gas is injected, usually at the bottom, and random mixing is produced by the ascending bubbles. In the ALR, the major patterns of fluid circulation are determined by the design of the reactor, which has a channel for gas-liquid upflow—the riser—and a separate channel for the down flow (Fig. 18). The two channels are linked at the bottom and at the top to form a closed loop.

Fig. 17A: The picture of an ALR

The gas is usually injected near the bottom of the riser. The extent to which the gas disengages at the top, in the section termed the gas separator, is determined by the design of this section and the operating conditions. The fraction of the gas that does not disengage, but is entrapped by the descending liquid and taken into the downcomer, has a significant influence on the fluid dynamics in the reactor and hence on the overall reactor performance.

Airlift Reactor Morphology

Airlift reactors can be divided into two main types of reactors on the basis of their structure (Fig. 18): (1) external loop vessels, in which circulation takes place through separate and distinct conduits; and (2) baffled (or internal-loop) vessels, in which baffles placed strategically in a single vessel create the channels required for the circulation. The designs of both types can be modified further, leading to variations in the fluid dynamics, in the extent of bubble disengagement from the fluid, and in the flow rates of the various phases.

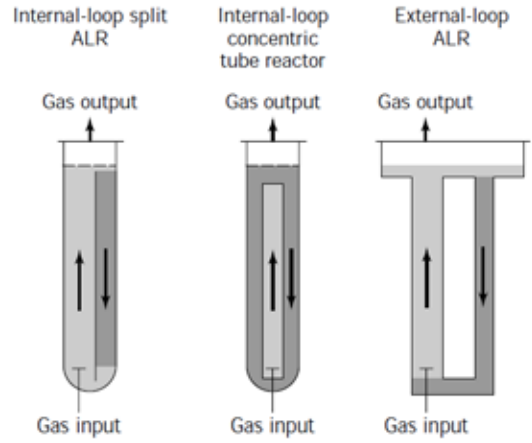

Fig. 18: Different types of ALRs

All ALRs, regardless of the basic configuration (external loop or baffled vessel), comprise four distinct sections with different flow characteristics:

- **Riser**. The gas is injected at the bottom of this section, and the flow of gas and liquid is predominantly upward.
- **Downcomer**. This section, which is parallel to the riser, is connected to the riser at the bottom and at the top. The flow of gas and liquid is predominantly downward. The driving force for recirculation is the difference in mean density between the downcomer and the riser; this difference generates the pressure gradient necessary for liquid recirculation.
- **Base**. In the vast majority of airlift designs, the bottom connection

zone between the riser and downcomer is very simple. It is usually believed that the base does not significantly affect the overall behavior of the reactor, but the design of this section can influence gas holdup, liquid velocity, and solid phase flow.

- **Gas separator**. This section at the top of the reactor connects the riser to the downcomer, facilitating liquid recirculation and gas disengagement. Designs that allow for a gas residence time in the separator that is substantially longer than the time required for the bubbles to disengage will minimize the fraction of gas recirculating through the downcomer (Fig. 19).
- Momentum, mass transfer, and heat transfer will be different in each section, but the design of each section may influence the performance and characteristics of each of the other sections, since the four regions are interconnected.

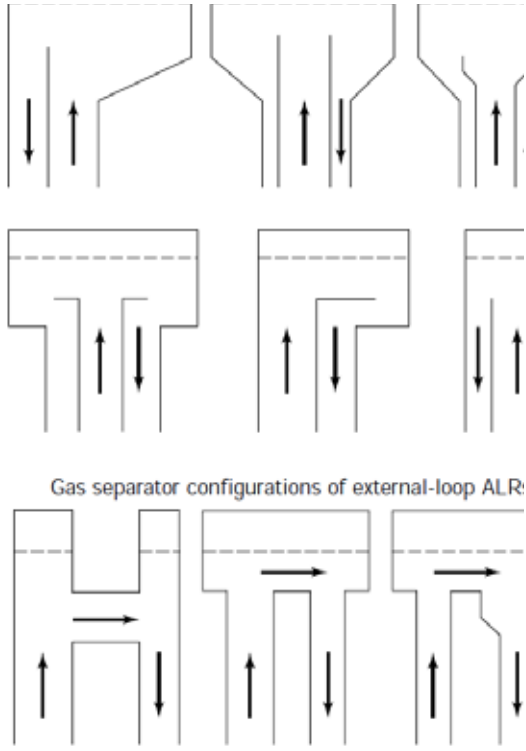

Fig. 19: Different types of gas separators.

Advantages of Airlift Bioreactors

For the growth of microorganisms, ALRs are considered to be superior to traditional stirred-tank fermenters despite the fact that the conventional fermenters provide the major requirements for culturing microorganisms: gas–medium interface for the supply of oxygen and the removal of waste gases; means of agitation to ensure proper nutrient distribution and to minimize damage resulting from addition of concentrated acid or base (for pH control); means of heat transfer (for temperature control); and a contamination-free environment. Therefore, the reason for the more successful growth reported in ALRs appears to lie in the difference in the fluid dynamics between ALRs and the more conventional fermenters. In conventional stirred tanks or bubble columns, the energy required for the movement of the fluids is introduced focally, at a single point in the reactor, via a stirrer or a sparger, respectively.

Consequently, energy dissipation is very high in the immediate surroundings of the stirrer and decreases away from it toward the walls. Similarly, shear will be greatest near the stirrer, since the momentum is transferred directly to the fluid in that region, which, in turn, transfers this energy to the slower-moving, more distant elements of the fluid. This results in a wide variation of shear forces; for example, the maximum shear gradient in a stirred tank with a flat-blade turbine has been reported to be approximately 14 times the mean shear gradient. Cells in culture may thus be exposed to contrasting environments in a mechanically stirred vessel, either to minimal shear forces that may generate potentially undesirable gradients in temperature and in substrate, metabolite, and electrolyte concentrations or, alternatively, to highly turbulent zones, with no problems of heat or mass transfer, but with very high shear gradients that may endanger cell integrity or exert some influence on cell morphology and metabolism. Changes in the morphology of microorganisms associated with high shear forces in the medium have frequently been observed. The nature of the relationship between such morphological changes and the rates of growth and metabolite production is still not properly understood, although it may be of great importance in the design and scale-up of bioreactors.

In ALRs, as in bubble columns, the gas is injected at a single point, but in ALRs the direct contribution of gas injection to the dynamics of the system is small; circulation of liquid and gas is facilitated by the difference in gas holdup

between the riser and the downcomer, which creates a pressure difference at the bottom of the equipment:

$$\Delta P_b = \rho_L g(\varphi_r - \varphi_d)$$

where ΔP_b and the pressure difference, ρ_L is the density of the liquid (the density of the gas is considered to be negligible), g is the gravitational constant, and ϕ_r and ϕ_d are the fractional gas holdup of the riser and downcomer, respectively. The pressure difference forces the fluid from the bottom of the downcomer toward the riser, generating fluid circulation in the ALR. Since ϕ_r and ϕ_d are both average values integrated along the height of the reactor, it follows that there are no focal points of energy dissipation and that shear distribution is homogeneous throughout the ALR. There is thus a relatively constant environment, with minimization of sharp changes in the mechanical forces acting on suspended particles. Because good mixing is required, shear forces cannot be avoided completely. One of the most critical points is the bottom, where there is a sharp 180° turn. Shear-sensitive mammalian and plant cells in culture should benefit from such an environment. Currently, the research and development of new bioreactors for mammalian cells is indeed focusing on the issue of shear-related damage to suspended cells. Mammalian and plant cells in culture are more susceptible than microorganisms to the reactor conditions. Mammalian cells, which lack the rigid cell wall of microorganisms, have a larger size (one order of magnitude) than microorganisms and are very sensitive to mechanical stress. Plant cells have a rigid cellulose wall, but they are also much larger than microorganisms (usually by about an order of magnitude) and are therefore also sensitive to reactor conditions. Kolmogoroff's model of isotropic turbulence indicates that serious damage may occur at relatively large values of the length scale.

The last length is a parameter of the model and indicates the size of the eddy where energy starts to be dissipated by viscous resistance. Indeed, it has been observed that plant cells, in spite of their rigid wall, are shear-sensitive, and difficulties have been found in stirred-tank cultures. This is especially true when large-scale systems are considered. Although high agitation rates may be detrimental to cell growth, low agitation rates lead to an increase in the number and size of cell aggregates—also an undesirable phenomenon. The aggregates are formed as a result of daughter cells failing to separate after

division and as a consequence of the stickiness of the polysaccharides excreted by the cells, especially at the end of the growth phase. An optimal shear rate between these two extremes must be found for each culture. It has recently been shown experimentally that velocity fluctuations related to turbulent shear are relatively homogeneously distributed in an ALR. The measurements of fluctuating velocity made by Tan *et al.* show that the liquid turbulence in ALRs is homogeneously distributed in both the riser and the downcomer. It thus seems reasonable to assume that the homogeneity of the stress forces is the main advantage offered by ALRs and that this homogeneity is responsible for the success of shear-sensitive cultures in the ALR type of fermenter. Another advantage of the ALR is the mechanical simplicity of the device. The absence of a shaft and of the associated sealing, which is always a weak element from the point of view of sterility, confers on the ALR an obvious advantage over agitated tanks. This consideration is especially important in processes involving slow-growing cultures, such as animal and plant cells, for which the risk of contamination is large.

All the points mentioned above are particularly relevant for sophisticated processes in which the product is usually of high value. But ALRs may be used also for processes involving low-value products, in which case efficiency of energy use may well become the key point for design, as in the use of ALRs for wastewater treatment. The superiority of ALRs over mechanically agitated contactors in terms of mass transfer rates for a given energy input has been demonstrated by Legrys. Comparison of the efficiency of oxygen transfer, that is, the mass of oxygen absorbed per unit energy invested and unit time, showed that the efficiency of the ALR is among the highest in agitated systems. The ALRs are particularly suited to processes with changing oxygen requirements because aeration efficiency and performance are relatively insensitive to changes in operating conditions. Performance decreases markedly in mechanically stirred systems as the energy input (or oxygen transfer rate) increases, but it is quite constant in ALRs (Fig. 20).

The efficiency of ALRs decreases relatively slowly as the energy input per unit volume of reactor is increased, as is shown in Figure 21. In contrast, in the operation of stirred tanks, the mass transfer rate can be easily increased by increasing the power input, but this improvement is achieved at the cost of a considerable decrease in the efficiency of oxygen transfer. This decrease may

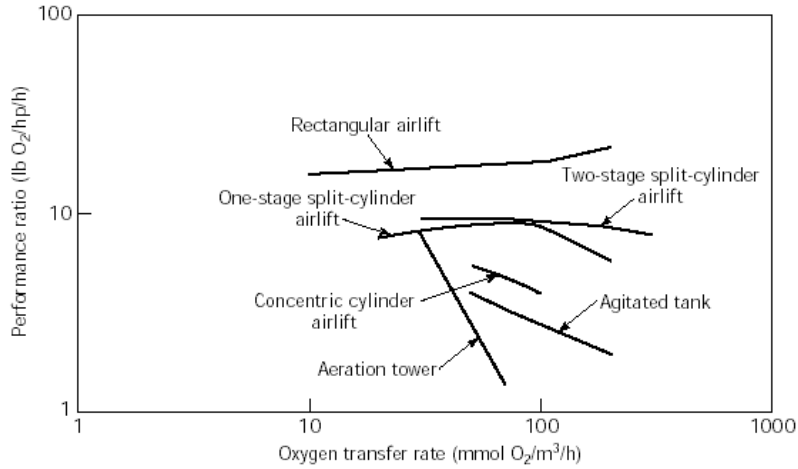

Fig. 20: Performance ratio as a function of oxygen-transfer rate, showing that aeration efficiency and performance are relatively insensitive to changes in operating conditions in different types of ALRs versus an agitation tank and an aeration tower. Adapted from Orazem and Erickson.

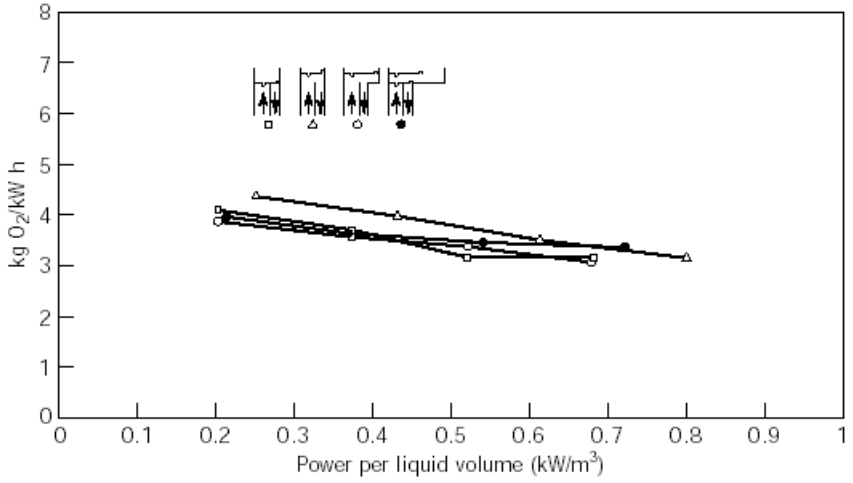

Fig. 21: -Aeration efficiency as a function of pneumatic power of gas input per unit volume in a straight-baffle ALR. The level indicated corresponds to no-aeration conditions. Adapted from Siegel *et al.*

constitute a crucial disadvantage in a process like wastewater treatment, where the energy input is an important element in the cost of the final product and flexibility of operating conditions is required because of the constant change of feed composition and flow rate. Energy economy in the ALR may be improved

by placing a second sparger in the upper part of the downcomer. If the liquid velocity is greater than the free rising velocity of the bubbles generated, the gas is carried down, resulting in a longer contact time between the bubble and the liquid. This diminishes the energy requirements, since part of the gas is injected against a lower hydrostatic pressure.

The advantages described above counterbalance the obvious disadvantage of ALRs, which is the requirement for a minimum liquid volume for proper operation. Indeed, the changes in liquid volume in these reactors are limited to the region of the gas separator, since the liquid height must always be sufficient to allow liquid recirculation in the reactor and must therefore be above the separation between the riser and the downcomer.

Fluid Dynamics

The interconnections between the design variables, the operating variables, and the observable hydrodynamic variables in an ALR are presented diagrammatically in Figure 22. The design variables are the reactor height, the riser-to-downcomer area ratio, the geometrical design of the gas separator, and the bottom clearance (C_b, the distance between the bottom of the reactor and the lower end of the draft tube, which is proportional to the free area for flow in the bottom and represents the resistance to flow in this part of the reactor). The main operating variables are primarily the gas input rate and, to a lesser extent, the top clearance (C_t, the distance between the upper part of the draft tube and the surface of the nonaerated liquid). These two independent variables set the conditions that determine the liquid velocity in the ALR via the mutual influences of pressure drops and holdups, as shown in Figure 22. Viscosity is not shown in Figure 22 as an independent variable because in the case of gas–liquid mixtures, it is a function of the gas holdup (and of liquid velocity in the case of non-Newtonian liquids), and because in a real process, it will change with time due the changes in the composition of the liquid.

FLOW CONFIGURATION

Riser. In the riser, the gas and liquid flow upward, and the gas velocity is usually larger than that of the liquid. The only exception is homogeneous flow, in which case both phases flow at the same velocity. This can happen only with very small bubbles, in which case the free-rising velocity of the bubbles is

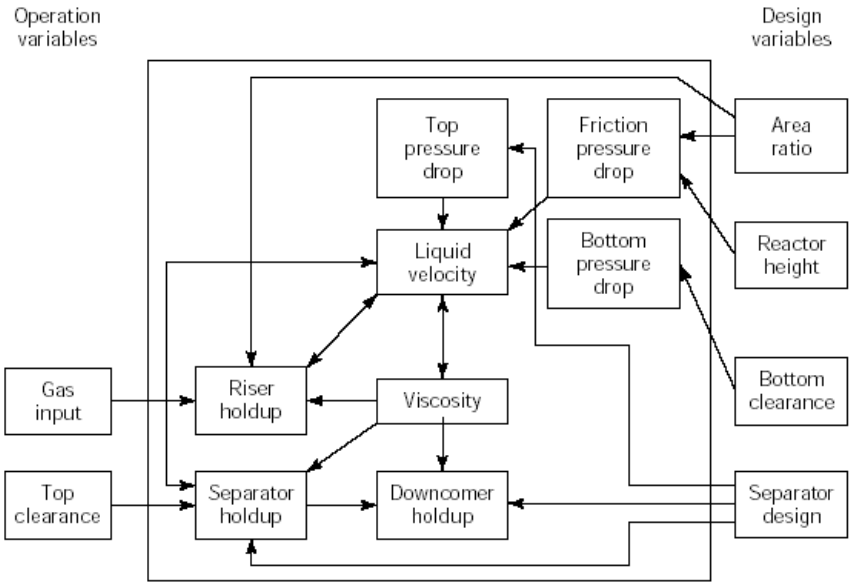

Fig. 22: Interaction between geometric and fluid dynamic variables in an ALR. Adapted from Merchuk *et al.*

negligible with respect to the liquid velocity. Although about a dozen different gas–liquid flow configurations have been developed, only two of them are of interest in ALRs:

1. Homogeneous bubbly flow regime, in which the bubbles are relatively small and uniform in diame ter and turbulence is low.
2. Churn-turbulent regime, in which a wide range of bubble sizes coexist within a very turbulent liquid.

The churn-turbulent regime can be produced from homogeneous bubbly flow by increasing the gas flow rate. Another way of obtaining a churn-turbulent flow zone is by starting from slug flow and increasing the liquid turbulence, by increasing either the flow rate or the diameter of reactor, as can be seen in Figure 23. The slug-flow configuration is important only as a situation to be avoided costs, because large bubbles bridging the entire tower cross-section offer very poor capacity for mass transfer.

Downcomer. In the downcomer, the liquid flows downward and may carry bubbles down with it. For bubbles to be entrapped and flow downward, the

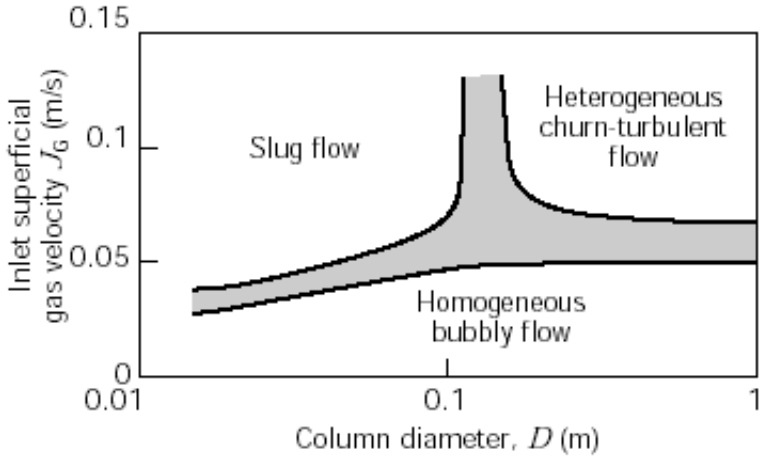

Fig. 23: Map of flow configurations for gas–liquid concurrent flow in a vertical tube. Adapted with permission from Wiswanathan.

liquid velocity must be greater than the free-rise velocity of the bubbles. At very low gas flow input, the liquid superficial velocity is low, practically all the bubbles disengage, and clear liquid circulates in the downcomer. As the gas input is increased, the liquid velocity becomes sufficiently high to entrap the smallest bubbles. Upon a further increase in liquid velocity larger bubbles are also entrapped. Under these conditions the presence of bubbles reduces the cross-section available for liquid flow, and the liquid velocity increases in this section. Bubbles are thus entrapped and carried downward, until the number of bubbles in the cross-section decreases, the liquid velocity diminishes, and the drag forces are not sufficient to overcome the buoyancy. This feedback loop in the downcomer causes stratification of the bubbles, which is evident as a front of static bubbles, from which smaller bubbles occasionally escape downward and larger bubbles, produced by coalescence, escape upward. The bubble front descends, as the gas input to the system is increased, until the bubbles eventually reach the bottom and recirculate to the riser. When this point is reached, the bubble distribution in the downcomer becomes much more uniform. This is the most desirable flow configuration in the downcomer, unless a single pass of gas is required. The correct choice of cross-sectional area ratio of the riser to the downcomer will determine the type of flow.

Gas Separator: The gas separator is often overlooked in descriptions of experimental ALR devices, although it has considerable influence on the

fluid dynamics of the reactors. The geometric design of the gas separator will determine the extent of disengagement of the bubbles entering from the riser. In the case of complete disengagement, clear liquid will be the only phase entering the downcomer. In the general case, a certain fraction of the gas will be entrapped and recirculated. Fresh gas may also be entrapped from the headspace if the fluid is very turbulent near the interface. The extent of this entrapment influences strongly gas holdup and liquid velocity in the whole reactor. It is quite common to enlarge the separator section to reduce the liquid velocity and to facilitate better disengagement of spent bubbles. Experiments have been reported in which the liquid level in the gas separator was high enough to be represented as two mixed vessels in series. This point will be analyzed further in the section devoted to mixing.

GAS HOLDUP

Gas holdup is the volumetric fraction of the gas in the total volume of a gas–liquid–solid dispersion:

$$\varphi_i = \frac{V_G}{V_L + V_G + V_S}$$

where the sub indexes L, G, and S indicate liquid, gas, and solid, and *i* indicates the region in which the holdup is considered, that is, gas separator (s), the riser (r), the downcomer (d), or the total reactor (T).

The importance of the holdup is twofold: (1) the value of the holdup gives an indication of the potential for mass transfer, since for a given system a larger gas holdup indicates a larger gas–liquid interfacial area; and (2) the difference in holdup between the riser and the downcomer generates the driving force for liquid circulation. It should be stressed, however, that when referring to gas holdup as the driving force for liquid circulation, only the total volume of the gas is relevant. This is not the case for mass transfer phenomena, in this case, the interfacial area is of paramount importance, and therefore some information on bubble size distribution is required for a complete understanding of the process. Because gas holdup values vary within a reactor, average values, referring to the whole volume of the reactor, are usually reported. Values referring to a particular section, such as the riser or the downcomer, are much more valuable, since they provide a basis for determining liquid velocity and mixing. However, such values

are less frequently reported. The geometric design of the ALR has a significant influence on the gas holdup. Changes in the ratio A_d/A_r, the cross-sectional areas of the downcomer and the riser, respectively, will change the liquid and gas residence time in each part of the reactor and hence their contributions to the overall holdup. Gas holdup increases with decreasing A_d/A_r.

Gas Holdup in Internal Airlift Reactors. These take into account liquid properties and geometric differences within a particular design. Most of the correlations take the form:

$$\varphi_r = a(J_G)^{\alpha}\left(\frac{A_d}{A_r}\right)^{\beta}(\mu_{ap})^{\gamma}$$

where ϕ_r is the gas holdup in the riser, J_G is the superficial gas velocity (gas volumetric flow rate per unit of cross sectional area), μ_{ap} is the effective viscosity of the liquid, and α, β, γ, and a are constants that depend on the geometry of the reactor and the properties of the liquid. The correlation can be used to predict the holdup in a system that is being designed or simulated as a function of the operating variables, the geometry of the system, or the liquid properties. Such correlations are effective for fitting data for the same type of reactor (*e.g.*, a split-vessel reactor) with different area ratios or even different liquid viscosities, but they are mostly reactor-type specific. The cyclic flow in the ALR complicates the analysis of the system. The riser gas holdup depends strongly on the geometric configuration of the gas–liquid separator and the water level in the gas separator. This has been shown experimentally in a split-vessel rectangular ALR, but the premise can essentially be extended to any internal loop ALR. Analysis of the system revealed that these factors influence the gas disengagement and hence the gas recirculation in the downcomer. When this influence is taken into account and the holdup is plotted against the true gas superficial velocity, $J_{G,true}$, which is defined as the sum of the gas superficial velocity due to the freshly injected gas, Q_{in}, and to the recirculated gas, Q_d, that is,

$$J_{G,true} = \left(\frac{Q_{in} + Q_d}{A_r}\right)$$

then all the data for the different gas separators may be represented by a single relationship, such as equation 3. In other words, if the actual gas flow is known, the influence of gas recirculation (which depends on Ad/Ar and the design of

the gas separator) has been already taken into account and does not need to be considered again. Nevertheless, this simple approach has a drawback in that the true gas superficial velocity is difficult to measure because the gas recirculation rate is usually not known. A method for evaluation of the extent of the maximum gas recirculation has recently been developed and will be discussed later in this article. Thus, correlations that take into account all the variables, which may be easily measured, remain the option of choice. Table 1 shows most of the correlations of this type that have been proposed for the riser holdup in internal loop ALRs. Comparison of a number of these correlations shows that there is reasonable agreement between the predictions of the different sources (Fig. 24). Figure 24 can be used as an example of the actual state of-the-art in ALR design. A number of correlations have been proposed, and three variables (Ad/Ar, lap, and JG) have been tested by most researchers. The ranges in which these variables were studied varies from source to source. In addition, some other variables (such as bottom clearance, top clearance or gas separator design, and surface tension) have been used by some authors but ignored by others. One example is the disengagement ratio defined by Siegel and Merchuk (64), which represents the mean horizontal path of a recirculating bubble relative to the external diameter and is equivalent to the parameter obtained by dimensional analysis (1) as:

$$M = \frac{D_S}{4D}$$

where D is the diameter of column and Ds the diameter of gas separator. If this parameter is not taken into account, then studies of the influence of the top clearance (42,65) are incomplete and difficult to extrapolate to other designs. The same can be said about the filling factor (66) given by the ratio of the gas separator volume to the total volume. The foregoing discussion thus explains why all the correlations coincide for some ranges of these secondary variables while in other ranges they may diverge. In addition, in some cases the number of experiments may not have been sufficient to provide correlations or they may have been ill-balanced from the statistical point of view. The obvious solution to this problem lies in the collection of a large and detailed bank of reliable data that will constitute the basis for correlations with greater accuracy and validity. The safest procedure for the prediction of the gas holdup in an ALR under design is to take data provided by researchers who have made the

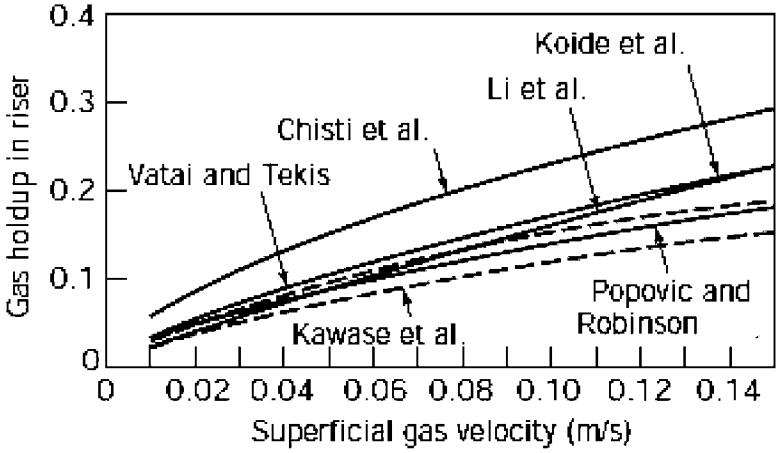

Fig. 24: Some correlations proposed for prediction of gas holdup in the riser of internal-loop ALRs. Gas holdup (ϕ_r) is presented as a function of superficial gas velocity (J_G). Other parameters related to geometry and physicochemical properties that were used in the calculations are shown on the figure.

measurements in that particular type of reactor with the same physicochemical properties of the system.

Gas holdup in the downcomer is lower than that in the riser. The extent of this difference depends mainly on the design of the gas separator. The downcomer gas holdup is linearly dependent on the riser holdup, as a consequence of the continuity of liquid flow in the reactor. Many expressions of this type have been published. At low gas flow rates, ϕ_d is usually negligible, since most of the bubbles have enough time to disengage from the liquid in the gas separator. This usually happens at the low gas flow rates frequently used for animal cell cultures. The gas holdup in the separator is very close to the mean gas holdup in the whole reactor as long as the top clearance C_t is relatively small (one or two diameters). For larger top clearances, the behavior of the gas separator begins to resemble that of a bubble column, and the overall performance of the reactor is influenced by this change.

External-Loop Airlift Reactors: From the point of view of fluid dynamics, neither the external configuration (shape and architecture) nor the fact that both riser and downcomer are easily accessible is the most important difference between external- and internal-loop reactors. The most important point is that the gas separator of the external-loop ALR is built in such way

that gas disengagement is usually much more effective in this type of reactor. In concentric tubes or split vessels, the shortest path that a bubble has to cover from the riser to the downcomer is a straight line across the baffle that separates the two sections. In the case of external-loop ALRs, there is usually a minimum horizontal distance to be covered, which increases the chances of disengagement of the bubbles. In this case, it is worth pointing out that if gas does appear in the downcomer, then most of it will be fresh air entrained in the reactor because of interfacial turbulence or vortices that appear in the gas separator above the entrance to the downcomer. In many of the studies reported in the literature on holdup in external-loop ALRs, total disengagement is attained. No such data are available for the concentric tubes of split vessel ALRs, since total disengagement is possible only at very low gas flow rates. Several authors have presented their results of gas holdup as the gas velocity versus the superficial mixture velocity, based on the drift flux model of Zuber and Findlay. These authors derived general expressions for prediction of the gas holdup and for interpretation of experimental data applicable to non- uniform radial distributions of liquid velocity and gas fraction. The drift velocity is defined as the difference between the velocity of the particular phase (U) and the volumetric flux density of the mixture (J) where:

$$J = J_G + J_L$$

The drift velocities of the gas and liquid phases may thus be expressed as:

$$J_G = U_G - J$$

$$J_L = U_L - J$$

Zuber and Findlay derived the relationship, which has been shown to be more than adequate to provide a correlation of gas holdup measurements in tower reactors with high liquid velocities, such as ALRs:

$$U_G = \frac{J_G}{\varphi} = C_0 J + \frac{\frac{1}{A}\int \varphi(U_G - J)dA}{\frac{1}{A}\int \varphi \cdot dA}$$

where A is cross-sectional area, $C0$ is distribution parameter, J is superficial velocity, JG is superficial gas velocity, UG linear gas velocity, and u is gas holdup. Equation describes the relationship between the gas velocity in a two-phase

flow and the volumetric flow density of the mixture, J. As stressed by Zuber and Findlay, J has the advantage of being independent on space coordinates for both one-dimensional flow and multidimensional irrotational flows. The distribution parameter C0 is given by

$$C_0 = \frac{\frac{1}{A}\int_A \varphi J \cdot dA}{\left[\frac{1}{A}\int_A J \cdot dA\right]\left[\frac{1}{A}\int_A \varphi \cdot dA\right]}$$

The value of C_0 depends mainly on the radial profile of the gas holdup. Zuber and Findlay calculated $C_0 = 1$ for a flat profile and $C_0 = 1.5$ for a parabolic profile. Experimental values have been reported in the range of 1.03–1.2 for up flow and 1.0–1.16 for down flow. Equation shows that this parameter is a function of the profiles of velocities and holdup. The last term of the right-hand side of equation is the weighted mean value of the drift velocity:

$$U_{GI} = U_G - J$$

The drift velocity of a swarm of bubbles can be evaluated by using the expression given by Zuber and Findlay.

$$U_{2J} = 1.53 \cdot \left[\frac{\sigma g \Delta\rho}{\rho_L^2}\right]^{0.25} (1 - \varphi)^{1.5}$$

where U_{2J} is the velocity of the swarm of bubbles, g is gravitational acceleration, ρ_L is the density of liquid, $\Delta\rho$ is the density difference, σ is the surface tension, and ϕ is the gas holdup. This equation is valid for bubble diameters of the order of 0.1 to 2 cm, which covers the population usually observed in ALRs. It has, however, been shown that a plot of U_G versus J gives a straight line, suggesting that a constant value of the drift velocity satisfactorily represents the two-phase flow in the riser of an external-loop ALR. In this plot, the distribution parameter was $C_0 = 1.03$, and U_{GS}, the value of the slip velocity of a bubble, was taken as the mean drift velocity. Siegel *et al.* applied the same model for the study of gas recirculation in a split-vessel ALR and obtained the values of $C_0 = 1.11$. The slip velocity that they obtained fitting their data to equation 8 was 0.238 m/s. It has been suggested that this simplification holds as long as coalescence is not a predominant factor in the process. It is very important to stress the

difference between holdup, ϕ, and the flowing volumetric concentration (β), which is defined as:

$$\beta = \frac{Q_G}{Q_G + Q_L} = \frac{J_G}{J}$$

Zuber–Findlay's drift flux model allows us to derive the following equation, which establishes a connection between the gas holdup and β.

$$\frac{\beta}{\varphi} = C_0 + \frac{U_{b\infty}}{J}$$

where C_0 is the distribution parameter, J is the superficial velocity, $U_{b\infty}$ is the terminal gas velocity, β is the flowing volumetric concentration, and ϕ is the gas holdup. Figure 25 gives a representation of the $\phi = \beta$ plane. The 45 degree line indicates that $\phi = \beta$, an equality that is true only for nonslip flow, where the velocity of the gas is equal to the velocity of the liquid. Such a situation can be visualized for the case of very small bubbles in a relatively fast liquid. In this case, there is no influence of one phase on the motion of the other. As indicated in Figure 25, all the points below the 45 degree line indicate operation situations in which the liquid is driven by the gas:

$$U_G > U_L;\ \varphi < \beta$$

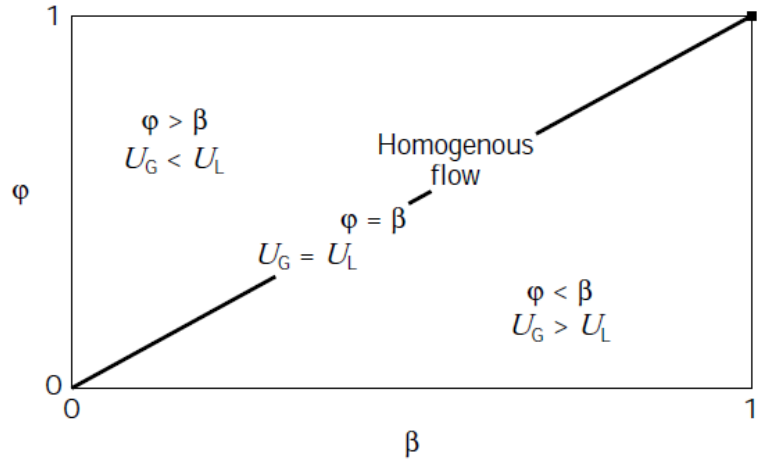

Fig. 25: Gas flow holdup (ϕ) vs. flowing volumetric concentration (β). The different zones in the plane ϕ-β identify the two phase flow.

This happens in the riser of ALRs. For all points above the line the opposite is true:

$$U_G < U_L;\ \varphi > \beta$$

This latter condition reflects the operation of the downcomer. A number of authors have measured the local holdup profile along the riser of an external-loop ALR. In general, it was found that the holdup increases with height. This finding concurs with the expected expansion of gas bubbles as regions of lower pressure are reached. Common sense indicates that this situation must be limited to a certain range; an increase in bubble size will enhance turbulence and result in an increase in bubble encounters, leading eventually to bubble coalescence. The larger bubbles will rise much faster, resulting in a decrease in holdup. Such a scenario was indeed observed by Merchuk and Stein, as is illustrated in Figure 27. Merchuk and Stein reported a maximum in the holdup profile for the case of a single-orifice gas distributor. For a multiple-orifice sparger, producing a more homogeneous bubble size distribution, a maximum was not observed within the studied length of the riser, which was 4 m. Literature data from different sources for gas holdup in the riser under conditions of little or no carryover of gas from the separator into the downcomer for different A_d/A_r and top clearance C_t may be represented by the simple exponential:

$$\varphi_r = \alpha J_G^{\beta}$$

where the constant _ depends on the friction losses in the loop, and b is usually a value between 0.6 and 0.7, as is illustrated in Figure 28. The fact that neither the area ratio nor the top clearance affects the gas holdup demonstrates the role of the gas–liquid separator in determining the performance of the reactor in general. In the absence of gas recirculation, there is no effect on these variables. Moreover, this means that under conditions of no gas entrainment from the separator to the downcomer, it is possible to predict the riser gas holdup as a function of the riser superficial gas velocity alone, which is of great importance for design purposes. It is accepted that liquid velocity has a mild negative effect on gas holdup in the riser. This effect is usually studied by reducing the liquid flow; this is achieved by adding resistance to the liquid loop by means of a valve or other controlled obstruction under conditions of low or nil gas recirculation. Such experiments, which are relatively simple in external-loop ALRs, indicate that the holdup decreases as the liquid velocity is increased from zero (bubble

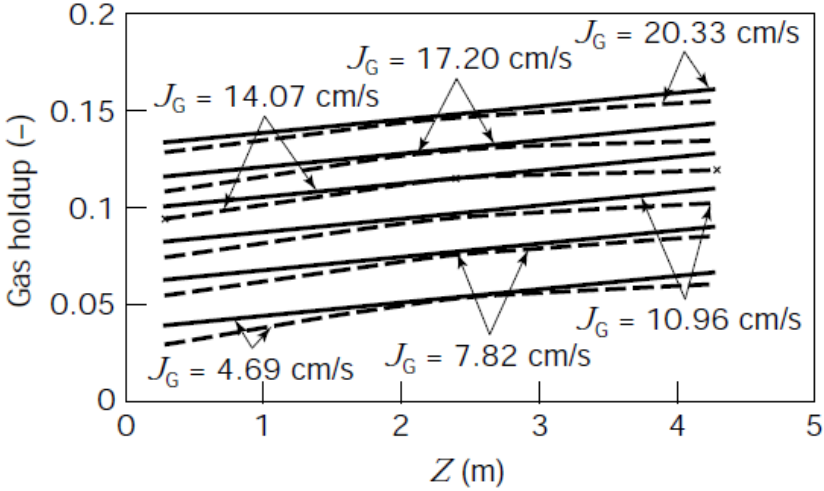

Fig. 27: Dependence of the riser gas holdup in a 4-m high external-loop ALR with a multiple-orifice sparger (solid lines) and a single-orifice sparger (broken lines)

column) to 0.3 m/s (which is close to the bubble free-rise velocity). For higher velocities, the effect of U_L is small. These findings add to our understanding of the fluid dynamics in the column. At liquid velocities that are smaller than the bubble free-rising velocity, the liquid transported in the wake of the bubbles, which must return downward to balance the mass flux, is the cause of the meandering and loops that typically appear in bubble column operation. As the overall liquid flux increases, the patterns straighten out, the bubbles begin to ascend in a straight pattern, and the holdup goes down. When the liquid velocity is higher than the free-rise velocity of the bubbles, piston flow of bubbles ensues in the tube, and the decrease in holdup for further increases in liquid velocity is due solely to the change in the ratio of gas–liquid volumetric flow rates. When there is gas recirculation, the area ratio A_d/A_r becomes an important variable affecting gas holdup. The effect of A_d/A_r starts in the region in which gas entrainment from the separator to the downcomer occurs. If it is assumed that the riser cross-sectional area A_r remains unchanged and the downcomer cross-sectional area Ad is increased, then it can be expected that the liquid velocity in the riser will increase as a result of the smaller resistance to flow in the loop, which in turn leads to a decrease in the riser gas holdup. An increase in A_d/A_r will result in a decrease in the liquid velocity in the downcomer, which leads to a decrease in the gas recirculation, since fewer bubbles are entrapped

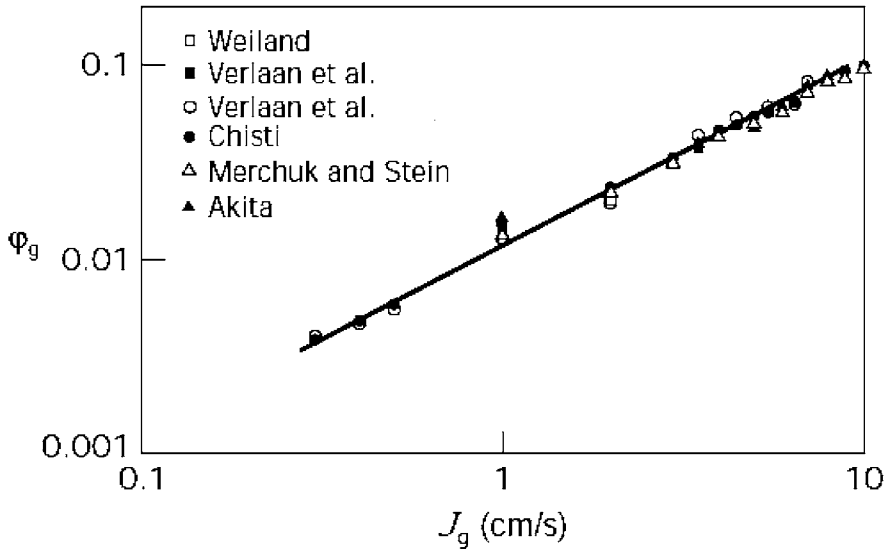

Fig. 28: Gas holdup reported by various sources for the riser of airlift reactors under conditions of little or no gas recirculation. The data correspond to different A_d/A_r ratios.

in the downcomer. The final outcome of increasing A_d/A_r is thus a decrease is the riser gas holdup. A similar argument can be applied in the discussion of the effect of reactor height on the riser gas holdup, that is, an increase in the height of the downcomer will result in a higher liquid velocity, which will in turn lead to a decrease, as in the former case, in the holdup in the riser. In contrast, an increase in A_d/A_r will lead to an increase in the extent of bubble entrapment in the downcomer, which will serve to inject some additional gas into the riser. On the other hand, an increase of gas holdup in the downcomer diminishes the driving force for recirculation, as shown in equation, and this will moderate the increase of liquid velocity generated by the larger height. This feedback control of the liquid velocity is one of the characteristics particular to ALRs.

Table shows most of the expressions published for the correlation of experimental data obtained in external-loop ALRs. Some of these expressions are presented in Figure. The differences between the predictions obtained with the different correlations are probably due to the design of the gas separator. The equation given by Popovic and Robinson seems to give an average of the proposed correlations.

Effects of Liquid Rheology. The effect of rheology on the reactor behavior and performance is of great interest because in most biotechnological

Table: Gas Hold-up in External-Loop ALR

No.	Formula
1	$\varphi_r = \frac{0.6\rho_G^{0.062}\rho_l^{0.069}\mu_G^{0.107}}{\mu_l^{0.053}s_l^{0.185}} \cdot \frac{J_{Gr}^{0.936}}{(J_{Gr} + J_{lr})^{0.474}}$
2	$\varphi_r = 0.16\left(\frac{J_G^2}{J_{lr}}\right)^{0.56}\left(1 + \frac{A_d}{A_r}\right)$
	$\varphi_d = 0.89\varphi r$
	$\varphi_r = 1.07Fr^{0.333}$
3	$Fr = \frac{J_G^2}{gD_r}$
4	$\varphi = 0.55J_{Gr}^{0.78}F^{0.2}D_r^{0.42}$
	$F = \frac{V_{ls}}{V_l}$
5	$\varphi_r = 0.203\frac{Fr_*^{0.31}}{Mo^{0.012}}\left(\frac{J_{Gr}}{J_{lr}} \cdot \frac{A_r}{A_d}\right)^{0.74}$
	$Mo = \frac{g(\rho_l - \rho_G)}{\sigma_l\rho_l^2} \cdot K^4\left(\frac{8J_{lr}}{D_r}\right)^{4(n-1)}\left(\frac{3n+1}{4n}\right)^{4n}$
	$Fr_* = \frac{(J_{lr} + J_{Gr})^2}{gD_r}$
6	$\varphi_d = 0.997\varphi_r$
7	$\varphi_r = 0.16\left(\frac{J_{Gr}}{J_l}\right)^{0.56}\left(1 + \frac{A_d}{A_r}\right)$

processes an increase in biomass provokes changes in the rheology of the fluid, especially in the case of mycelial growth. This effect is enhanced when in addition to the biomass growth, a product of the process is released into the medium in appreciable amounts. A good example of this scenario is the biosynthesis of polysaccharides, which cause an increase in the liquid viscosity. The effect of viscosity on gas holdup in bubble columns has been studied by a number of authors. The main problem to be overcome is that of non-Newtonian flow. If the viscosity is not constant, but changes with changes in the shear rate, then the evaluation of shear rates becomes particularly relevant for the identification of the system. Several authors have confronted this issue. Nishikawa *et al.*

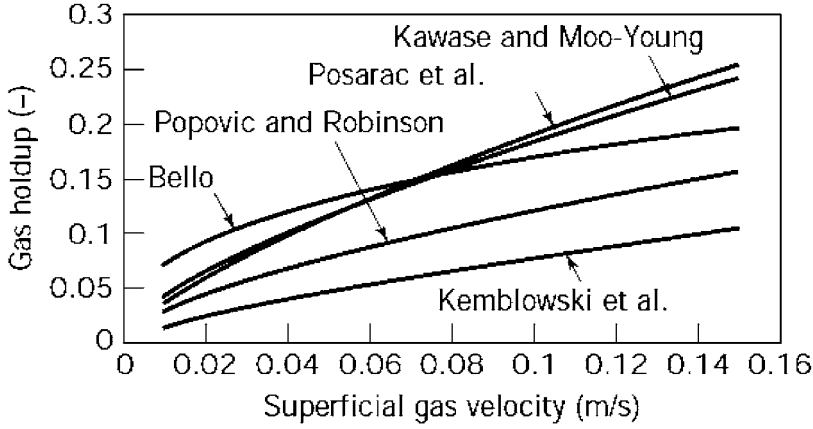

Fig. 29: Some correlations proposed for prediction of gas holdup in the riser of external ALRs. The gas holdup is presented as a function of the superficial gas velocity.

analyzed the problem of heat transfer in a bubble column with non-Newtonian liquids. They found a direct proportionality between the superficial gas velocity and the global shear rate:

$$\gamma = 5000 \cdot J_G \quad (J_G > 0.04\text{m/s})$$

This global shear rate was then used to calculate a global viscosity. In shear-sensitive cultures, the definition of a global shear rate in itself is of great importance. A number of researchers, Henzler, Kawase and Moo-Young, Schumpe and Deckwer have followed the approach of Nishikawa *et al.* but have suggested different proportionality constants relating the global shear rate to the superficial gas velocity. This approach is questionable from the rheological point of view because it will predict the same shear rate for a certain superficial gas velocity, no matter which liquid is used. El-Tamtamy *et al.* introduced an improvement by calculating the shear rate from the bubble velocity divided by the bubble diameter. However, accurate evaluation of the latter two parameters is difficult. Henzler and Kauling suggested relating the shear rate to power input based on dimensional analysis by expressing the shear rate as a function of the power input per unit volume, $(P/[V\rho\nu])^{1/2}$. Their analysis gives different shear rates for liquids that are rheologically different.

The above-described relationships predict different shear rates that vary in up to three orders of magnitude. It is thus generally agreed that the correct

solution is still to be found. Recently, a more general approach, known as a global approach, has been proposed by Merchuk and Ben-Zvi (Yona). The shear stress in a bubble column was defined as being equal to the acting force, which can be calculated from the power input divided by the sum of the areas of all the bubbles:

$$\tau = \frac{P}{L_R} S_{ab}$$

where L_R is an effective length that represents the mean circulation path of a bubble in the system considered, P is the power input, S_{ab} is the total surface of all of bubbles, and τ is the shear stress. Assuming ideal gas isothermal expansion, the power input P can be calculated. The interfacial area can be evaluated from correlations or can be obtained by direct measurement if available. A correlation taking into account other variables, like sparger configuration, surface tension, etc., will broaden the range of applications of this approach. If a constitutive equation describing the rheology of the system is available (such as the power law, which has been reported to correspond to many biological systems), equation facilitates the calculation of a global shear force acting on the liquid. The shear rate can be in this case expressed as:

$$\gamma = \left[\frac{\tau}{k}\right]^{1/n}$$

where γ is shear rate and k is behavior coefficient, and equation can be now used to express γ as

$$\gamma = \left[\frac{P_1 J_G \ln\left(\frac{P_1}{P_2}\right)}{aL_R^2 \kappa}\right]^{1/n}$$

where the subindexes 1 and 2 represent the two extremes of the section considered. Equation thus gives a global shear rate that is a function of both fluid dynamics and rheology. This approach has been found to be useful for the presentation of results on mass transfer rates in bubble columns. In contrast to the marked influence of rheology on gas holdup in bubble columns, the data available for ALRs show clearly that the effect of liquid viscosity is less dramatic,

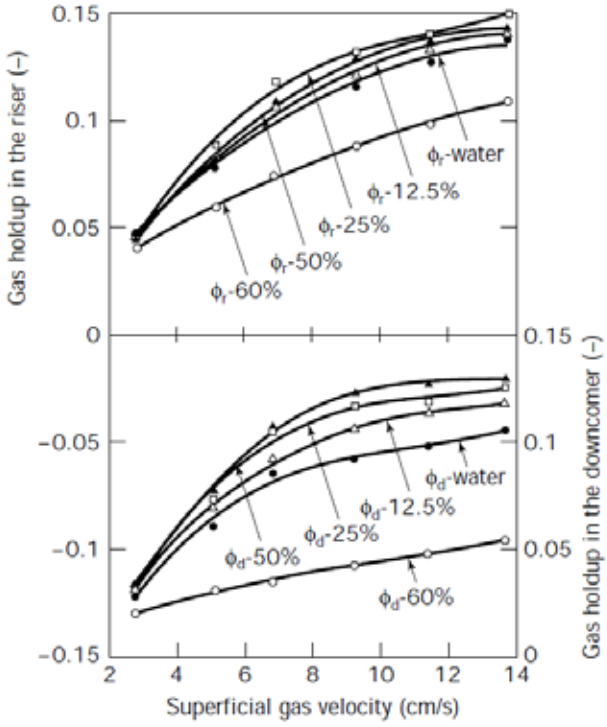

Fig. 30: Effect of liquid viscosity on the gas holdup in the riser and in the downcomer of an internal-loop ALR. The viscosity corresponding to the solutions used was 4–14 mPa s. Percentages refer to percent glycerol in water seen.

but not simpler. Figure 30 illustrates the effect of the addition of glycerol to water in an internal-loop ALR. At low concentrations of glycerol, a moderate increase of the gas holdup is evident, particularly in the downcomer but also in the riser. These increases are caused by the lower free rise velocity of the bubbles, which increase the gas retention due to the longer residence time. In addition, the entrapment of the bubbles is increased, and this is reflected mainly in ϕd. When the concentration of glycerol becomes too high, a strong decrease of the gas holdup is seen.

This decrease is probably due to the onset of coalescence, which produces larger bubbles that ascend faster in the liquid and easily disengage in the gas separator. The viscosities corresponding to these solutions ranged from 4 mPa s to 14 mPa s. In Figure 31, the addition of carboxymethyl cellulose (CMC) to water is shown. The change in CMC concentration had only a slight effect on

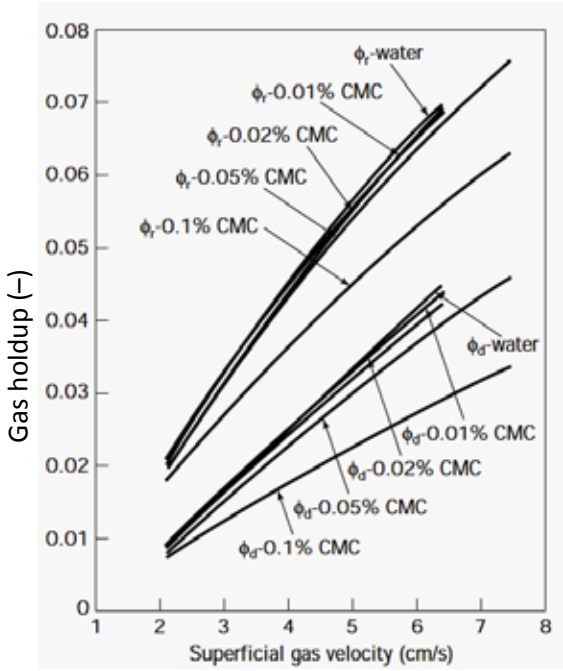

Fig. 31: -Effect of liquid rheology on the gas holdup in the riser and in the downcomer of an internal-loop ALR with a non-Newtonian liquid. The apparent viscosity corresponding to the solutions used, calculated for γ= 50 s^{-1}, was 5–56 mPa s.

the gas holdup for additions in the range 0.01 to 0.05% CMC. Only for solutions with concentrations higher than 0.5% CMC was an appreciable decrease in holdup seen.

Effect of Liquid Level. The influence of the liquid level C_t on the gas holdup is exerted as a consequence of changes in the extent of disengagement of the bubbles in the gas separator. This influence is therefore dependent on the geometric design of this section. Whether a bubble will disengage or will be entrapped into the downcomer depends on the interrelationship of several parameters—the free rising velocity of the bubble $U_{b\infty}$ (a function of size and viscosity), the liquid velocity in the downcomer U_{Ld} (a function of the difference in gas holdup between the riser and the downcomer and frictional losses), and the residence time of the bubble in the gas separator (a function of geometric design and liquid height). For a given bubble size, if U_{Ld} is smaller than the $U_{b\infty}$ corresponding to the smallest bubble, then there is no carryover. For smaller bubbles, the balance between the time required to cover the path from the end

of the riser to the zone near the entrance of the downcomer and the time needed for disengagement will give the fraction of bubbles recirculated. It should nevertheless be kept in mind that this is a feedback process. A higher bubble disengagement rate leads to a lower gas holdup in the downcomer, which in turn increases the liquid velocity, enabling larger bubbles to be trapped, until the system eventually reaches a steady state. Due to the above-explained influence of the geometric design, the influence of the liquid height is completely different in internal- and external-loop ALRs. In internalloop reactors, an increase in C_t increases the zone of the separator in which the gas holdup is higher, and as a result, the gas holdup increases. The extent of this increase depends, as said earlier, on the free-rise velocity of the bubbles.

Figure 32 shows the gas holdup in the riser and downcomer of a 30-liter ALR for two values of the top clearance, C_t = 0.178 m and C_t= 0.308 m, for two different liquids, water and a 0.5% CMC solution. It can be seen that although for water C_t has a small effect, this is not so for the more viscous solution. In the latter, the lower rising velocity of the bubbles causes a greater number of bubbles to be entrained and carried down by the liquid. Thus, the residence time in the disengagement section becomes very important in determining the

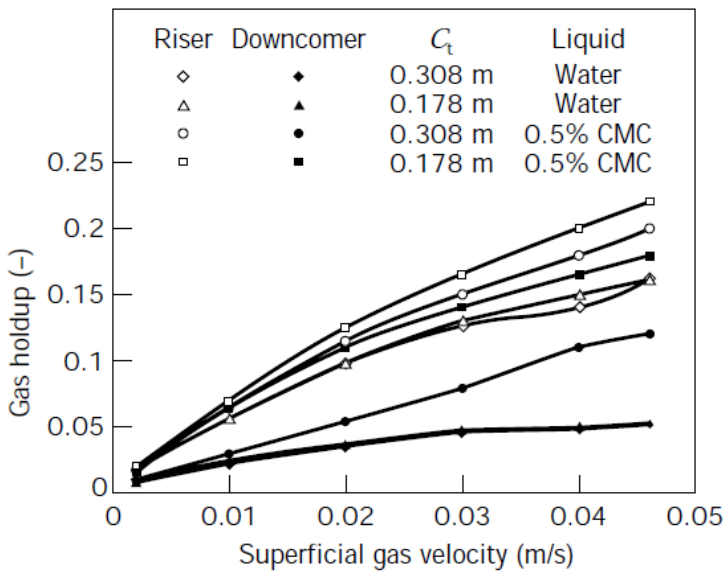

Fig. 32: Riser and downcomer gas holdup in an internal-loop ALR for two different top clearances and two liquids.

fraction of bubbles that recirculate. A lower C_t will give a shorter residence time in the separator, a larger bubble recirculation, and, hence, a larger gas holdup. In external-loop ALRs, the opposite effect is obtained, as may be seen in Figure 33. The data in Figure 33, obtained for a 4-m high external-loop ALR, show that the holdup in the riser decreases as C_t increases. This is due to the construction of these reactors, in which much of the gas that enters into the downcomer is trapped from the headspace due to the turbulence in this zone. An increase in

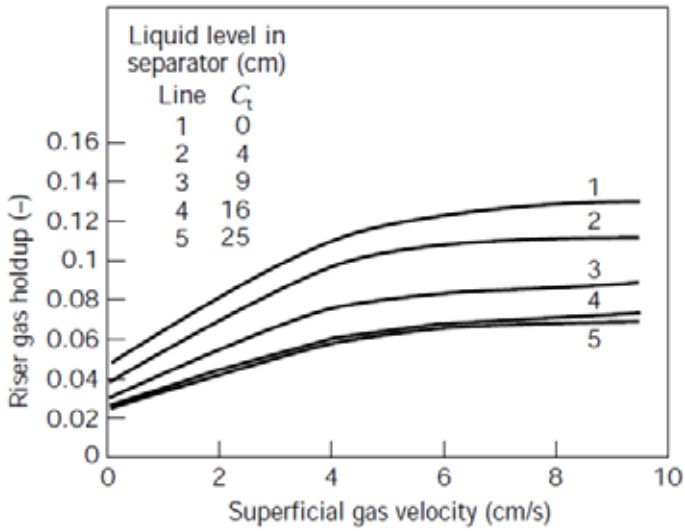

Fig. 33: Gas holdup in the riser of an external-loop ALR for several top clearances.

the liquid height serves to reduce the amount of gas trapped, so that less gas circulates in the downcomer and the liquid velocity increases. The final result is a reduction in the gas holdup, both in the riser and the downcomer.

Gas Recirculation

The degree to which gas flowing in the riser is entrapped and recirculated through the downcomer is an important variable, since it influences not only the flow configuration in the downcomer, but also the overall performance of the ALR. The liquid velocity depends mainly on the difference in holdup between the riser and the downcomer, and it in turn influences the gas holdup in the riser. Despite the importance of recirculation, very little quantitative data are available on this phenomenon. Siegel *et al.* evaluated the gas recirculation in a split-vessel ALR by an indirect method based on holdup measurements. From

their results, shown in Figure 34, it may be seen that the recirculation rate remains fairly constant for changing gas flow rates in the riser for high values of the last variable. Thus, the recirculation rate is determined largely by the geometric configuration of the gas–liquid separator and the liquid level in the separator. Three zones are evident in Figure 34; they represent operating conditions giving oscillating, borderline, and straight bubble flow in the downcomer. Oscillating flow patterns produce much larger fractions of gas retained in the downcomer, but they are much more sensitive to J_G. At low superficial gas velocity, the recirculation increases very sharply with J_G. The bubbles exhibit an oscillating swirling flow pattern, with some larger bubbles escaping toward the top. The borderline condition is defined as oscillatory bubble flow at a low gas flow rate that shifts to straight bubble flow with increasing input gas flow rate.

The straight flow operation zone is distinguished by bubble flow in a straight, well-defined flow pattern for all the input gas flow rates studied. If a straight bubble flow pattern is desired, the reactor should be operated at high riser gas flow rates, at which the reactor will shift toward stable operation. Lubbert *et al.* attempted to evaluate the recirculation of gas during the cultivation of yeast (*Saccharomyces cerevisiae*) on waste from a starch factory in a 4-m^3 pilot plant. They used microprocessor-aided pseudostochastic tracer input and cross-correlation techniques, which facilitated very reduced tracer feeds due to a high signal-to-noise ratio. The response to a pulse of helium was measured directly at the surface of the liquid in the separator by a quadruple mass spectrometer. The peak obtained showed pronounced shoulders (Fig. 35) which could be interpreted as superimposition of a second peak that represents the helium tracer one loop after. The fitting of such a model to the experimental data suggested recirculation of 25% of the gas. This figure is in the range of the recirculation rates presented by Siegel *et al.*, considering

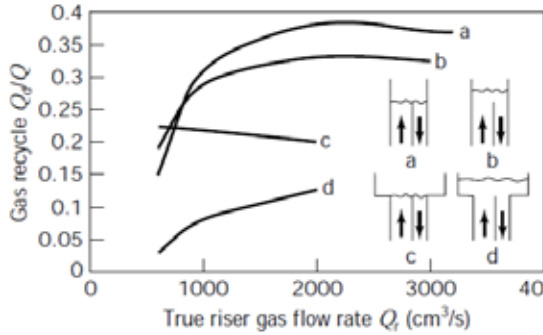

Fig. 34: Gas recirculation in a split-cylinder ALR. The level indicated corresponds to no-aeration conditions.

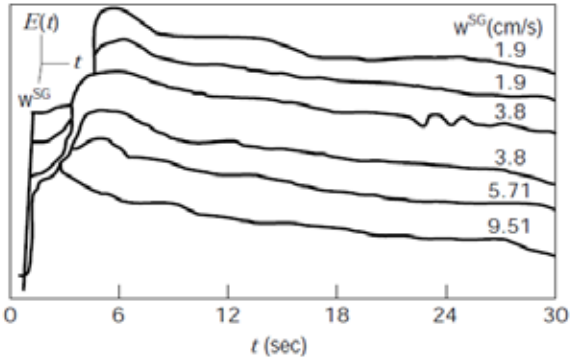

Fig. 35: Response to a pulse of helium in an airlift reactor. The pronounced shoulders could be interpreted as the result of superimposing a second peak, which represents the He tracer one loop after.

the differences in the coalescing properties of the liquids used in these two works and the corresponding differences in the downcomer holdup. Recently, Merchuk and Berzin developed a mathematical model based on the application of the first law of the thermodynamics to each of the regions of an ALR. This model facilitates the evaluation of the maximum liquid recirculation possible in the system. The calculation is based on the premise that the gas recirculated must be compressed from the pressure at the top of the downcomer to the pressure at its bottom. The mathematical expression that gives this maximal gas recirculation is:

$$Q_d = \frac{Q_L(P_2 - P_3) + Q_L\rho_L gh - \frac{1}{2}\rho_L C_d A_d(1 - \varphi_d)U_L^\beta}{P_4 \ln\left(\frac{P_3}{P_2}\right)}$$

where Q_d is the gas flow rate in the downcomer, Q_L is the liquid circulation flow rate, P_i is pressure at point i of the reactor (1 is top of the riser, 2 is top of the downcomer, 3 is bottom of the downcomer, 4 is bottom of the riser), C_d is the hydraulic resistance coefficient, A_d is the downcomer cross-sectional area, U_L is the linear liquid velocity, g is the gravitational acceleration, p_L is the liquid density, and Q_d is the downcomer gas holdup. The calculation of ϕd thus requires knowledge of the liquid flow rate, the pressures, and the geometry of the reactor. This equation represents the maximum recycling of gas in the downcomer, which will take place only if all the energy dissipated in the downcomer is invested in gas compression.

Liquid Velocity

The liquid velocity is one of the most important parameters in the design of ALRs. It affects the gas holdup in the riser and downcomer, the mixing time, the mean residence time of the gas phase, the interfacial area, and the mass and heat transfer coefficients. Circulation in ALRs is induced by the difference in hydrostatic pressure between the riser and the downcomer as a consequence of a difference in gas holdup. Liquid velocity—like gas holdup—is not an independent variable, because (see Fig. 22) the gas flow rate is the only variable that can be manipulated. As shown in Figure 22, the geometric design of the reactor will also influence the liquid velocity, but this remains constant during operation. Experiments have been carried out in devices specially designed to artificially change the resistance to flow, with the aim of studying the effect of the velocity at a fixed rate of aeration. The information emerging from these experiments indicates that an increase in the liquid velocity leads to a decrease in the mean residence time of bubbles in the riser and hence of the gas holdup in the riser. In practice, when the gas flow rate is increased, the higher liquid velocity increases the carryover of bubbles from the gas separator into the downcomer; the carryover dampens the liquid flow by reducing the hydrostatic driving force. As a result, the overall change in liquid velocity is tempered.

Liquid Velocity Measurement. Several different methods can be used for measuring the liquid velocity. The most reliable ones are based on the use of tracers in the liquid. If a tracer is injected and two probes are installed in a section of the tube, the velocity of the liquid traveling the distance between probes can be taken directly from the recorded peaks, as the quotient of the distance between the two electrodes and the time required by the tracer to travel from the one to the other. The latter is obtained as the difference of between the first moments of the two peaks. A second method is to calculate the liquid velocity (U_L) from the circulation time (t_c) and holdup (ϕ) as:

$$U_L = \frac{\text{liquid volume}}{t_c \times A \times (1 - \varphi)}$$

where A is cross-sectional area. In this case, only one electrode is necessary, ϕ is the holdup at the point at which the electrode is installed, and the circulation time is obtained from two successive peaks recorded by the electrode.

Modeling of Liquid Flow. A number of expressions are available for

the estimation of the liquid velocity. Two main methods have been used for the modeling of two-phase flow in ALRs—energy balances and momentum balances. The energy was used to balance approach to obtain a relationship between superficial gas velocity, holdup, and liquid velocity. Lee *et al.* calculated U_L by a similar type of model for a series of published data for concentric and external-loop ALRs and from their own results for split vessels. In both the above-mentioned models, constants accounting for friction losses were obtained by adjusting the models to the experimental data, on the other hand, managed to express the results of his energy balance and Freedman and Davidson in a relationship free of empirical constants. His results, however, fit the experimental data only qualitatively, and the fit is satisfactory only for very small diameters. An improvement of this method was suggested by Clark and Jones, who took into account the radial distribution of the gas holdup through the drift flux model. However, the values of the distribution coefficient C_0 needed for satisfactory fitting of the experimental data for lager diameters is far from the range usual in this type of flow. Chisti and Moo-Young extended a model originally proposed by Bello, based on an energy balance over the airlift loop. Their expression for the average superficial liquid velocity is:

$$U_{Lr} = \left(\frac{2gH_d(\varphi_r - \varphi_d)}{\frac{K_t}{(1-\varphi_r)^2} + K_B\left(\frac{A_r^2}{A_d}\right)\frac{1}{(1-\varphi_d)^2}} \right)^{0.5}$$

where U_L is the superficial liquid velocity, A_r is the riser cross-sectional area, A_d is the downcomer cross-sectional area, H_d is the downcomer height, K_b and K_t are the hydraulic pressure loss coefficients, Q_r is the riser gas holdup, and Q_d is the downcomer gas holdup. By choosing suitable values for the friction coefficients in each case, the authors showed that much of the published data on liquid velocity for the different types of ALRs could be satisfactorily correlated by equation. Only one coefficient has to be adjusted, since the authors assume that Kt, the friction coefficient at the top of the loop, is negligible in concentric-tube type reactors and that in external-loop reactors Kt can be taken as equal to K_b, the friction coefficient for the bottom of the loop. Equation has thus been adopted by many scientists. Wachi *et al.* claimed that their derivation of the same equation gives a clearer physical meaning to the adjustable parameters.

Equation can also be also derived from a simple momentum balance. Chisti *et al.* presented an empirical correlation for K_b obtained by comparison of results obtained from several sources:

$$K_b = 11.402 \cdot \left(\frac{A_d}{A_b}\right)^{0.789}$$

where A_b is the minimal cross section at the bottom of the airlift reactor and A_d is the downcomer cross-sectional area. Equation has the particularly that the gas flow rate, which is the main, and often the only, manipulable variable in the operation, is not present directly, but exerts its influence through the gas holdup. Therefore, either experimental data or a valid mathematical expression for the gas holdup in both the riser and the downcomer are required. Chisti and Moo-Young extended this model further in order to facilitate the prediction of liquid circulation in ALRs operating with pseudoplastic fluids, such as mold suspensions. This improvement is very important, since many commercial fermentation processes involve such non-Newtonian liquids. Kemblowski *et al.* presented a method for the prediction of gas holdup and liquid circulation in external-loop ALRs. In their experiments there was almost no gas recirculation, because of the large size of the gas separators used. Garcia Calvo presented an ingenious model based on energy balances and on an idea originally proposed by Richardson and Higson, and Garcia Calvo and Leton extended the model to bubble columns. The model is based on the assumption that the superficial gas velocity (J_G) in any region can be considered to be the sum of two streams (J´ _ and J´´) as follows. The J´stream has a velocity equal to that of the liquid and can therefore be treated by the laws of homogeneous two-phase flow (no slip between the bubbles and the liquid). The second stream (J´´) is considered to be responsible for all the energy loses at the gas–liquid interface. The concept in itself is simple and elegant, and it is possible to envisage its application even to the flow in the downcomer, where $U_G < U_L$. In such a case, we would divide the gas flow rate into two parts as follows: One part would be larger than the actual flow rate, *i.e.*, it would have the same velocity as the liquid. In order to arrive at the actual gas flow rate, the second flow rate must have the reverse direction. This type of gas flow can actually be seen under certain conditions, such as when there is coalescence of bubbles and larger bubbles ascend along the walls of the downcomer. Another technique used by several researchers to

predict liquid velocity is the momentum balance of the ALR. This method has been used by Blenke in jet-loop reactors and by Hsu and Dudukovic, Kubota *et al.*, Bello, Koide *et al.*, and Merchuk and Stein. The latter authors presented a simple model for the prediction of the liquid velocity as a function of the gas input in an ALR. They assumed that the pressure drop between the bottom and the top of their external-loop reactor could be expressed as a continuation of the downcomer, using an equivalent length L_E. This length was set as an adjustable parameter describing the pressure loss in the loop. Kubota *et al.* used a similar approach for the analysis of Imperial Chemical Industries' deep-shaft reactor. They were able to simulate the operation of the reactor and to predict the minimum air supply required to prevent flow reversal. Verlaan *et al.* used a similar model, in combination with the expression of Zuber and Findlay, to calculate the friction coefficients from experimental data reported by several authors for a wide range of reactor volumes. Koide *et al.* presented an analysis of the liquid flow in a concentric-tube ARL that was also based on a momentum balance. The main difference between this model and that used by Merchuk and Stein was that Koide *et al.* used a convergence–divergence flow model for the bottom and the top of the loop. At the bottom, the effect of flow reversal on the pressure drop was included in the effective width of the gas-liquid flow path under the lower end of the draft tube hl, which was smaller than the actual gap. Miyahara *et al.*, who studied both the bubble size distribution in an internal-loop ALR and the pressure drop at the top and the bottom of the draft tube, also presented a model facilitating the prediction of the liquid velocity. Other models use the drift-flux model presented in previous equations, as:

$$U_{Lr} = \frac{J_{Gr}\left(\frac{1}{\varphi_r} - C_0\right) - U_{GJ}}{C_0(1 - \varphi_r)}$$

U_{GJ} can be taken from previous equation. The range of variation of C_0 is rather narrow, as shown in the previous section, and therefore it is not difficult to make a judicious guess as to the value of C_0 in an unknown system. The drift flux model has also been used together with energy balances or with the momentum balance. Some studies on liquid measurement present the results in the form of empirical correlations. The usefulness of these correlations depends on the amount of data and the number of parameters taken into

account. Most of those correlations are shown on Table 3, and some of them are presented in Figure 36. In general, the superficial liquid velocity increases with an increase in the superficial gas velocity, but its rate of increase is much lower at high superficial gas velocities. From Table 3, it can be seen that the riser-to-downcomer cross-sectional area ratio and the reactor height are the main parameters that affect the superficial liquid velocity at constant superficial gas velocity. The superficial liquid velocity increases with an increase in A_d/A_r. The effect of the properties of the liquid, such as viscosity, surface tension, and ionic strength, on the superficial liquid velocity are much milder in ALR than in bubble columns. It is expected that increasing the liquid viscosity will decrease the liquid velocity because of frictional losses, but this, in turn, will increase the gas holdup in the riser and consequently increase the driving force for liquid recirculation. Hence, it seems that these two effects balance each other

Table: Liquid Circulation Velocity in ALRs

No.		Formula
1	ELR	$J_{Lr} = 1.55 J_{Gr}^{0.33} \left(\frac{A_d}{A_r}\right)^{0.74}$
	ILR	$J_{Lr} = 0.66 J_{Gr}^{0.33} \left(\frac{A_d}{A_r}\right)^{0.78}$
2	Bubbly	$J_{Lr} = 0.024 J_{Gr}^{0.322} \left(\frac{A_d}{A_r}\right)^{0.794} \mu_{ap}^{-0.395}$
	Slug flow	$J_{Lr} = 0.052 J_{Gr}^{0.322} \left(\frac{A_d}{A_r}\right)^{0.794} \mu_{ap}^{-0.395}$
3	Slug flow	$J_{Lr} = 0.23 J_{Gr}^{0.322} \left(\frac{A_d}{A_r}\right)^{0.97} \mu_{ap}^{-0.39}$
4		$J_{Lr} = 2.858 J_{Gr}^{0.482} \left(\frac{A_d}{A_r}\right)^{0.97} 416 \mu_{ap}^{-0.0105}$
5		$J_{Lr} = \left[\frac{2gH_d(\varphi_r - \varphi_d)}{K_b\left(\frac{1}{(1-\varphi_r)^2} + \left(\frac{A_d}{A_r}\right)^2 \frac{1}{(1-\varphi_d)^2}\right)}\right]^{0.5}$
		$K_b = 11.4 \left(\frac{A_d}{A_r}\right)^{0.79}$

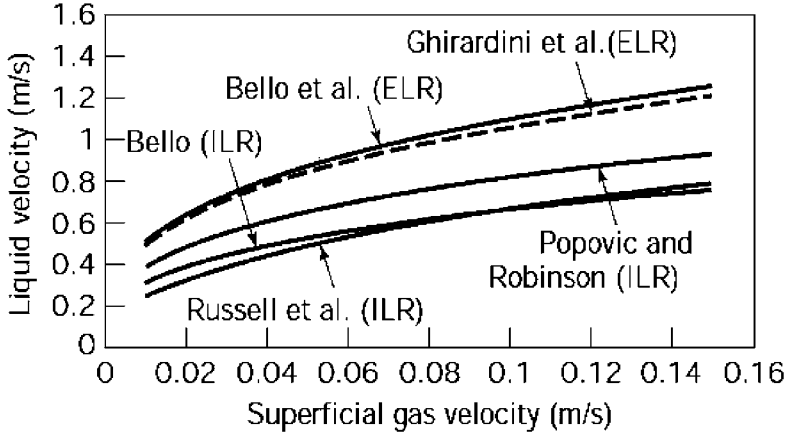

Fig. 36: Liquid velocity predicted by some of the proposed correlations from Table. ILR, internal-loop ALR; ELR, external-loop ALR.

partially and result in a milder effect on the superficial liquid velocity. The effects of the surface tension and the ionic strength are also exerted via their influence on the gas holdup, as analyzed above. As a rule, it can be recommended that the Zuber-Findlay expression be used when the holdup is known and the liquid circulation velocity is high. For low liquid velocity, a correlation obtained in a piece of equipment as similar as possible to the one under design should be used.

Liquid Mixing

For the design, modeling, and operation of ALRs, a thorough knowledge of mixing behavior is necessary. This is of particular importance during the process of scale-up from laboratory-scale to industrial-scale reactors. The optimum growth rate of a microorganism or the optimum production rate of a specific secondary metabolite usually relates to well-defined environmental conditions, such as pH range, temperature, substrate level, limiting factors, dissolved oxygen, and inhibitor concentration in a specific well mixed laboratory-scale vessel. Because of the compromises made during scale-up, it is difficult to keep, at different scales of operation, the same hydrodynamic conditions established in the laboratory; mixing on an industrial scale may not be as good as mixing on a laboratory scale. In smaller-scale reactors it is easier to maintain the optimal conditions of pH, temperature, and substrate concentration required for maximum productivity of metabolites in a fermenter. Furthermore, in fermentation systems efficient mixing is required to keep the pH within the

limited range, giving maximum growth rates or maximum production of the microorganism during addition of acid or alkali for pH control. Mixing time—or the degree of homogeneity—is also very important in fed-batch fermentation, where a required component, supplied either continuously or intermittently, inhibits the microorganisms or must be kept within a particular concentration range. A large number of commercially important biological systems are operated in batch or fed-batch mode. In this operation mode, fast distribution of the incoming fluid is required, and the necessity for understanding the dynamics of mixing behavior in these vessels is obvious. Even for batch systems, good control of the operating conditions, such as pH, temperature, and dissolved oxygen, requires prior estimation of mixing so that the addition rates can be suitably adjusted Deviation of the pH or temperature from the permitted range may cause a damage to the microorganism, in addition to its effect on the growth and production rates. Moreover, a knowledge of the mixing characteristics is required for modeling and interpreting mass and heat transfer data. A parameter used frequently to represent mixing in reactors is the mixing time (t_m). It has the disadvantage that it is specific to the reactor design and scale, but it is easy to measure and understand. Mixing time is defined as the time required to achieve the desired degree of homogeneity (usually 90–95%) after the injection of an inert tracer pulse into the reactor. The so-called degree of homogeneity (I), is given by:

$$I = \frac{C - C_m}{C_m}$$

where C is the maximum local concentration and C_m is the mean concentration of tracer at complete mixing. A more comprehensive way of analyzing mixing, applicable to continuous systems, is a study of the residence time distribution (RTD). Although ALRs are usually operated in a batch-wise manner, at least in the laboratory, advantage is taken of the fact that the liquid circulates on a definite path to characterize the mixing in the reactor. Hence, a single-pass RTD through the whole reactor or through a specific section is usually measured. Based on the observed RTD, several models have been proposed.

These models have the advantage of reducing the information of the RTD to a small number of parameters, which can later be used in design and scale-up. The axial dispersion model, which has the advantage of having a single

parameter, is widely accepted for the representation of tower reactors. This model is based on visualization of the mixing process in the tower reactor as a random, diffusion-like eddy movement superimposed on a plug flow. The axial dispersion coefficient D_z is the only parameter in the formulation:

$$\frac{\partial C}{\partial \tau} = D_z \frac{\partial^2 C}{\partial z^2} + U_L \frac{\partial C}{\partial z}$$

where C is the concentration of a tracer. The boundary conditions depend on the specific type of tower reactor. This model is attractive, since it has a single parameter, the Bodenstein number (Bo), which is used to describe the mixing in the reactor:

$$Bo = \frac{U_L L}{D_z}$$

where L is the characteristic length. When the *Bo* number tends to infinity, the mixing conditions are similar to those of a plug-flow reactor, and the reactor can be considered as well-mixed for low *Bo* numbers. The alternative approach of Buffham and Mason states that the mixing characteristics of a piece of equipment should be expressed as the variance r^2 of the distribution obtained by injection of a pulse of tracer without adopting any mechanistic model. The relationship between *Bo* and r^2 depends on the reactor configuration. The approach of Buffham and Mason facilitates the presentation of mixing characteristics free of any modeling assumptions. The variance r^2 is the second moment of the distribution and carries information on the spread of the distribution around the mean value (first moment). Nevertheless, most of the data on mixing in bioreactors are presented either as t_m or as overall *Bo* numbers, which can be obtained by relatively simple experiments of pulse injection. Single-pass mixing in the ALR is due to mixing in the individual and interrelated sections of the reactor—riser, separator, downcomer, and bottom. Repeated passage mixing is the sum of the mixing in the subsequent passages. The latter is usually reported as the mixing time (t_m), the former as Bo or r^2. Indeed, these parameters are interrelated, and knowledge of Bo or t_m is sufficient for calculating, theoretically, the mixing time based on the deviation of the envelope of the maxima in the response curve to a pulse, which is a measure of the degree of inhomogeneity. Verlaan *et al.* and Lin *et al.* correlated their results as follows:

$$t_m = MBo$$

where M is a constant equal to 0.093 or to 0.089. The coefficient M given by Verlaan *et al.* is in exact agreement with the theoretical relationship derived by Murakami *et al.* for Bo > 50 and a degree of inhomogeneity, I =0.05. Equation shows that the circulation path, which enters in the definition of Bo, has a linear effect on the mixing time. If the mean circulation time and the axial dispersion coefficients are known, it is possible to theoretically estimate the mixing time using equation. Experimental details must, however, be carefully planned to avoid complications. Note that in order to simplify data processing it is important to inject the signal and to measure the response at exactly the same point (often the position of the injection point is not specified despite its effect on the mixing time). In a study of the effect of the injection point on the dynamics of the mixing time, then it was concluded that the gas–liquid separator is the best choice for tracer injection for short mixing times. Fields and Slater reported a marked dependence of the respiratory quotients upon the injection point of methanol during unlimited fed-batch growth of *Methylophilus methylotropus* in a concentric-tube ALR. The lines in Figure 19 show experimental data for Bo (as overall values) reported for different types of ALR (in which the reactor is considered as a single unit). The dimensions of the reactors are given in Table. Because of the definition of the overall Bo, the values are specific to the reactor for which they were obtained and can be used only as indication of trends and orders of magnitude. As explained above, the ALR is, in fact, a combination of

Table: Bodenstein Number as a Function of the Superficial Gas Velocity

Curve number	Authors	Type	A_d/A_r	H/D_r	Liquid	Ref.
1	Weiland	External loop	0.25	85	Water	44
2	Weiland	External loop	0.25	85	2-propanol 1.65%	44
3	Weiland	External loop	0.25	85	CMC 50%	44
4	Lin et al.	External loop, unbaffled	0.11	20	Water	119
5	Lin et al.	External loop, baffled	0.11	20	Water	119
6	Lin et al.	External loop, unbaffled	0.11	40	Water	119
7	Bello et al.	External loop	0.69	12	Water	45
8	Bello et al.	External loop	0.69	12	Water	45
9	Bello et al.	External loop	0.11	20	Water	45
10	Moor Nagar	External loop	1.0	30	Water	122
11	Fields and Slater	Concentric tube	1.56	10.5	Water	114
12	Fields and Slater	Concentric tube	1.56	21	Water	114
13	Fields and Slater	Concentric tube	1.56	10.5	Water, antifoam	114
14	Fields and Slater	Concentric tube	1.56	10.5	1% Ethanol	114
15	Bello et al.	Concentric tube	0.13	39.65	Water	112
16	Bello et al.	Concentric tube	0.56	55.6	Water	112
17	Verlaan et al.	External loop, total *Bo* number	0.25	16.5	50 mM KCl aqueous solution	79
18	Verlaan et al.	*Bo* number in the riser	0.25	16.5	50 mM KCl aqueous solution	79
19	Verlaan et al.	*Bo* number in the downcomer	0.25	16.5	50 mM KCl aqueous solution	79
20	Verlaan et al.	External loop, total *Bo* number	0.25	16.5	50 mM KCl aqueous solution	79

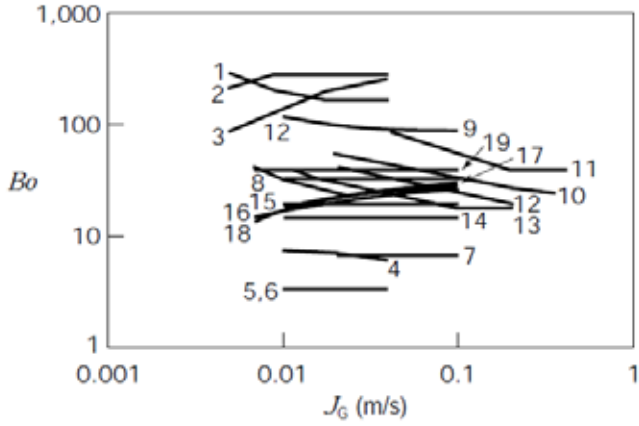

Fig. 37: Global Bodenstein numbers reported for ALRs as a whole unit.

several regions having quite different fluid dynamic characteristics. The overall mixing is the result of the contributions of each of them, and the overall Bo represents this combination for a particular reactor. This value thus has some limitations for extrapolation to other configurations or scales. Because each section has different mixing characteristics (it may have a different cross-section, flow configuration, etc.), from a strictly engineering point of view, the mixing in each of the sections of the ALR should be defined and considered separately. One way of obtaining information on the mixing characteristics of each of the regions of the ALR is the simultaneous measurement of the response in the ALR at several points, so that after one single pulse injection the response of each section in the loop can be obtained. This method of measurement has the advantage that multiple measurements are made for the same tracer injection experiment. This enables us to check the consistency of the liquid velocity results obtained, since independent measurements can obtained in the same run, as can be seen in Figure 38. The results for *Bo* obtained by Verlaan in an external-loop ALR are shown in Figure 39 (the much higher *Bo* in the downcomer was explained by the fact that the data were obtained under conditions of complete gas disengagement so that only liquid flowed). The results indicated that most of the mixing took place in the gas separator, and both riser and downcomer could be considered as plug-flow conduits. The same conclusions were drawn for internal-loop ALRs by Merchuk *et al.* by analysis of mixing times: the shift in results for mixing times obtained with different probes in response to the same impulse perturbation indicated that the riser and the downcomer were

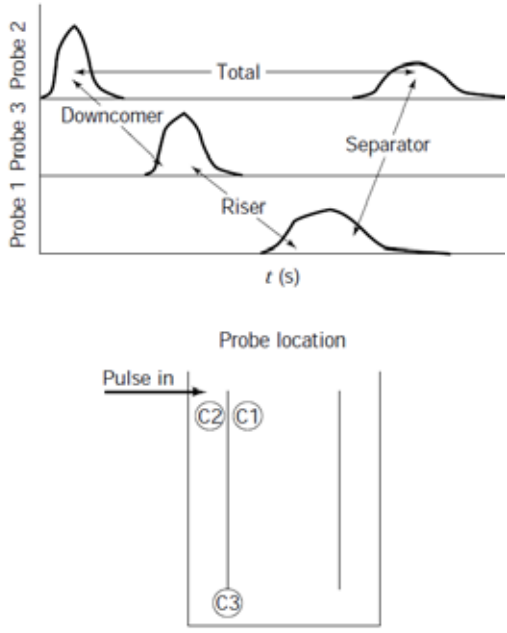

Fig. 38: Response of three electrodes in the riser, separator, and downcomer to a pulse of electrolyte. The information that can be obtained from a single experiment is indicated by the arrows.

introducing a pure delay in the response, that is, that they behaved as plug-flow sections. Indeed, the simplest model of an ALR, from the point of view of fluid dynamics, is a combination of two plug-flow reactors, representing the riser and the downcomer, and a perfectly stirred tank, representing the gas

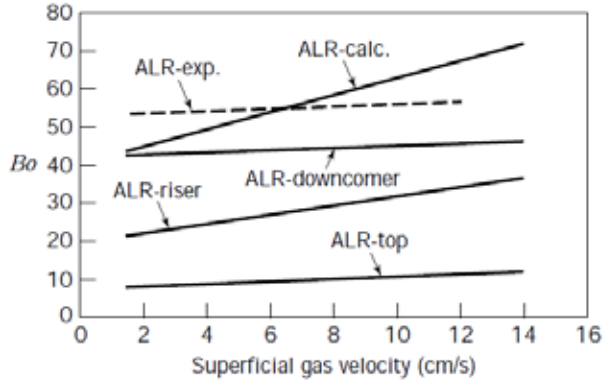

Fig. 39: Bodenstein numbers as a function of the superficial gas velocity in an external-loop ALR. ALR-exp, experimental values for the whole reactor; ALR-calc, calculated values for the whole reactor.

separator (Fig. 40). Merchuk and Yunger showed that this simple model could take into account the mixing in the ALR. The validity of using this simple model as a first approximation is supported by experimental evidence that shows that the mixing time decreases when the separator volume increases. When the volume of the separator is increased substantially without changing the reactor diameter, the gas separator becomes tall and slender and may depart from total mixing behavior. It has been reported that under such conditions the circulation time measured from two successive peaks of a probe is not influenced by changes in the top clearance. This indicates that the gas separator acts as two interconnected well-mixed regions, one of them (the lower one in Figure 41) being the link between riser and downcomer, as shown schematically in Figure 41.

The extent of mixing in the gas separator of internal loop ALRs can probably be compared to that in a bubble column of the same dimensions. In the case of external loop ALRs, the extent of mixing depends on the geometric design. In special designs, like the channel-loop reactor, a different approach must be taken. However, in general, a rule of thumb may be recommended: consider that all the mixing takes place in the gas separator, and calculate the degree of mixing in it using published data for bubble columns. Correlations available for

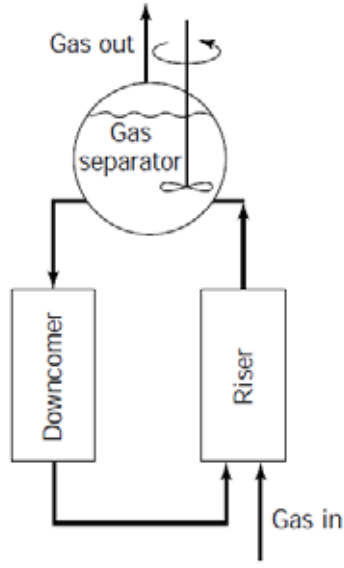

Fig. 40: Simple model of an ALR representing the riser and the downcomer as plug-flow reactors and the gas separator as a perfectly mixed region.

bubble columns can thus be used. Godboole and Shah recommend the use of the correlation proposed by Deckwer *et al.*

$$D_Z = 0.678 \cdot D^{1.4} \cdot J_G^{0.3}$$

where D_Z is the dispersion coefficient and D is the column diameter, or the relationship proposed by joshi:

$$D_Z = 0.33(U_c + J_L)D$$

where JL is the superficial liquid velocity and Uc is the cell circulation velocity given by

$$U_C = 1.31\left[gD\left(J_G - \frac{\varphi_G}{1 - \varphi_G} J_L - \varphi_G U_{b\infty}\right)\right]$$

where $U_{b\infty}$ is the terminal bubble velocity. The liquid superficial velocity (J_L) can be easily calculated for external-loop reactors, and for internal loop reactors, J_L may be taken as half the liquid velocity in the riser. The viscosity may also play a role in the rate of mixing. An increase in liquid viscosity will increase the energy dissipation in the loop and result in an increase in mixing time and *Bo*. In non-Newtonian fluids, however, the behavior may be different, as shown in Figure 42. It has been reported that in the case of the addition of polymers that confer pseudoplastic behavior to the liquid, low concentrations produce a decrease of the mixing time. This can be explained in terms of the drag reduction due to the presence of polymers in the boundary layer near the walls. Fields *et al.* found that the mixing time increased for concentrations of the natural polymer, xanthan gum, above the critical concentration. (The critical concentration is a theoretically

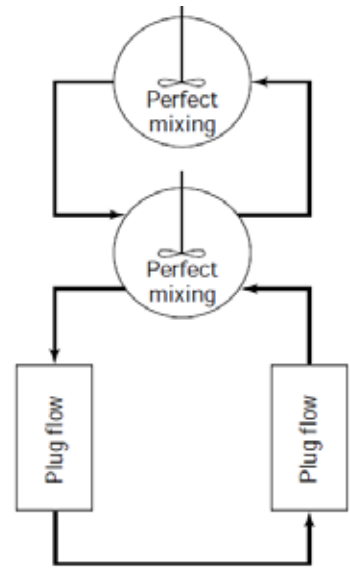

Fig. 41: Schematic representation of the effect of a tall slender gas separation region in a concentric-tube ALR.

calculated value at which appreciable overlapping of polymer molecules occurs and which marks the onset of a rapid increase of the apparent viscosity.

Mixing in the Gas Phase

For all practical purposes, the gas in the riser of an ALR exhibits plug flow behavior. Only for extremely high J_G or hindered liquid circulation will the axial dispersion of the bubbles have some effect on the gas RTD. In the downcomer, the gas flow is almost plug-flow when the bubble recirculation is fully developed. But at the stage at which a stationary phase of suspended bubbles appears at the top of the downcomer, appreciable dispersion will occur. This zone has a large degree of mixing due to coalescence and consequent rise of larger bubbles amid smaller ones, with repeated events of breakup and coalescence. However, this type of operation has no relevance to practical applications. It is an operation mode to be avoided at all costs. Indeed, no data on mixing under these conditions have been reported. The main question related to the mixing of the gas phase is, in fact, related to gas recirculation. When a particular gas flow has developed in the downcomer, part of the gas is being recirculated. A pulse of gas tracer at the inlet would produce, as a response, a series of pulses, separated one from the other by the gas circulation time. In practice, not many of these pulses would be detected, due to dilution and disengagement of the tracer in each pass through the separator. The only reported study on gas phase mixing in an ALR is that of Frehlich *et al.* The distribution of the gas residence times in two reactors, one of 0.08 m^3 and the other of 4 m^3, was measured using pseudostochastic tracer

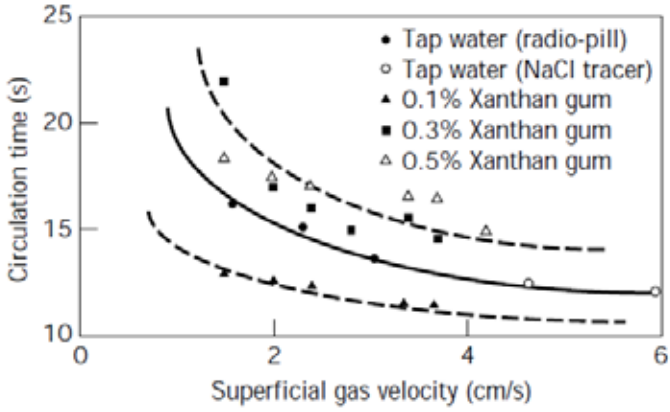

Fig. 42: Variation of mean circulation times with J_G for several solutions. Adapted with permission from Fields and Slater

signals and a mass spectrometer. The values of *Bo* were calculated from the first and second peaks, indicating the main gas stream and the recirculation. Figure 43 shows the *Bo* obtained for a laboratory-scale ALR. The values obtained in a pilot plant were of the same order.

Energy Dissipation and Shear Rate in Airlift Reactors

ALRs are being increasingly used in processes involving shear-sensitive cells (mammalian, insect, and plant cell cultures). This situation has created the need for considering shear stress as one of the parameters relevant in the design of such reactors. Although the a priori evaluation of shear rates is a matter that has been studied for many years in stirred tanks, information on this subject is scanty for pneumatically stirred reactors. The first approach made in this direction in pneumatically agitated vessels was that of Nishikawa *et al.*, who were interested in the problem of heat transfer to a non-Newtonian liquid in a bubble column. This study was extended to mass transfer by Nakanoh and Yoshida, who proposed the expression:

$$\gamma = 5000\ J_G$$

This expression has been widely accepted despite the criticism sometimes leveled at it. Some modifications have thus been proposed, which, like the original approach, were based on data for bubble column performance and therefore have limited application for ALRs. Recently, a method facilitating the

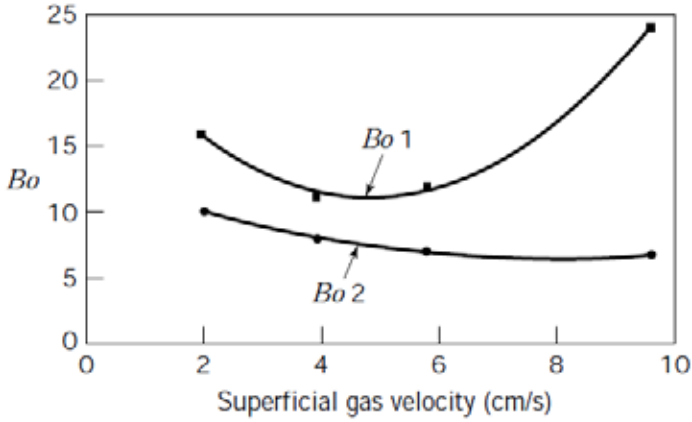

Fig. 43: Bodenstein numbers of the first and second peaks of the gas residence time distribution in an 80-L internal-loop ALR, as a function of the gas superficial velocity.

prediction of the distribution of the energy dissipated in an ALR, based on a simple thermodynamic approach, has been developed. Energy dissipation was considered to occur in the ALR by two main mechanisms, wall friction and bubble-associated dissipation (ideal gas behavior was assumed). The work done by the gas on the liquid (and *vice versa*) was expressed assuming isothermal expansion of the bubbles. The energy dissipation inside the gas phase was considered negligible. The general energy balance was written as:

$$\Delta(PQ) + \Delta E_p + E_D = W_S$$

In this equation, the first term represents the flow work lost by the system under consideration, E_D is the energy dissipated per unit of time, and W_S is the shaft work done by the surroundings on the system under consideration. The schematic representation of the concentric-tube ALR in Figure 44 indicates the different points in the reactor considered in the mathematical expressions. The expressions found for the energy dissipated in each zone were the following:

Riser

$$(E_d)_R = Q_L(P_4 - P_5) - Q_L\rho_L gh - Q_r P_4 \ln\left(\frac{P_5}{P_4}\right)$$

Gas separator

$$(E_d)_S = Q_L(P_5 - P_2) - Q_{in}P_4 \ln\left(\frac{P_1}{P_5}\right) - Q_d P_4 \ln\left(\frac{P_2}{P_5}\right)$$

Downcomer

$$(E_d)_d = Q_L(P_2 - P_3) - Q_L\rho_L gh - Q_d P_4 \ln\left(\frac{P_3}{P_2}\right)$$

Bottom

$$(E_d)_b = Q_L(P_3 - P_4) - Q_d P_4 \ln\left(\frac{P_4}{P_3}\right)$$

Results of this model of an ALR can also be used to estimate the global shear rate in each region of the reactor, according to the global approach presented Merchuk and Ben-Zvi (Yona). The shear stress in the liquid of each region of the reactor can be defined as the energy dissipated divided by the mean path of circulation in the region and by the sum of the areas of all the bubbles. For the region *i* in the ALR.

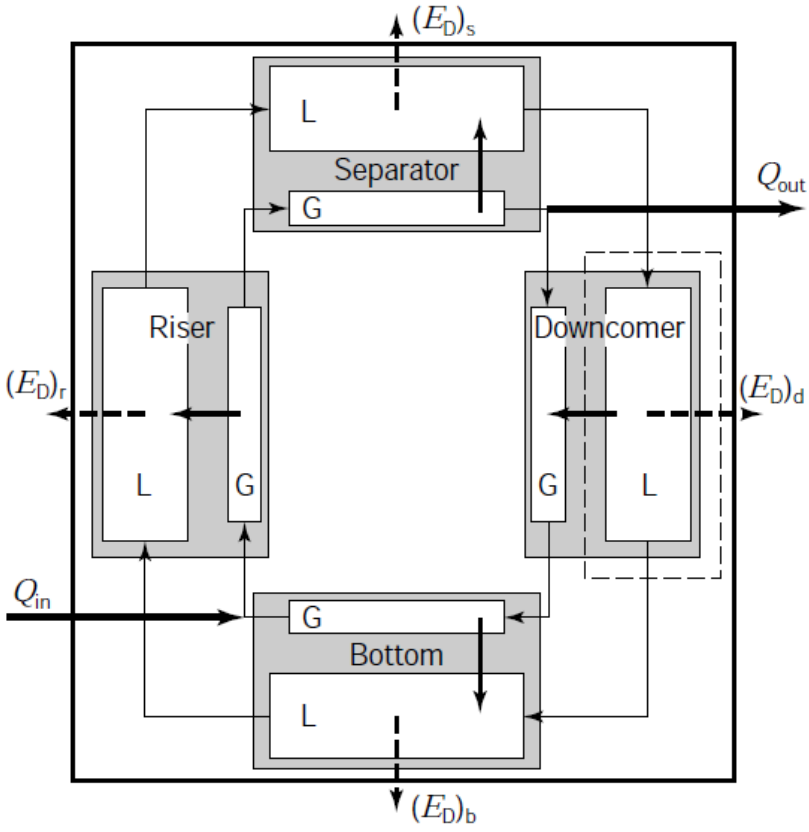

Fig. 44: Schematic description of the variables in the thermodynamic model for energy dissipation distribution in an ALR.

$$\tau_I = \frac{(E_d)_{bulk,I} t_I}{a_I h_I^2 A_I}$$

where t_i is the residence time of the liquid, h_i is the effective length, and a_i is the specific interfacial area, in the region i.

A global shear rate γ_i can be calculated for each region i as

$$\gamma_I = \frac{\tau_I}{\mu}$$

where μ is the effective viscosity of the fluid. For liquids exhibiting different types of rheological behavior, the corresponding constitutive equation must be used. Such an approach has been used for the interpretation of shear effects on mammalian cells and algal growth.

MASS TRANSFER

The volumetric mass transfer coefficient (k_La) is the rate of gas transfer across the gas-liquid interface per unit of driving force (the driving force is the gas concentration gradient between the liquid and the gas). The mass transfer coefficient k_La can be seen as the product of two terms: the mass transfer coefficient k_L and the specific interfacial area a. Both terms depend on a series of variables that can be grouped into three categories: (1) static properties of the liquid, such as density, diffusivity, and surface tension; (2) dynamic properties of the liquid (related to liquid flow), such as rheological parameters; and (3) liquid dynamics. In general, the variables in group 1 do not change very drastically. The variables in groups 2 and 3, however, may span wide ranges.

Mass Transfer Rate Measurements

Methods for the determination of k_La in a reactor can be grossly classified as steady-state and non-steady-state methods. In the steady-state methods, the rates of oxygen uptake in steady-state operation are evaluated, either by measurement of inlet and outlet rates of oxygen or by direct analysis of a compound that reacts with the oxygen, as in the case of the sulfite method. One of the problems associated with these procedures is that the changes in oxygen concentration in the gas streams are usually small, and the errors of measurement thus have a substantial influence. When a chemical is added to the system, there is the question of whether the addition has provoked changes in the physicochemical properties, which thus become different from the properties of the original system. Transient methods may be applied to follow the response of the dissolved oxygen concentration in the system after a step-change of oxygen concentration in the inlet gas stream. These methods have the advantage that addition of an alien material is not required and that a single concentration is measured. The correct use of this method has been analyzed in depth by Linek *et al.* One important point to take into account is the dynamics of the oxygen electrode. The lag in the response of the oxygen electrode makes it necessary to discern between the electrode response and the real oxygen concentration, especially when close to a sharp change in concentration. A correct analysis should also include the model of the dynamic behavior of the electrode. In order to simplify these procedures, approximations based on truncation of parts of the response curve have been proposed. These methods

are based on truncating the first part of the electrode response obtained in a transient experiment. Once the error included in the value of k_La is set, the extent of truncation is fixed, allowing simplification of the analysis of the remainder of the curve. It should be kept in mind that this simplification implies the loss of part of the information, and due care should be given to statistical analysis of the results. Variations of the method have been proposed to minimize disturbances in the system by introduction of step variations of agitation or pressure. In this way, the method can be applied to bioreactors during real operation of the system. One problem that may appear in the measurement of mass transfer rates, especially when viscous liquids are used, is related to the presence of very small bubbles that are depleted of oxygen very rapidly but do not disengage in the gas separator, thus constituting an inert volume of gas in the reactor. Kawase and Moo-Young analyzed the use of transient absorption of CO_2 for the determination of k_La and concluded that the error due to small bubble retention was much smaller than that in the case of O_2. Whatever the

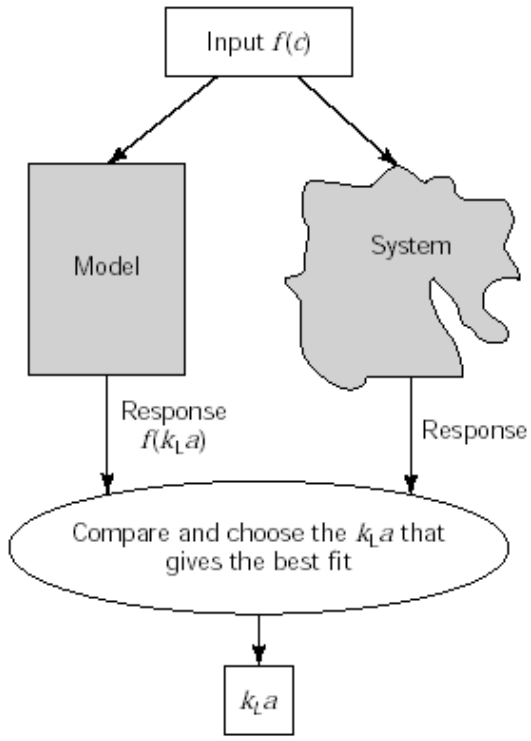

Fig. 45: Steps in the determination of the mass transfer coefficient (k_La).

method used for the determination of k_La, the process of data elaboration is basically the same as is shown schematically in Figure 45. The measured variable (usually oxygen concentration) is compared to the value predicted by a mathematical model of the process. The model includes k_La as a parameter, and the value of k_La that gives the best fit is chosen. It is thus obvious that the choice of the model is very important, and poor assumptions on flow characteristics of gas or liquid phases may lead to errors and deviations from the true values. All the models are a simplified (amenable to mathematical treatment) description of the system. It should be kept in mind, therefore, that k_La is not a property of the system, but a parameter of the model adopted. If total mixing is assumed in the model adopted, the mass transfer coefficient obtained will consequently be limited. The assumption of complete mixing is such a common practice that many reports do not even specify explicitly that this has been done, and in many texts the mass transfer coefficient k_La is defined by the equation:

$$\text{OTR} = k_1a(C^* - C)$$

It is often forgotten to state that this equation is valid only for perfectly mixed systems. Strictly, the different sections of ALRs (riser, downcomer, and gas separator) have different flow characteristics, and the mass transfer coefficient may be expected to differ from one region to another. Some researchers have assumed that the contribution of the downcomer to the overall mass transfer is negligible and have reported values of k_La that are, in fact, the entire mass transfer divided by the volume of the riser. The fact that the values of the mass transfer coefficient are calculated and reported in different ways introduces some ambiguity into the published data; special care should therefore be taken when comparing data or using published mass transfer coefficients for design purposes. The assumption of perfect mixing in the liquid phase may be questionable in the case of tall reactors. One very simple method to verify this assumption is the simultaneous measurement of the response of the concentration to a step-change in the inlet. In a perfectly mixed system, the location of the probe should be irrelevant. Figure 46 shows the response of three probes, one located at the end of the riser, one at the inlet of the downcomer, and one at the bottom of a split-cylinder ALR. The difference between the figures stems from a different gas separator section, which changes the fluid dynamics in the system. In one case the system behaved as perfectly mixed, because of the large volume of the gas separator and the faster liquid circulation. In the other

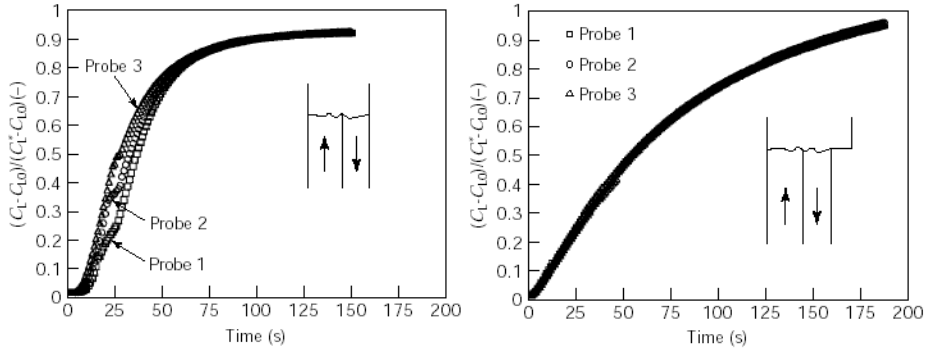

Fig. 46: Response of three probes, one located at the end of the riser, one at the inlet of the downcomer, and one at the bottom of a split-cylinder ALR.

(closed system in the figure), the responses of the three electrodes were clearly different, calling for a different analysis. The validity of the criterion, originally proposed by Andre *et al.*, that compares the circulation time in the reactor (t_c) with the characteristic time for mass transfer, which is the inverse of the mass transfer coefficient, was thus confirmed:

$$t_c \cdot k_L a < 0.5$$

If this condition is not fulfilled, the bioreactor cannot be considered as a perfectly mixed volume, and more sophisticated ways of analysis are required. In this case, the mathematical model, and, consequently, the analysis of the experimental data become much more complicated. Nevertheless, this approach has been used and the mass transfer experiments render values of $k_L a$ for each of the regions of the ALR. Figure 47 shows the results reported by Hwang and Lu in an internal loop ALR. The graph shows that the mass transfer takes place at the highest rate in the riser. Values for the downcomer are 50% lower, and those for the gas separator are intermediate between the riser and the downcomer. The overall mass transfer rate is the result of the balance between the volumes and rates in the three sections.

Bubble Size and Interfacial Area

As said earlier, the interfacial area per unit volume is an important component of the volumetric mass transfer coefficient. In fact, it is the part of $k_L a$ that is most susceptible to changes in operation variables and fluid properties. The mass transfer coefficient k_L varies only within a limited range,

but the interfacial area is the main component responsible for the changes in mass transfer rate due to variations in turbulence, initial bubble size, and liquid properties. The methods for measurement of the interfacial area are based either on rapid chemical reactions or on direct measurement of bubble size. If a mean bubble size can be defined, then the interfacial area can be evaluated with the aid of the holdup measurement, since, in a population of homogeneous bubble size, it can be applied:

$$a = \frac{6\varphi}{d_s}$$

where the Sauter mean diameter (d_S) is given by

$$d_S = \frac{\sum n_i d_i^3}{\sum n_i d_i^2}$$

and n_i is the number of bubbles of diameter d_i

There are very few published data on bubble size applicable to ALRs. For the riser, the correlation presented by Miyahara *et al.* for the volumetric mean diameter of the bubbles in the riser of a concentric-tube ALR can be used:

$$\bar{d}\left(\frac{g\rho_L}{\sigma d_0}\right)^{1/3} = f(N_W)$$

where d_0 is the diameter of the sparger orifice and σ the surface tension,

$$N_W = \frac{We}{Fr^{0.5}}$$

and the function $f(N_W)$ is different for each range of N_W:

$$\begin{aligned} f(N_W) &= 2.9 && N_W < 1 \\ f(N_W) &= 2.9N_W^{-0.188} && 1 < N_W < 2 \\ f(N_W) &= 2.9N_W^{-0.5} && 2 < N_W < 4 \\ f(N_W) &= 3.6 && 4 < N_W \end{aligned}$$

Data on bubble size in the downcomer of an ALR were published by Popovic and Robinson. No data on interfacial area measured by chemical methods have been published.

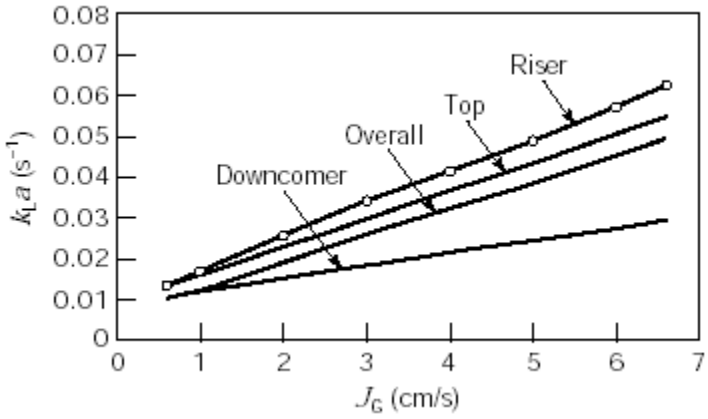

Fig. 47: Influence of the superficial gas velocity on overall k_La and on the k_La in each of the regions of an ALR.

Data Correlations for Mass Transfer Rate

There are two ways of correlating experimental data from ALRs. *First*, the hydrodynamic point of view suggests that the movement of the fluid in the reactor determines its overall behavior; the gas superficial velocity is therefore the more appropriate independent variable. *Second*, the thermodynamic point of view is based on a consideration of energy balance, a more global approach to the system. This will lead to correlation of the phenomena in the system as a function of the energy input. Indeed, it is easier to compare mass transfer coefficients in ALRs with those in conventional reactors when the data are presented as a function of the total power input (both mechanical and pneumatic) per unit volume of the medium (Fig. 48). Figure 49 shows data for mass transfer

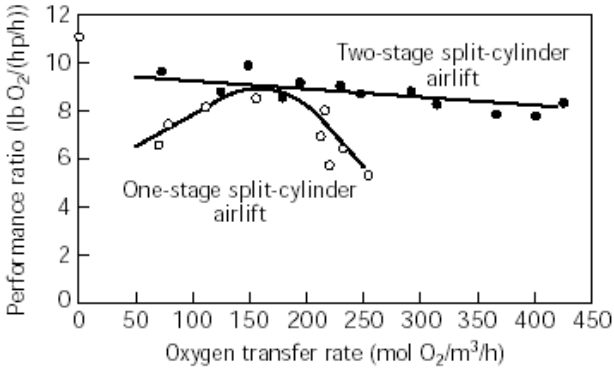

Fig. 48: Performance of ALRs. Adapted from Orazem and Erickson.

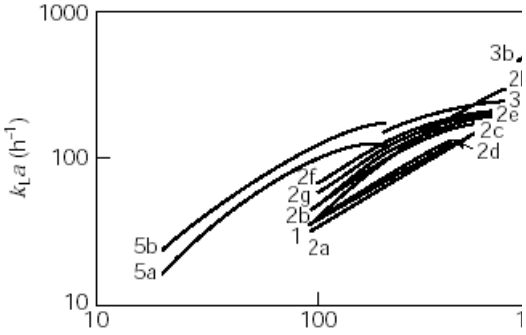

Fig. 49: Mass transfer coefficients as a function of specific power input.
With permission from Siegel *et al.*

coefficients as a function of specific power input. References and geometric characteristics can be seen in Table.

Selected of correlations proposed for the prediction of mass transfer coefficients are shown in Tables for internal- and external-loop ALRs, respectively, and the predictions are compared in Figures 50 and 51. Among the internal-loop reactors, two correlations presented for reactors with a rectangular cross-section are shown.

For external-loop ALRs, the correlation by Popovic and Robinson is recommended. In the case of internal-loop ALRs, most of the correlations predict similar values. The correlation of Merchuk *et al.* can be recommended on the basis that more geometric parameters have been taken into account, and this gives

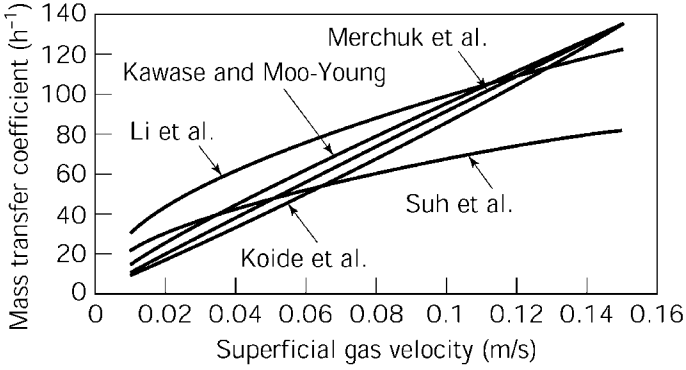

Fig. 50: Mass transfer coefficient $k_L a$ as a function of gas superficial velocity for internal-loop ALRs. Correlations are presented in Table 6.

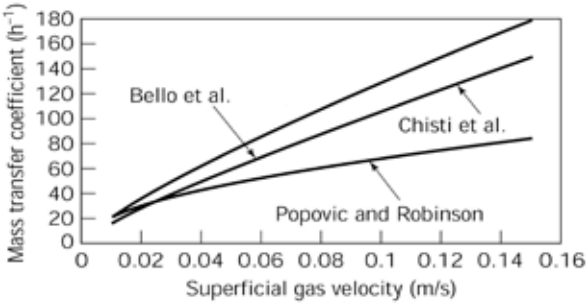

Fig. 51: Mass transfer coefficient k_La as a function of gas superficial velocity for internal-loop ALRs. Correlations are presented in Table 6.

greater generality. Nevertheless, the general considerations already expressed when analyzing other correlations in this chapter are valid here as well.

Heat Transfer

Because of the relatively low reaction rates of processes involving microorganisms and cells, it may—in a very general way—be said that heat-effect problems related to local variations of temperature are not common in bioreactors. Even in the case in which polymeric products are released into the medium and very high viscosity is reached, heat transfer is not the controlling step, because such viscous media will hinder the mass transfer and heat generation will consequently be limited. In such cases the main point of focus is thus, mass, rather than heat, transfer. Reactions catalyzed by immobilized enzymes, however, may require different considerations, because of higher reaction rates. There is a far greater body of published data on heat transfer in bubble columns than in ALRs, and some of the basic observations are valid

Table: Mass Transfer in ALRs

Curve no.	Reactor type	Height (cm)	*D* Riser (cm) draught tube	*D* Downcomer (cm) reactor tube	A_d/A	Ref.
1	Concentric tube	143	21	30	1.04	150
2a	External loop	180	15.2	76 + 10.2	0.69	45
2b	External loop	180	15.2	7.6	0.25	45
2c	External loop	180	15.2	5.1	0.11	45
2d	Concentric tube	180	8.9	15.2	0.56	45
2e	Concentric tube	180	7.6	15.2	0.35	45
2f	Concentric tube	180	5.1	15.2	0.13	45
2g	Bubble column	180	0	15.2	0.00	45
3a	Rec. split vessel; all experiments, except high recirculation and two spargers	435–450	9 × 250	7 × 25	0.78	32
3b	Rec. split vessel; high recirculation and two spargers	435–450	9 × 25	7 × 25	0.78	32
4	External loop	850	10	5	0.25	78
5a	Concentric tube	170	11.7	20	1.96	44
5b	Concentric tube	170	17.6	20	0.26	44

Table: Mass Transfer in Internal-Loop ALRs

No.	Formula	Ref.
1	$Sh = 3 \cdot 10^4 Fr^{0.97} M^{-5.4} Ga^{0.045} \left(1 + \frac{A_d}{A_r}\right)^{-1}$	1
2	$Sh = 2.66 Sc^{0.5} Bo^{0.715} Ga^{0.25} \left(\frac{D_r}{D}\right)^{-0.429} \varphi^{1.34}$	151
3	$k_L a = 0.0343 J_{Gr}^{0.524} \mu_{ap}^{-0.255}$ $\gamma = 5000 J_{Gr}$ for $J_{Gr} \geq 0.04\ \mathrm{ms}^{-1}$ $\gamma = 5000 J_{Gr}^{0.5}$ for $J_{Gr} \leq 0.04\ \mathrm{ms}^{-1}$	48
4	$Sh = 0.68 n^{-0.72} Fr^{0.38n+0.52} Sc^{0.38-0.14n}$	59

for both types of reactor. The heat transfer rate in bubble columns is much larger than that expected from single-phase flow. This is a result of the bubble-driven turbulence and liquid recirculation, which are characteristic of the flow in pneumatically agitated reactors. Several correlations have been proposed for the prediction of the heat transfer coefficient in these reactors. Recently, Kawase and Moo-Young (62) presented an expression that satisfactorily fits most of the published data. The model is based on Levich's three-zone concept and Kolmogoroff's isotropic turbulence theory and has no empirical adjustable parameters. The model can take into consideration non-Newtonian behavior of the liquid and predicts the enhancement of the heat transfer due to the shear-thinning effect of the fluid. The dimensionless expression may be written as:

$$Nu = 0.075(10.3n^{-0.63})^{\beta} n^{1/3} (Pr^*) \frac{1}{3} Fr^{-\beta} (Re^*)^{\beta+3(n+1)}$$

with

$$\beta = \frac{4 - n}{6(n + 1)}; \quad Pr^* = \frac{\kappa D^{1-n}}{\left(\frac{\kappa}{C_p}\right) J_G^{1-n}}; \quad Re^* = \frac{D^n J_G^{2-n}}{\left(\frac{k}{\rho}\right)}$$

where the symbols defined in "Nomenclature" have been used.

Table: Mass Transfer in External-Loop ALRs

No.	Formula	Ref.
1	$K_L a = k_1 J_{Gr}^{0.8}\left(1 + \frac{A_d}{A_r}\right)^{-2}$	45
	Water $K_L = 0.75\mu^{-0.8}\sigma^{-0.2}$	
	NaCl $K_L = 0.79\mu^{-0.8}\sigma^{-0.2}$	
2	$k_L a = 0.5 \cdot 10^{-2} J_{Gr}^{0.52}\left(1 + \frac{A_d}{A_r}\right)^{-0.85} D_l^{0.5}\rho_l^{1.03}\sigma_l^{-0.25}\mu_{ap}^{-0.89}$	88
	or in simplified form:	
	$k_L a = 1.911 \cdot 10^{-4} J_{Gr}^{0.52}\left(1 + \frac{A_d}{A_r}\right)^{-0.85} \mu_{ap}^{-0.85}$	
	$k_L a = 0.24 J_{Gr}^{0.837}\left(1 + \frac{A_d}{A_r}\right)^{-1}$	
3	in case of suspended solids:	152
	$k_L a = (0.349 - 0.102 C_s) J_{Gr}^{0.837}\left(1 + \frac{A_d}{A_r}\right)^{-1}$	
4	$k_L a = 913\left(\frac{P}{VD}\right)^{1.04} (U_L)^{-0.15}$	32
5	$k_L a = (0.349 - 0.102 C_s\left(1 + \frac{A_d}{A_r}\right)^{-1} J_{Gr}^{0.837}$	152

For Newtonian liquids, this equation reduces to:

$$Nu = 0.134^{1/3}(Pr)^{1/3}Fr^{-1/4}(Re)^{3/4}$$

Kawase and Moo-Young compared their model with data and correlations published by various investigators and found satisfactory agreement for both Newtonian and non-Newtonian liquids.

For ALRs, the flow in the reactor may be similar to that in bubble columns if the internal recirculation is high, or it may be even closer to net two-phase flow in pipes, in which case the equations for heat transfer in pipes can be used. Blakebrough *et al.* studied heat transfer rates in an external-loop airlift fermentor used for culturing *Aspergillus niger.* They concluded that the enhancement of the heat transfer rate could be explained by disturbances in the liquid layer near the surface caused by the presence of the microorganisms.

Three-Phase Airlift Reactors

The special qualities of the ALR stem, as stated before, from its fluid dynamic characteristics. One such characteristic is the directionality of the liquid flow. Independently of superimposed fluctuations, a clear net flow is present in the reactor, with exception of the gas separator in internal-loop designs. Therefore, it is to be expected that the fluidization capacity of the ALR will be markedly superior to that of a bubble column. Several studies have been conducted on the suspension of solids in ALRs, particularly on the use of this type of device for catalytic processes in the chemical industry, where the solid support is usually heavy. In this regard, a very important point is the minimum gas superficial velocity that leads to complete solid fluidization. Hysteresis has been observed in some cases; once total fluidization has been attained, the superficial velocity can be reduced to values lower than that required to reach this state. This is due to the high pressure drop related to passage of liquid through a bed of solids, before fluidization, as compared to the drag forces required to maintain the solid in suspension after all the solids are suspended.

Contradictory data on the effect of the suspended solids on the reactor performance have been reported. Fan *et al.* claimed that the overall gas holdup increased due to the presence of the solids, whereas Koide *et al.* showed the opposite effect on the gas holdup and reported a small decrease in $k_L a$ as well. It is possible that these discrepancies are due to the use of different solids. One of the properties of solids that is often overlooked is wettability. Small bubbles may adhere on wet table solids, leading to a change in the apparent density of the particle and thus changing their solid circulation velocity.

In the case of suspended solids that take an active part in the process, the mass transfer rate from the liquid to the solid may become the limiting step. The dependence of particle size on the mass transfer to the suspended solids has been studied by several authors. All the comments made above relate to heavy solids. This situation is not very frequent in biological processes, with the exception of biolixiviation or the special case of microbial desulphuration of coal. In most of the biological processes that may take place in an ALR, the solids are either cells, clumps of cells, or supports that are not much denser than the medium. Therefore, neither fluidization nor the distribution of solids in the reactor constitutes a problem. Assa and Bar found very small variations in the axial distribution of animal and plant cells suspended in an internal-loop ALR.

This is due to the small free-falling velocity of the solids, which is the reason for the difference in loading between the riser and the downcomer when heavy particles are used. Because of the small difference between solid and medium density, the movement of the particles usually present in biological processes is not as dependent on gravity forces as on liquid and bubble movement. In this case, the transport of liquid in the wake of the bubbles may be considered to be the prevailing transport mechanism. Snape and Thomas proposed a Monte Carlo algorithm for modeling particle movement by this mechanism in bubbly flow to predict distribution of circulation times in the reactor. Koide *et al.* conducted a broad study of gas holdup and mass transfer rates in an internal-loop ALR containing Ca-alginate beads, which are often used for cell immobilization.

It is found that solid loading had a negative effect on both parameters, but the particle diameter had no influence in the range studied (1.8 mm < d_p < 3.98 mm). Chang *et al.* studied the influence of suspended pellets (cylindrical pellets of immobilized penicillin acylase) on the mixing time in an internal-loop ALR. They found mixing time increased when the solid volumetric concentration was raised up to 15%. For higher concentrations the trend inverted, and the mixing time decreased. No such effects were observed with heavier solids. Increases in gas superficial velocity and in top clearance both lead to decreases in mixing time in all cases.

FIXED-BED BIOREACTORS

Introduction

Catalytic fixed-bed reactors are the most important type of reactor for the synthesis of large-scale basic chemicals and intermediates. In these reactors, the reaction takes place in the form of a heterogeneously catalyzed gas reaction on the surface of catalysts that are arranged as a so-called fixed bed in the reactor. In addition to the synthesis of valuable chemicals, fixed-bed reactors have been increasingly used in recent years to treat harmful and toxic substances. For example, the reaction chambers used to remove nitrogen oxides from power station flue gases constitute the largest type of fixed-bed reactors as regards reactor volume and throughput, while automobile exhaust purification represents by far the most widely employed application of fixed-bed reactors. With regard to application and construction, it is convenient to differentiate

between fixed bed reactors for adiabatic operation and those for non-adiabatic operation. Since temperature control is one of the most important methods of influencing a chemical reaction, adiabatic reactors are used only where the heat of reaction is small, or where there is only one major reaction pathway; in these cases no adverse effects on selectivity or Yield due to the adiabatic temperature development are expected. The characteristic feature of adiabatic reaction control is that the catalyst is present in the form of a uniform fixed bed that is surrounded by an outer insulating jacket (Fig. 52a). Since the incoming reaction gases in most cases must be heated to the ignition temperature of the catalytic reaction, adiabatic reaction control is often coupled with heat exchange between the incoming and exiting reaction gas resulting in so-called autothermal reaction control. This type of reaction control offers certain specific features and development perspectives.

Reactions with a large heat of reaction as well as reactions that are extremely temperature-sensitive are carried out in reactors in which indirect heat exchange occurs via a circulating heat transfer medium integrated in the fixed bed. Since in most cases the task of the heat-transfer cycle is to maintain the temperature in the fixed bed within a specific range, this concept is frequently described as an "isothermal fixed-bed reactor". However, isothermal reaction control does not provide optimum selectivity or yield in all cases, and for this reason the concept of heat exchangers integrated in the fixed bed is also being increasingly

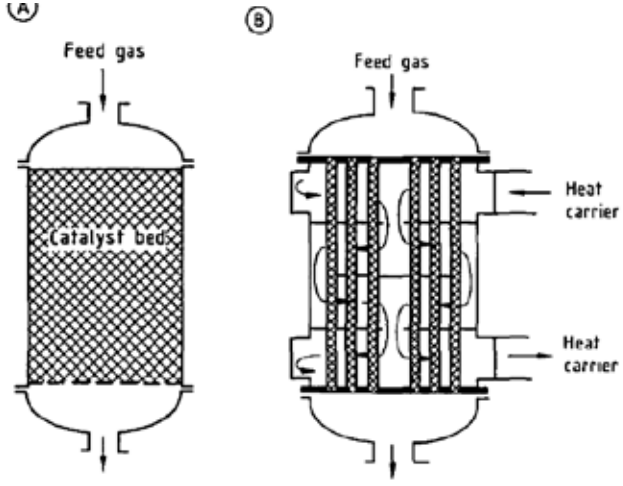

Fig. 52: Basic types of catalytic fixed-bed reactors (A) Adiabatic fixed-bed reactor; (B) Multitubular fixed-bed reactor

used to achieve non isothermal temperature profiles. The most common arrangement is the multitubular fixed-bed reactor, in which the catalyst is arranged in the tubes, and the heat carrier circulates externally around the tubes (Fig. 52b). Fixed-bed reactors for industrial syntheses are generally operated in a stationary mode (*i.e.*, under constant operating conditions) over prolonged production runs, and design therefore concentrates on achieving an optimum stationary operation. However, the non-stationary dynamic operating mode is also of great importance for industrial operation control. In particular, fixed-bed reactors with a strongly exothermic reaction exhibit and, at times, surprising operational behavior which is also discussed. Within a production plant the reactor may justifiably be regarded as the central item of apparatus. However, compared to the remaining parts of the plant for preparing the feed and for separating and working-up the products, often it is by no means the largest and most cost-intensive component. In many cases the achievable conversion in the reactor is limited for thermodynamic (equilibrium) and kinetic reasons (selectivity). It is then usual to separate the material discharged from the reactor into products and unreacted feed components (see Fig. 53), which are recycled to the feedstock. This recycling procedure involves costs

1. For product separation
2. For recycle compression
3. For repeated heating and cooling of the circulating material to the reaction temperature and the temperature of the separating device

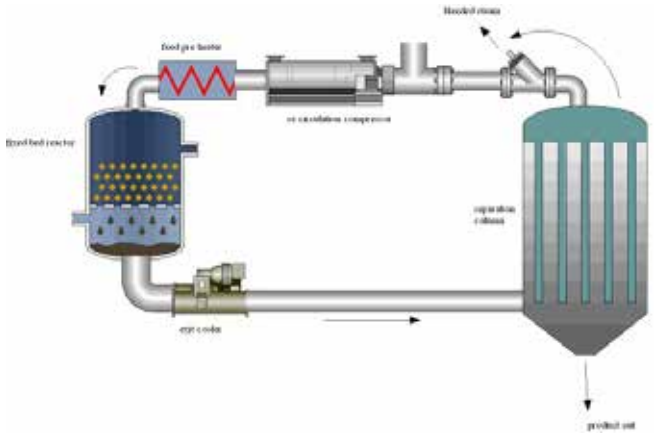

Fig. 53: Reaction cycle for synthesis reactions with incomplete conversion (a) Fixed-bed reactor (b) Feed preheater (c) Exit cooler (d) Recirculation compressor (e) Separation column.

4. Due to loss of product resulting from the need to remove part of the circulating material to limit the amount of inert substances or byproducts in the recycle stream (bleed stream).

To minimize these costs it is therefore necessary to maximize the conversion in the reactor and avoid as far as possible inert accompanying substances in the reaction mixture. With irreversible reactions (*e.g.*, partial oxidations) the trend is therefore towards a highly concentrated, approximately stoichiometric feed composition, which may occasionally be in the explosive range.

Catalyst Forms for Fixed-Bed Reactors

The heart of a fixed-bed reactor and the site of the chemical reaction is the catalyst. The processes taking place on the catalyst may formally be subdivided into the following separate steps:

1. Diffusion of the reactants from the gas space through the outer gas - particle boundary layer, macropores, and micropores
2. Chemisorption on active centers
3. Surface reactions
4. Desorption of the products
5. Back-diffusion of the products into the gas space.

Since most reactions take place with a considerable heat of reaction, a corresponding heat transport is superimposed on the mass transport. The control of the microkinetics, consisting of micropore diffusion, chemisorption, surface reaction, and desorption, is the task of the catalyst developer and is not discussed further here. If the catalyst is specified together with its micro kinetic properties, then reaction conditions (feedstock concentrations, pressure, temperature profile, and residence time) can be found that lead to optimum yields. The reaction engineer must determine these conditions and ensure that they are maintained in an industrial reactor. In the case of selectivity-sensitive multistep reactions, any deviation from the optimum values inevitably leads to a decrease in yield. This applies to deviations from the uniform residence time distribution due to flow dispersion and flow bypass phenomena in the fixed bed, as well as to deviations from uniform reaction conditions in the catalyst as a result of mass-transport resistance in the particles and the outer boundary layer. The influence of mass-transport resistance in the particles can

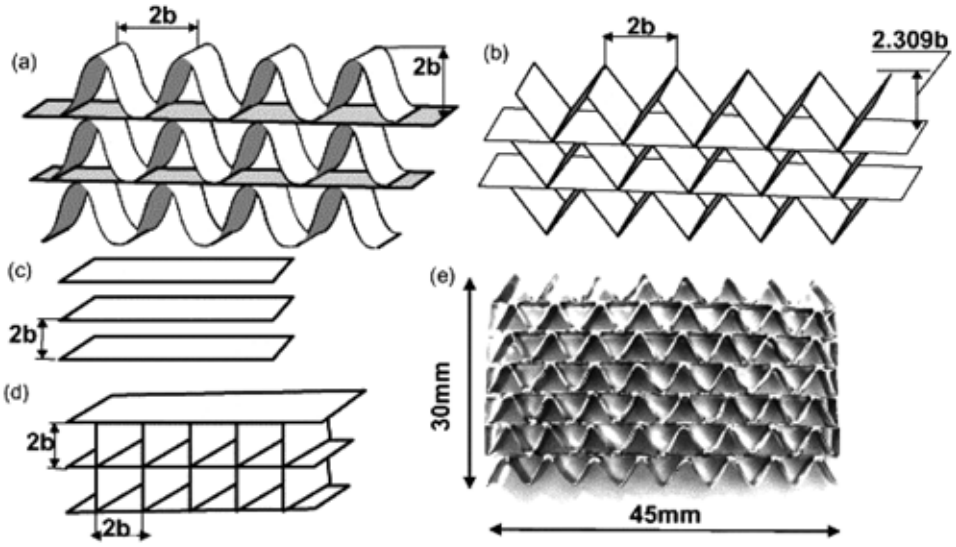

Fig. 54: Showing Different type of Monolith Catalysts (a) (b) and (e) the corrugated monolith, (c) the parallel-monolith and (d) the square-monolith.

only be excluded if the critical reaction rate is substantially lower than the mass transport velocity. This leads on the one hand to the need for good external mass transfer (*i.e.* to reasonable flow conditions in the packed bed), as well as to short diffusion paths in catalyst particles and sufficiently large pores. On the other hand (in the case of exothermic reactions) the local reaction rate must be controlled and limited by the packed-bed temperature. Temperature control thus plays a predominant role in selective reaction control in general and in particular in the case of exothermic multistep reactions. Under non-adiabatic conditions, catalysts must therefore be assembled and arranged in the fixed bed in such a way as to ensure good heat transport to the heat-transfer medium.

A further requirement placed on the catalyst is a low flow pressure loss. This applies particularly if the reaction conversion in a single through put is low, so that the reaction has to be carried out with a large circulating gas ratio (Fig. 53), as well as to off-gas purification, in which large off-gas streams must be handled with minimal additional cost. Finally, the catalyst should be available in a sufficiently high concentration in order to keep the construction volume of the reactor low. The decisive parameters here are the specific external catalyst surface a_p (= square meters of catalyst surface per cubic meter reactor volume)

for reactions controlled by external mass transfer, the catalyst fraction I - ε, where ε = cubic meters of free gas space per cubic meter of reactor volume, describing the void fraction of the fixed bed. The above requirements are to some extent contradictory, which has led to the proposition of a large number of different catalyst forms and arrangements. However, only a few of these have proved really effective in practical operation. Suitable catalyst forms and arrangements include random packings of spheres, solid cylinders, and hollow cylinders, as well a uniformly structured catalyst packings in the form of monoliths with parallel channels, parallel stacked plates, and crossed, corrugated-plate packets.

Gas-Catalyst Mass and Heat Transfer

Random Packings

Industrial fixed-bed reactors are generally operated with a cross-sectional loading $G_z \geq$ I kg gas per square meter of reactor cross section per second. This loading produces a sufficiently strong turbulence in random packing.

As a result the external gas - catalyst mass-transfer resistance is small compared to the transport resistance in the catalyst pores. However, generally the thermal conductivity of the catalyst matrix is larger than of the gas. This

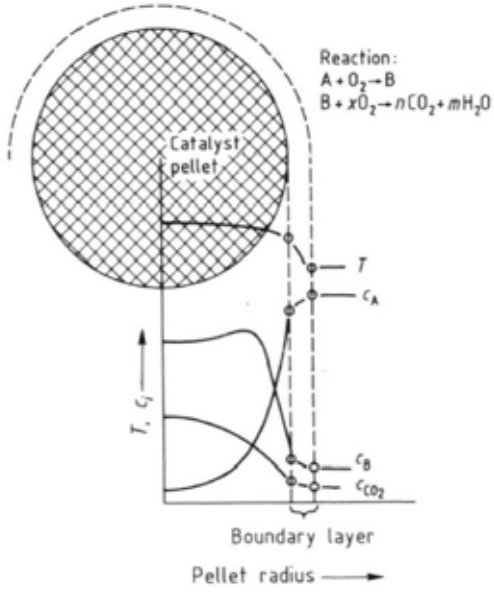

Fig. 55: Temperature and concentration profiles for a partial oxidation reaction in a spherical catalyst pellet.

means that the external gas - catalyst heat transport resistance exceeds the thermal conduction resistance in the catalyst particles. The temperature and concentration conditions established in a spherical catalyst are illustrated for a partial oxidation reaction in Figure 55. The conditions can be calculated from the model equation given in Model Reactors and Their Design Equation, under the assumptions made there. An essential precondition is that the catalyst particle is uniformly exposed over its entire surface to a flow with uniform temperature and concentration. This is, of course, never the case in random packings. Figure 56 shows the local mass-transfer distribution, providing an insight into the overall highly inhomogeneous conditions. The visualization technique is based on the reaction of traces of ammonia in the gas stream with a catalyst surface impregnated with manganese chloride solution. The conversion to manganese dioxide is already so fast under ambient conditions that it practically depends only on the external mass-transfer resistance of the gas boundary layer. The intensity of the dark coloration is thus directly proportional to the local reaction rate of the surface reaction. At a constant ammonia concentration in the gas flow it is thus also proportional to the local mass transfer, and if the mass-transfer and heat transfer are equivalent, also to the local heat transfer.

Figure 56 shows that the local conditions in random packings are much more complex than assumed in current conventional models. Nevertheless, the models for fixed beds containing a large number of catalyst particles over the cross-section can provide reliable information if it is borne in mind that they only describe the mean value of a process that varies greatly a regards detail.

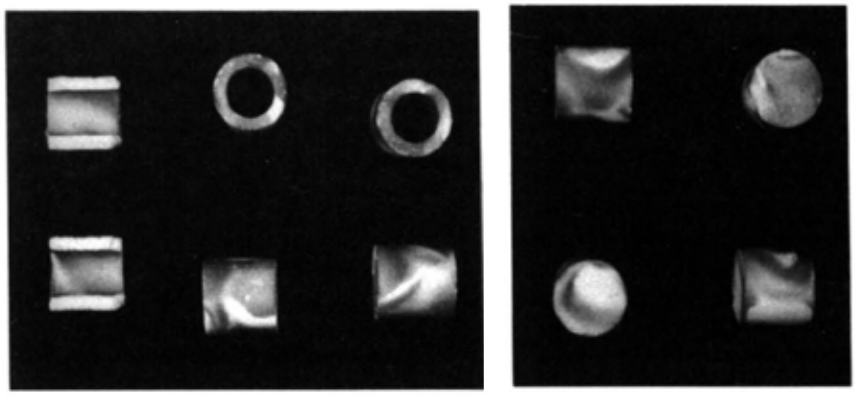

Fig. 56: Local mass-transfer distribution at the surface for individual cylindrical or ring-shaped catalyst pellets in a fixed-bed packing.

Asymptotic dimensionless laminar now heat or mass- transfer coefficients $Nu = \alpha_w \cdot d_h/\lambda_G$ (constant wall conditions) and fanning friction factor I for pressure drop. $\Delta p = 2f(\eta Z_L/d_h^2) \cdot v_G$ for ducts of different cross section.

Geometry	*Nu*	*f*	d_h
	2.47	13.33	$2a/\sqrt{3}$
	2.98	14.23	a
	3.34	15.05	$2\sqrt{3}a$
	3.66	16.00	a
	7.54	24.00	$2a$

For the same reason, it is inappropriate to compare model predictions with a few local temperature or concentration measurement. Indeed, a certain degree of averaging is also necessary in the measurement procedure. The literature contains a number of correlation equations for the mean gas - catalyst mass transfer and heat transfer as a function of gas properties , catalyst geometry, and flow conditions. However, in practice they play only a minor role for catalyst packings since design and simulation calculations are frequently performed with a model that is quasi-homogeneous, at least with regard to temperature (Model Reactors and Their Design Equations. The reason for this are the above-mentioned strong local fluctuations, which make differentiation between the gas temperature and catalyst temperature difficult.

Monolith Structures

In contrast to random packings, the external heat transfer and mass transfer in monolith catalysts is much more uniform, but they can also become limiting factors at high reaction rates. This applies in particular to channel-type monoliths with narrow parallel channels. Where the flow is generally laminar

under industrial operating conditions. Example includes monolith catalysts with a square-channel cross section for automobile exhaust purification and for the removal of nitrogen oxides from flue gases.

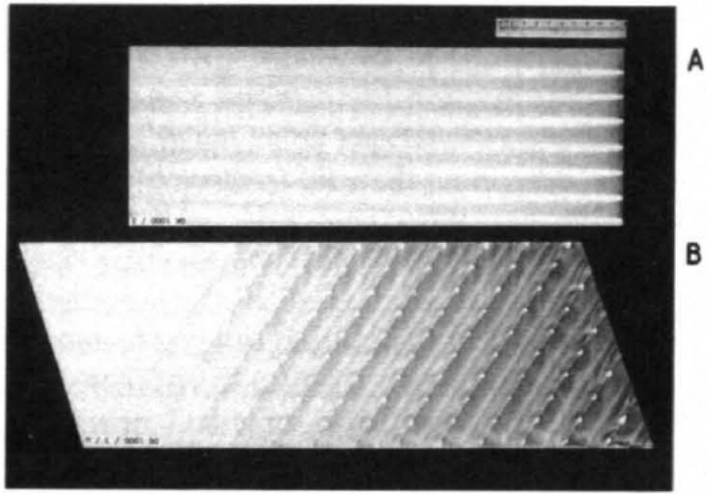

Fig. 57: Visualization of mass transfer in monolith structures (flow from left to right) (A) Square duct; (B) Corrugated monolith.

Figure 57 shows results of the visualization of the local mass transfer by using the ammonia manganese chloride reaction. The marked decrease in coloration in the flow direction is mainly the result of the increasing consumption of ammonia in the wall boundary layer, so that the reactants diffusing to the wall have to travel an ever increasing distance from the flow core (build up of the laminar boundary layer). The depletion is particularly pronounced in the corners, since two reaction surfaces meet here. The more acute their enclosed angle, the greater is the depletion in the corner region and the smaller is the contribution of the wall surface to further heat transfer and mass transfer. The efficiency of channel monoliths of equal cross-sectional area but different shape therefore decreases in the sequence: circle, hexagon, rectangle, triangle. This is illustrated in Table, which gives the asymptotic dimensionless mass-transfer and heat-transfer coefficients for tubes of the above cross sections. As Figure 58 shows, the asymptotic limiting value is established after a flow length roughly corresponding to times the hydraulic channel diameter. The asymptotic limiting value from Table can therefore be used to perform estimation calculations in

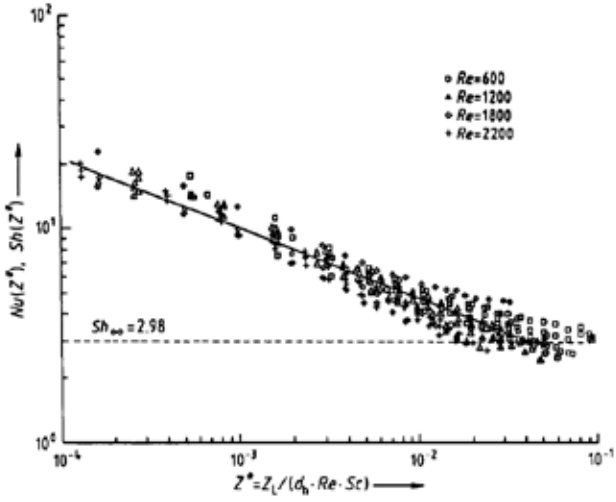

Figure 58

conventional industrial monolith catalysts with a large length-to-diameter ratio. For more accurate calculations the radically and axially variable velocity. Concentration and temperature profiles must also be taken into account. In contrast to the monolith types discussed so far, the flow conditions in corrugated-plate monoliths (Fig. 54 C) are turbulent under normal industrial velocities. The uniformity of the mass-transfer distribution depends on geometrical parameters (wave form, amplitude, wavelength, angle of incidence). The transfer coefficients are considerably higher than those of laminarly traversed channel monoliths (Fig. 57 B), but the pressure loss is also high. These structures offer considerable advantages for convective heat transport transverse to the flow direction and for transverse mixing, which are discussed in more detail in the following sections.

Flow and Pressure Loss in Fixed Beds

Conventional industrial catalyst forms differ considerably as regards pressure loss. For example, for equal mean dimensions and the same proportion of empty space random packages generally have a considerably higher pressure loss than monolith structures and among these corrugated structures have a higher pressure loss than monoliths with straight parallel channels. Mass transfer and heat transfer are strongly correlated with the pressure loss. For reasons of energy demand the catalyst form for a given process is chosen to combine the required mass transport and heat transport with the lowest

pressure loss. However, it should be borne in mind that the flow into the fixed-bed reactor is generally achieved by means of a feed pipe and a distribution hood. These must therefore be constructed so that the fixed bed or tube bundle is uniformly traversed and the gas residence time in each tube or each flow filament of the fixed bed is the same. This requirement can always be met simply if the pressure loss in the fixed bed or tube bundle is substantially greater than in the entrance hood. In this case it need only be ensured that the fixed bed is packed so uniformly that no flow bypass is formed or, in the case of a multitude reactor, the pressure loss is equalized in all the individual tubes of the bundle. Because the pressure loss increases with the square of the flow velocity, a uniform distribution of the flow then occurs automatically. Obtaining a uniform flow distribution is substantially more difficult if the pressure loss of the fixed bed is small. This holds in particular for monolith reactors with straight, laminarly traversed channels. The Hagen - Poiseuille equation is used to calculate the pressure loss in laminarly traversed monolith channels.

$$\Delta p = \frac{32 \eta Z_L v_G}{d_h^2} .$$

The pressure loss of packed tubes can be described either by means of a pressure loss coefficient and the pressure drop equation.

$$\Delta p = \zeta \cdot \frac{\varrho}{2} \cdot v_G^2$$

or by the Ergun equation

$$\Delta p = f_1 v_G + f_2 v_G^2$$

where for spherical packings:

$$f_1 = 150 \cdot \eta \cdot \frac{(1-\varepsilon)^2}{\varepsilon^3 \cdot d_p^2}$$

$$f_2 = 1.75 \cdot \varrho \cdot \frac{(1-\varepsilon)}{\varepsilon^3 \cdot d_p}$$

Thus the pressure drop depends very strongly on the void fraction ε of the packing. Of the standard forms for packed catalysts, hollow cylinders of thin wall thickness ($\varepsilon \approx 0.6$-0.8) are therefore preferred to spheres ($\varepsilon \approx 0.37$ -0.4) and solid cylinders ($\varepsilon \approx 0.35$).

The strong dependence of the pressure loss on the void fraction underlines the importance of packing catalyst beds carefully to avoid bypass flow due to local variations in the packing density. For the same reason the tubes of multitubular reactors for highly exothermic. Selectivity sensitive reactions are often filled uniformly by means of special devices and if necessary individually compensated for pressure loss.

The pressure loss coefficient s (Eq. 2.2) can be determined for typical packing forms.

Heat Transport Transverse to the Flow Direction

With non-adiabatic reaction control, heat must be transported perpendicular to the flow direction through the fixed bed to the heat exchange surfaces. At the usual mass flow rates of $G_r = 1\ \mathrm{kg\,m^{-2}s^{-1}}$, this heat transport takes place mainly by convection, *i.e.*, the fixed bed must be constructed so that flow components transverse to the main flow direction occur locally. Monolith structures with straight parallel channels are thus unsuitable for non-adiabatic reaction control.

In catalyst packing transverse flow components are automatically established as a result of the non-uniform arrangement and the twisted flow around the pellets. Hollow and full cylinders with a length-to-diameter ratio of 1 to 3 are particularly effective in this respect.

Despite the fact that radial heat transport in the form of twisted flow takes place mainly by convection. it is formally described by means of a so-called effective thermal conductivity λ_r transverse to the flow direction.

In addition to heat transport through the fixed bed perpendicular to the main flow direction the heat transport at the boundary between the fixed bed and heat exchange surface is also decisive for the heat exchange. The latter heat transport is generally described by a wall heat transfer coefficient α_w, in which the complex interplay between convective flow at the tube wall and conduction transport by contact between the fixed bed and the heat exchange surface is described in overall terms. However the correlations for α_w and λ_r, given in the literature do not adequately take account of the actual velocity distribution in packed tubes. Plug flow was generally assumed although the actual velocity profile is non-uniform with a pronounced slip at the wall. This is due to the fact

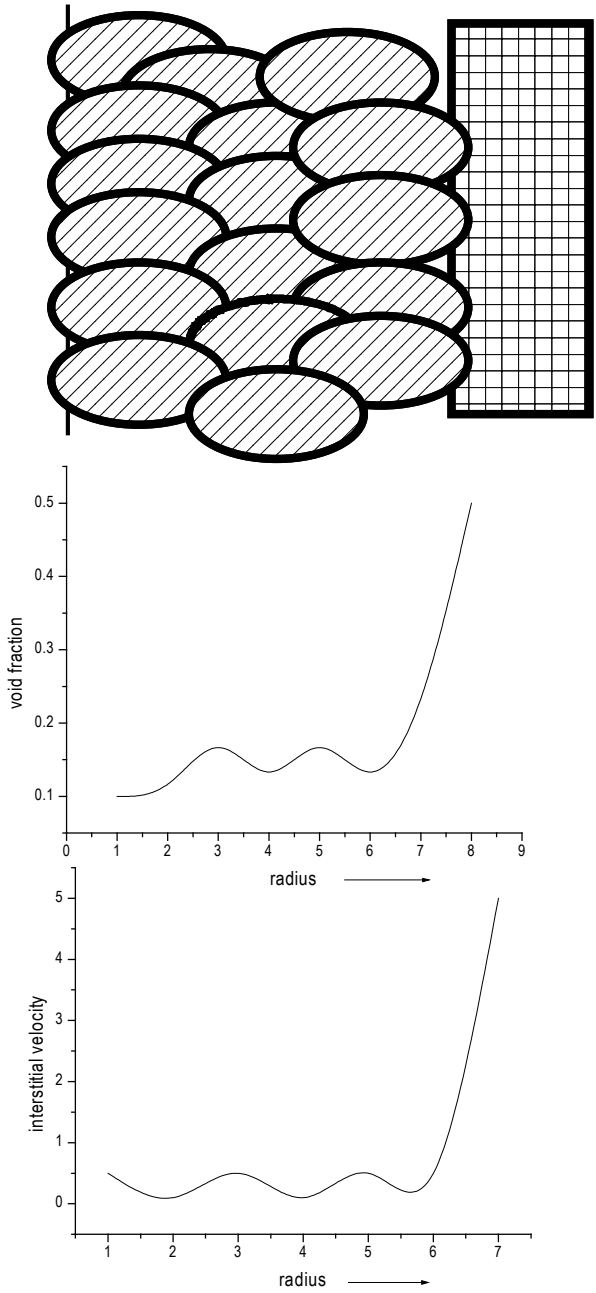

Fig. 59: The figure showing the radial distribution of the void fraction and axial velocity of the packed column with spheres.

that the pellets make only point contact with the wall,whereas they overlap and cross over one another inside the packing, thereby reducing the free volume and hence the velocity. The conditions for a spherical packing are illustrated schematically in Figure 59. The radially varying empty space distribution and velocity distribution must be taken into account in detailed reactor calculations as well as in the determination of accurate heat-transport parameters. Existing correlation equations for calculating the heat-transport parameters were obtained from heating or cooling experiments without reactions and assuming plug flow; they therefore permit only a semiquantitative evaluation. However, this is adequate for qualitative comparison of catalyst structures.

Comparison and Evaluation of Different Catalyst Forms

The choice of a suitable catalyst form is always an optimization problem that can be completely specified only for a specific process. Even then, however, weighting the performance function is not easy since, for example, small pressure losses uniform flow through the reactor and good mass- and heat-transfer properties generally represent opposing requirements. The following assessment is therefore only a rough guide.

Catalyst Forms for Adiabatic Operation

Decisive parameters for adiabatic operation include:

1. The active catalyst surface available per unit reactor volume
2. The quantity of the mass and heat transfer between the flowing gas and the active catalyst surface
3. The flow pressure loss
4. The uniformity of the flow through the reactor and thus the degree of utilization of the fixed bed

The major proportion of the active catalyst surface IS located In the interior of the porous catalyst structure. However if its assumed that, in the case of sufficiently fast reactions, the reaction site is restricted to a thin layer underneath the external surface then the active catalyst surface area can be taken as proportional to the specific external catalyst surface area a_p. If the uniform distribution of the flow entering the fixed bed is regarded as a separate problem, then for given kinetic conditions the evaluation may be restricted to three parameters, specific external surface area a_p gas-solid mass-transfer

coefficient k_G and the flow pressure loss. The evaluation becomes particularly simple if with single dominant reaction, the external gas-solid mass transfer limits the reaction, since in this case the specific reaction kinetics have no Influence. Assuming mass-transfer limitation, the material balance for the key component along the flow path is

$$\varepsilon \cdot v_G \cdot \frac{\partial c}{\partial z} = - k_G \cdot a_p \cdot c$$

If the reaction has a conversion of 99%, *i.e.* an outflow concentration of 1 % of the inflow concentration, the length of the fixed bed Z_L is, by integration. For

$$Z_L = - \frac{\ln 0.01 \cdot \varepsilon \cdot v_G}{k_G \cdot a_p} = \frac{4.6 \cdot \varepsilon \cdot v_G}{k_G \cdot a_p}$$

For the required reactor volume V_R with the cross-sectional area A:

$$V_R = Z_L \cdot A = 4.6 \cdot \frac{\dot{V}}{k_G \cdot a_p}$$

The computation is particularly simple for straight, laminarly traversed channels. The asymptotic limiting value given in Table for the square channel

$$Sh = \frac{k_G \, d_h}{D} \approx 3$$

gives, with $a_P = \frac{4}{d_h \cdot \varepsilon}$,

$$k_G \cdot a_p \approx \frac{12 \, D}{d_h^2 \cdot \varepsilon}$$

and

$$V_R = 0.38 \frac{\dot{V} \cdot d_h^2 \cdot \varepsilon}{D}$$

If Equation is used for the pressure loss, then for the laminarly traversed monolith channel.

$$\Delta p = \frac{12.28 \cdot \eta}{D} \cdot v_G^2 \cdot \varepsilon^2$$

Using the above equations, reactor variants for catalytic off-gas purification with a given volume now V were calculated in. The result is shown in Figure 2.7. The pressure drop of the fixed bed over the required reactor length is plotted; the curve parameter is the hydraulic diameter d_h of the monolith channel or packing body for different empty-tube gas velocities $v_e = \varepsilon \cdot v_G$. According to Equation (2.11) the required fixed bed volume V_R. with square monolith catalysts and a given throughput V depends only on dh , whereas the geometric arrangement (small bed cross section A and long bed length Z_L' or large bed cross section and short bed) has no innuence on V_R However, the bed cross-sectional area A for a given gas throughput V determines via

$$\dot{V} = A \cdot v_G \cdot \varepsilon$$

the inter-particle velocity v_G according to Equation this then appears as a quadratic term in the pressure loss. In conclusion a minimum catalyst volume with minimum pressure loss is obtained by using a very flat bed with a large now cross-sectional area A and small hydraulic channel diameter or particle diameter d_h. This result applies in general to all catalyst forms. The main difficulty with this arrangement the uniform distribution of the now velocity. Figure 60 shows the improvement in pressure loss that can be achieved by channel monoliths as compared to spherical packings. Other catalyst forms such as Raschig rings or corrugated-plate packets lie between these boundary curves.

Catalyst Forms for Isothermal Operation

In addition to the previously discussed quantities, the lateral heat-transport parameters of the fixed bed are further decisive parameters in isothermal reaction control. As shown in heat transport can be characterized by the effective thermal conductivity perpendicular to the main flow direction λ_R and the wall heat transfer coefficient α_W. Both quantities are strongly dependent on the filling or packing form. Since transport in the industrially interesting region mainly occurs by convection, they are approximately proportional to the mass throughput. For the purposes of overall comparison, the corresponding characteristic parameters are given in Figure 61 for some industrially Important

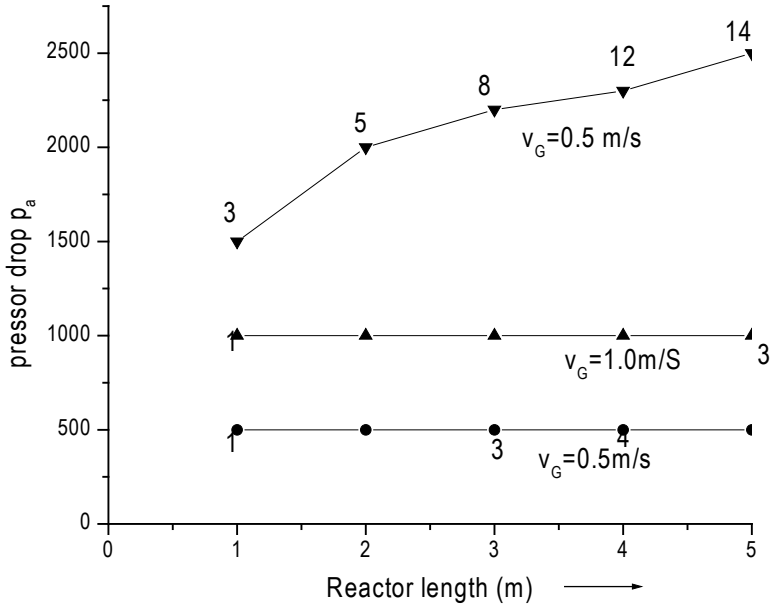

Fig. 60: Pressure drop over the fixed-bed length for a catalytic combustion reactor with given throughput and 99% conversion function of the hydraulic catalyst diameter d_h for different gas empty-tube velocities.

filling and packing forms in a tube of 50 mm internal diameter with a mass-flow velocity of G_z = 1 kgm^{-2} s^{-1} . The dimensions of the packing bodies were chosen so that their specific external surface area a_p is ca. 500 m^2/m^3. Under these conditions hollow, thin-walled cylinders have clear advantages over other package forms exhibiting the lowest pressure loss and the highest thermal conductivity. Only as regards wall heat transfer are they inferior to spheres or cylinders. However, good wall heat transfer is apparently less decisive from a reaction engineering viewpoint than good radial thermal conductivity, since the former can be compensated by an appropriate temperature profile of the heat-transfer medium whereas the radial thermal conductivity directly influences the uniformity of the reaction conditions over the tube cross section. On the other hand, solid cylinders with a large length-to-diameter ratio have good heat transport values, but at the cost of a very high pressure loss. Despite its poor heat transport properties, a monolith with straight, parallel channels, such as used for automobile exhaust control, is included in the comparison. Monolith forms have very high specific surfaces combined with a very low pressure loss.

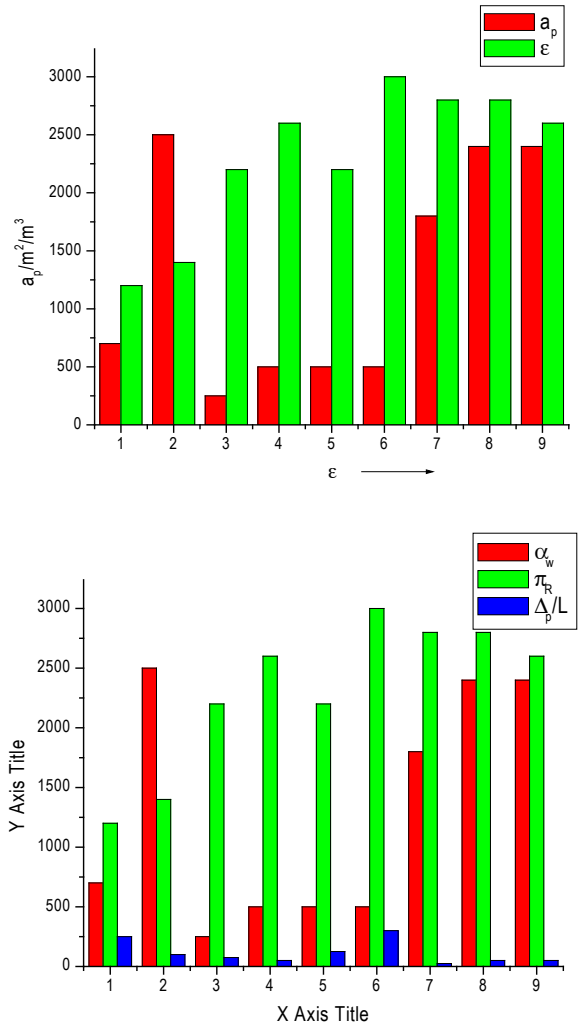

Fig. 61: Characteristic Parameters of the column packing

Crossed corrugated structures are considerably more favorable for isothermal reaction control. They have a very high radial thermal conductivity that is almost independent of the specific surface area; the latter can be varied over a wide range by means of the channel dimensions. The catalyst of a reaction tube can thus be structured so that wide packings of small specific surface area can be used in the region of the main reaction zone, while packings of increasingly narrower structure, *i.e.*, large specific surface area, are used downstream. In

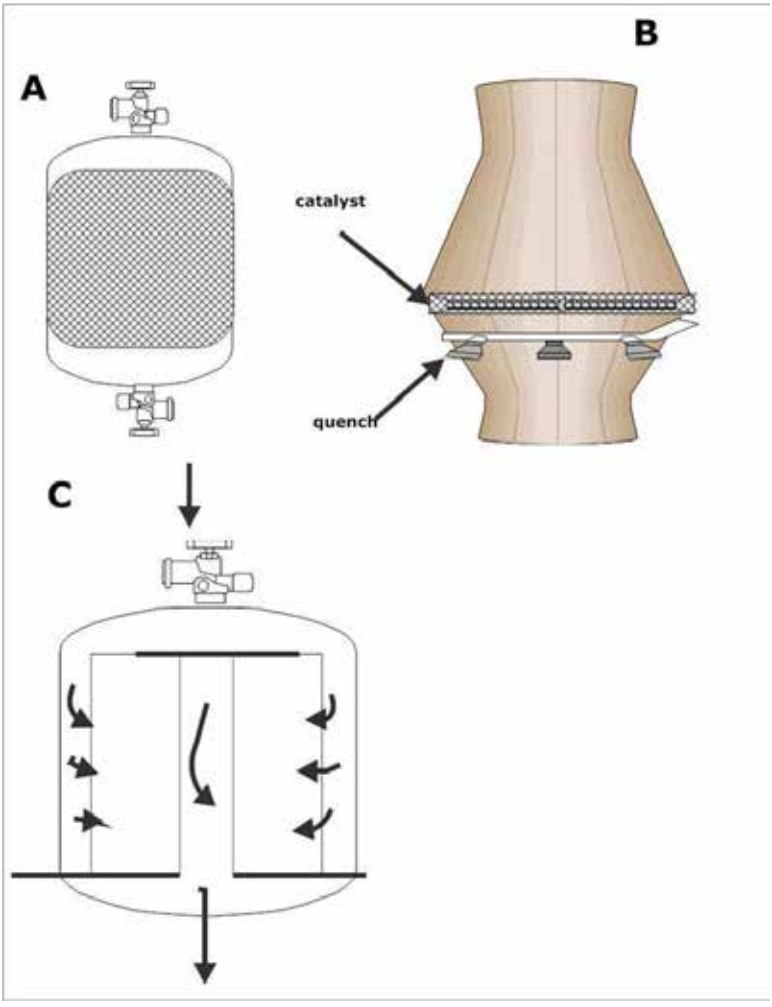

Fig. 62: Main design concepts for adiabatic reactors (A) Adiabatic packed-bed reactor; (B) Disk reactor; (C) Radial-flow reactor.

this way a more uniform reaction rate and temperature profile can be achieved over the tube length. However, it must be remembered that with crossed corrugated structures, convective radial heat transport occurs only in one plane perpendicular to the main flow direction. in addition the flow behavior in tubes of circular cross section is rather non-uniform over the circumference which is why It is advantageous to arrange short packing sections in series, each section being displaced by 90 degree. The heat transport parameters in Figure 61 were determined for structures arranged in this way.

A general problem in the use of monolith structures in reaction tubes is incomplete wall contact since individual tubes of multi-tubular reactors always have a diameter tolerance of ca. 1 mm and interlocking of the structure with the tube wall must be avoided, the bypass of flow at the wall is even greater than with random packings. Up to now there have been no specific investigations of the magnitude and effects of this phenomenon.

Adiabatic Reaction Control

Adiabatic fixed-bed reactors are the oldest fixed-bed reactor configuration. In the simplest case they consist of a cylindrical jacket in which the catalyst is loosely packed on a screen and is traversed in the axial direction (Fig. 62 A). To avoid catalyst abrasion by partial fluidization catalyst packings are always traversed from top to bottom. If fixed beds composed of monolith catalyst sections are used the flow direction is arbitrary. The requirement for a low pressure loss leads to a fixed bed of large diameter and low height (Fig. 62 B). Such an arrangement (disk concept) is used particularly when very short residence times, followed by direct quenching of the reactions are required. Examples include ammonia oxidation in nitric acid production (→ Nitric Acid, Nitrous Acid, and Nitrogen Oxides) and oxidative dehydrogenation on silver catalysts (*e.g.* synthesis of formaldehyde by dehydrogenation of methanol → Formaldehyde.

In the first case the "fixed bed" consists of several layers of platinum wire gauzes, and in the second case, of a porous silver layer several centimeters in height. The bed diameters can be up to several meters. On account of the difficulties involved with obtaining uniform flow as well as for structural reasons, the disk concept is limited to small catalyst volumes. The radial flow concept (Fig. 62 C) is used where large amounts of catalyst are involved.

The catalyst packing is accommodated in the space between two concentric screen rings or perforated plate rings and is traversed radically either from the inside to the outside or from the outside to the inside. This design is particularly suitable for large catalyst volumes as well as for operation at elevated pressure, since at moderate reactor diameters the catalyst volume can be varied over a wide range by altering the reactor length, without affecting the flow-through length of the packing. A critical feature of packed radial-flow reactors is the shape of the upper bed closure. A simple horizontal covering is not practicable

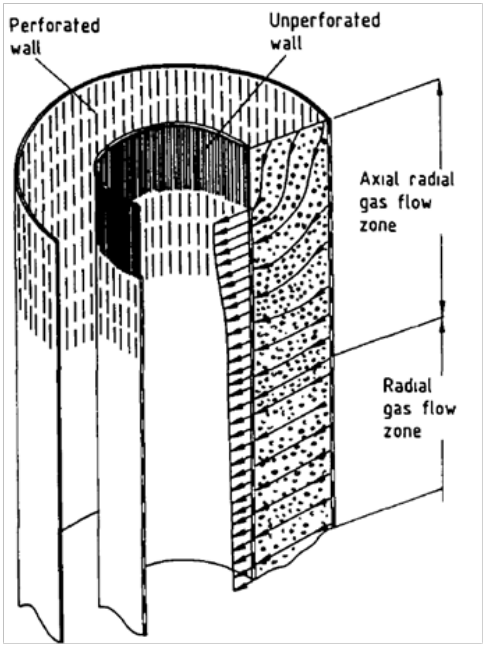

Fig. 63: Upper bed closure in a radial-flow reactor

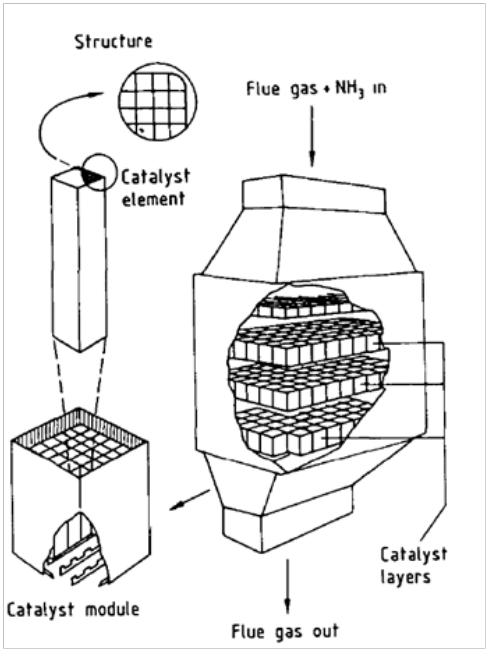

Fig. 64: Reaction chamber for removl of nitrogen oxides from power station flue gas

since a gap through which untreated gas can pass is then formed due to the unavoidable settling of the packing. The arrangement shown in Figure 62 has proved effective since it produces mixed axial and radial flow through the bed in the upper bed closure. The required geometrical shape must be determined by simulation of the local two-dimensional flow through the packing. The advantages of monolith catalysts with straight, parallel channels for adiabatic reactors have already been referred to in previous section. Since monolith catalysts are usually produced with a rectangular cross section, the fixed bed is constructed by arranging these individual monoliths in rows in the form of a large "box". Conventional DENOX reactors for removing NOx from power station flue gases are therefore designed as rectangular chambers (Fig. 64). The catalyst is often arranged in the form of several layers in sense, the spaces between the individual layers permitting cross-mixing, so that the influence of no-uniform flow as well as any possible local blockage of the next layer can be compensated to some extent. This is not easy to achieve particularly with low-pressure-loss monolith reactors and requires a careful design of the inflow hood.

On account of the low pressure loss, unfavorable flow conditions in the outflow hood may also affect the flow behavior through the catalyst bed. Figure 65 shows the velocity distribution in front of the monolith inlet for an industrially housed automobile catalyst. Since the flow cannot follow the sudden widening of the inlet funnel, one third of the total cross section is traversed at a velocity that is roughly three times the mean velocity. It can be estimated that, with uniform flow through the catalyst, half the catalyst volume would be sufficient for the same mean conversion. Also, bends in the feedpipe can lead to swirl-type components and thus contribute to non-uniform flow. Purely adiabatic fixed-bed reactors are used mainly for reactions with a small heat of reaction. Such reactions are primarily involved in gas purification, in which small amounts of interfering components are converted to non-interfering compounds. The chambers used to remove NOx from power station flue gases, with a catalyst.

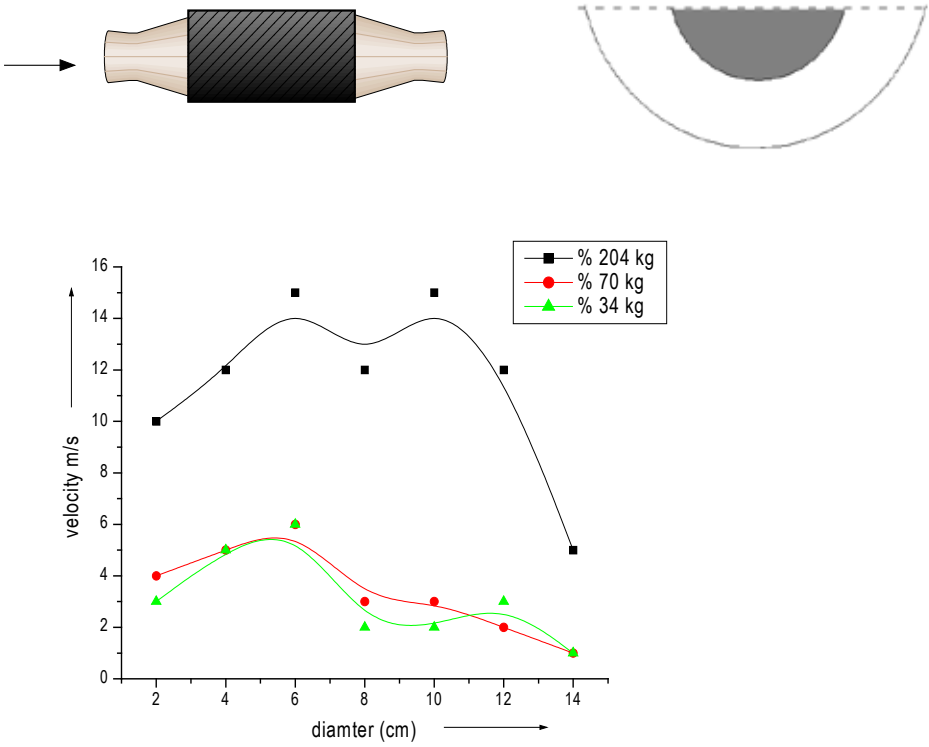

Fig. 65: Velocity distribution in an Industrially housed automobile catalyst.

Reaction Control with Supply or Removal of Heat in the Reactor

In the majority of fixed-bed reactors for industrial synthesis reactions, direct or indirect supply or removal of heat in the catalyst bed is utilized to adapt the temperature profile over the flow path as far as possible to the requirements of an optimal reaction pathway. Here a clear developmental trend can be observed, which is illustrated schematically in Figure 66. Development started with the adiabatic reactor (Fig. 66 A), which on account of the adiabatic temperature change could only be operated to give a limited conversion. Higher conversions were achieved at the same mean temperature level when several adiabatic stages were introduced, with intermediate heating or cooling after each stage. The simplest form involves injecting hot or cold gas between the stages (Fig. 66B). For a constant tube diameter, the main disadvantages of this temperature control strategy are cross-sectional loading, which increases from stage to stage, and the mixing of hot and cold streams which is energetically unfavorable. The composition is changed by injection which can have a positive or negative effect on the desired reaction. The next development was the replacement of injection cooling by interstate heat exchangers, through which the required or released heat of reaction is supplied or removed (Fig. 66 C). The development of reactors in which the heat-exchange surfaces are integrated in the fixed bed to supply or remove the heat of reaction as close as possible to the reaction site occurred in parallel with the development of multistage adiabatic reactors with intermediate heating or cooling. The multitubular fixed-bed reactor (Fig. 66 D) constitutes the oldest and still predominant representative of this class of fixed-bed reactors. Here the catalyst packing is located in the individual tubes of the tube bundle. The heat-transfer medium is circulated around the tube bundle and through an external heat exchanger. in which the heat of reaction is supplied or removed. Whereas with endothermic reactions circulating gas can be used as heat transfer medium for strongly exothermic reactions exclusively liquid or boiling heat-transfer media are used. Only in this way can the catalyst temperature (*e.g.,* in the case of partial oxidations) be held in the narrow temperature range necessary for selective reaction control. Initially, the integration of heat exchange in the fixed bed was utilized to ensure as isothermal a reaction control as possible, which is why reactors of the type shown in Figure 66 D are also commonly termed "isothermal reactors". They are characterized by reaction tubes of 20 – 80 mm internal diameter and a carefully

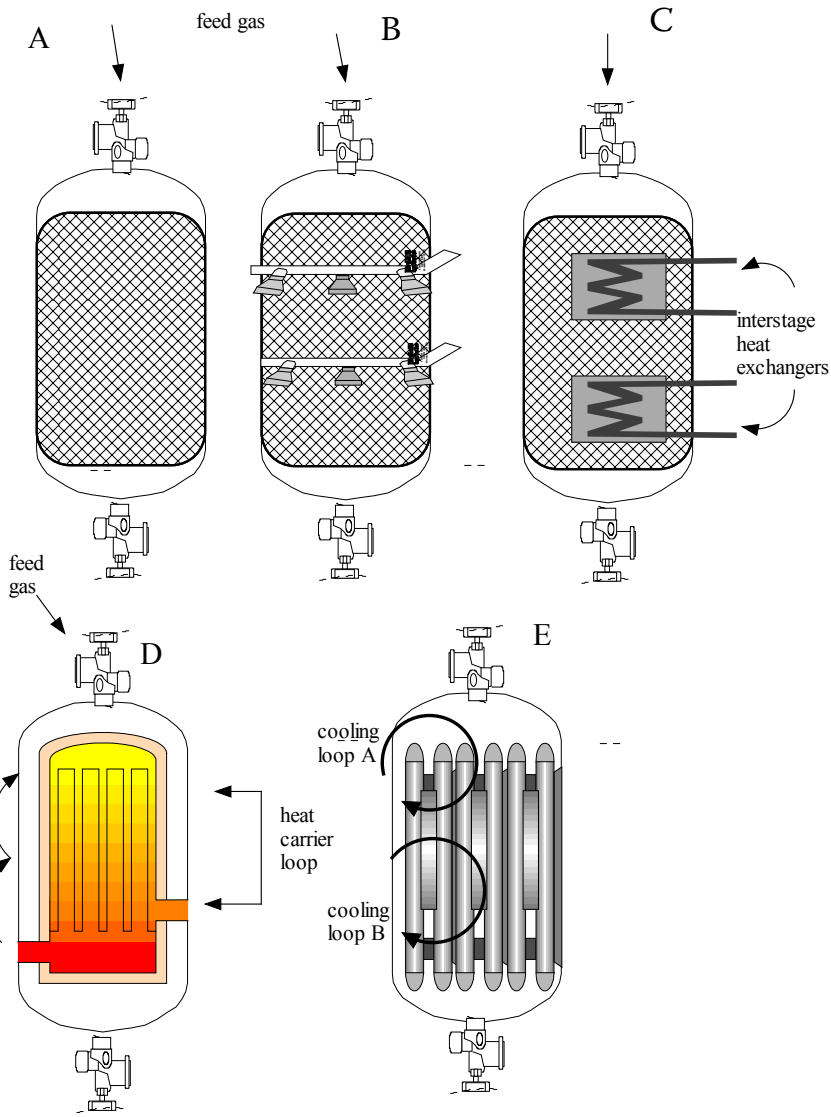

Fig. 66: Development of fixed-bed reactors (A) Single-bed adiabatic packed-bed reactor. (B) Adiabatic reactor with interstage gas feed (ICI concept). (C) Multibed adiabatic fixed-bed reactor with interstage heat exchange. (D) Multitubular fixed-bed reactor. (E) Multitubular fixed-bed reactor with two cooling circuits and non- isothermal cooling temperature.

designed flow control of the liquid heat-transfer medium, with largely constant heat-transfer condition throughout the tube bundle and maximum temperature changes of the heat-transfer medium in the tube bundle of a few degrees.

The latest concepts are aimed at establishing a freely selectable (within limits) optimum temperature profile over the tube length. This requires complex heat-transfer medium control with several sections and temperature levels (Fig. 66 E). The stimulus for the developments outlined in Figure 66 was the need for total raw material utilization as regards both mass and energy. This involves as main criteria the yield of primary end products (maximum), the yield of byproducts that must be removed and eliminated (minimum), the thermal energy consumption or recovery, and the mechanical energy requirements (gas compression, circulation of heat-transfer medium). In addition to the running costs, which are determined by the above criteria, the investment costs are decisive in an investment decision, and naturally rise sharply with increasing complexity of the reaction cycle.

On account of cost digression the projected plant size and the subsequent degree of utilization as well as the technological sophistication are decisive in calculating the product price. Several of the fixed-bed reactor variants illustrated in Figure 66 can depending on the location of the production site and the estimated output, be used for the same process. For example, multistage adiabatic reaction systems with intermediate superheated steam feed, multitubular reactors with circulating gas heating, and strictly isothermal designs with multitubular reactors heated with molten salt are currently used for the endothermic synthesis of styrene from ethylbenzene. Also, exothermic, equilibrium-limited reactions such as methanol synthesis are carried out in multistage adiabatic reactors with interstage cooling as well as in multitubular reactors. Overall, however, there is a trend towards the more highly integrated designs, which will accelerate with rising energy and raw material prices. Adiabatic multistage designs and reactors with heat exchange integrated in the fixed bed are discussed in the following sections. Autothermal reaction control, in which the heat of reaction of moderately exothermic reactions is utilized to heat the incoming feedstock.

Adiabatic Multistage Reactors with Interstage Heat Transfer

Adiabatic multistage fixed-bed reactors with intermediate cooling or heating are nowadays used particularly where the reaction proceeds selectively to give a single product but is limited by the equilibrium conditions. Intermediate cooling or heating is used to displace the gas temperature in the direction of higher equilibrium conversion. Typical examples include the synthesis of ammonia,

sulfur trioxide, and methanol. In these exothermic reactions the equilibrium conversion to the target product decreases with increasing temperature as shown in Figure 67 A. For a given conversion x a temperature can therefore be found at which the reaction rate, with respect to the target product, becomes a maximum. This temperature must be below the equilibrium temperature but not so low that the reaction becomes too slow for kinetic reasons.

The points obtained in this way can be joined to form a maximum reaction rate curve (Fig. 67 B). Since, in the case of adiabatic reaction control the temperature increases linearly with the achieved conversion Δx according to the equation,

$$\Delta T = -\frac{\Delta h_{\mathrm{R}} \cdot c_0}{\varrho_{\mathrm{G}} \cdot c_{\mathrm{pG}}} \cdot \Delta x$$

each adiabatic reaction pathway of an exothermic reaction lies on a straight line of gradient ΔT/Δx (see Fig. 67A).

A practicable reaction pathway for a multistage adiabatic reaction can thus be derived from Figure 67 by joining straight-line sections for the adiabatic reaction to vertical lines for the temperature reduction due to indirect intermediate cooling (Fig. 67C).

The kinetically optimum reaction pathway with the smallest required catalyst volume results when the trajectory follows, in a large number of small steps, the line of maximum reaction rate. In practice, the apparatus and equipment expenditure involved in a large number of stages must be weighed up against the savings in catalyst. Conventional multistage reactors for this class of reaction therefore have three to five stages. Figure 68 shows the layout of an ammonia synthesis reactor designed on this basis. For structural reasons the heat exchanger is incorporated between the inflow and outflow in the lowest part of the pressure casing.

The reaction gas then flows upward in the annular gap between the pressure casing and the fixed beds, whereby it is further heated and at the same time protects the pressure-bearing structural component against excessively high fixed-bed temperatures. The three adiabatic fixed-beds are traversed from top to bottom, part of the heat of reaction being utilized to generate steam in the two intermediate heat exchangers. To start up the cold reactor, hot gas

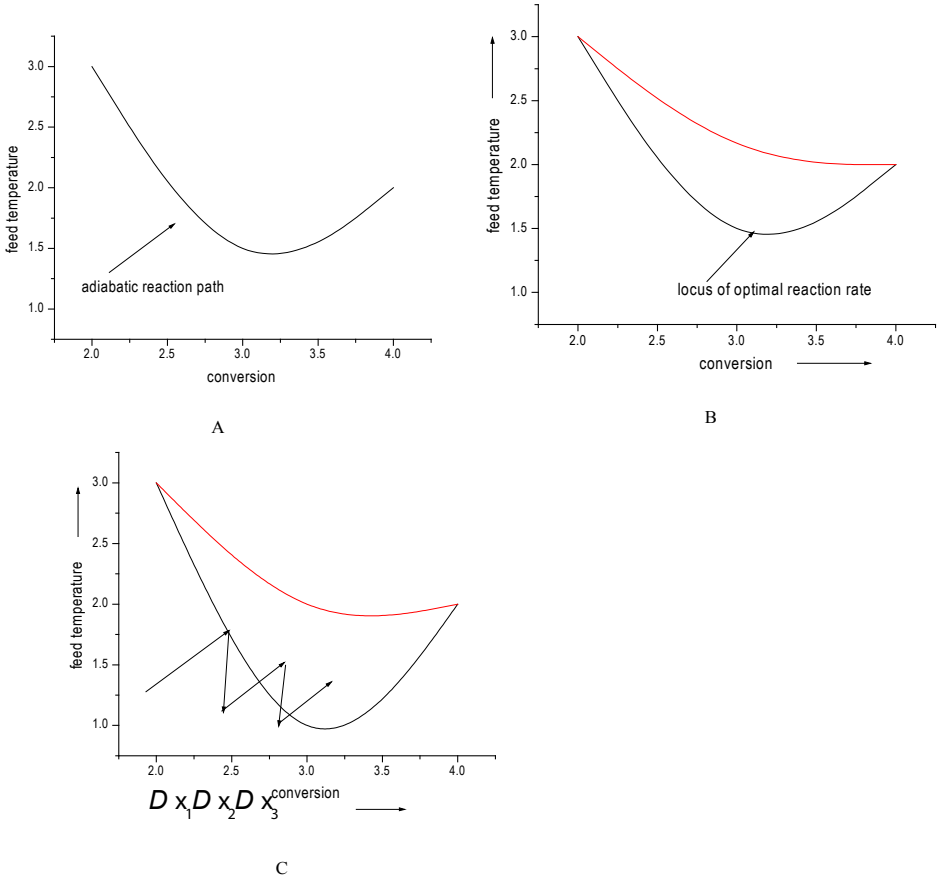

Fig. 67: Equilibrium limitations of the exothermic reactions (a) Equilibrium conversion as a function of temperature (b) Optimum reaction rate curve (c) Improvement of conversion by interstage cooling

must be added to the uppermost bed, for example through an external start-up preheater.

Industrial adiabatic multistage reactors often differ in many details from Figure 68 although they are of a comparable basic design. For example, radially instead of axially traversed beds can achieve a smaller pressure loss with a more favorable structural arrangement; heat exchange with the cold feedstock can be affected by heat exchange surfaces integrated in the first catalyst bed; or a cold gas quench can be used to achieve additional temperature regulation.

Modern, adiabatic multistage reactors may thus become so complex that the question arises whether a multitubular design according to Figure 66 D or E does not represent the more favorable alternative. The required heat-exchange surface area in the case where heat exchange is integrated in the fixed bed is smaller than in the case of free gas flow on account of the positive effect of the catalyst packing. Furthermore it does not involve any additional pressure loss and the optimum reaction rate curve can be better approximated by controlling the cooling temperature profile than by a stepwise temperature reduction.

On the other hand, a multistage arrangement may be considered for structural, operating technology, or kinetic reasons in the following cases:

1. If, in the case of large single-train plants subdivision into several individual items of apparatus is necessary for reasons of transport or construction

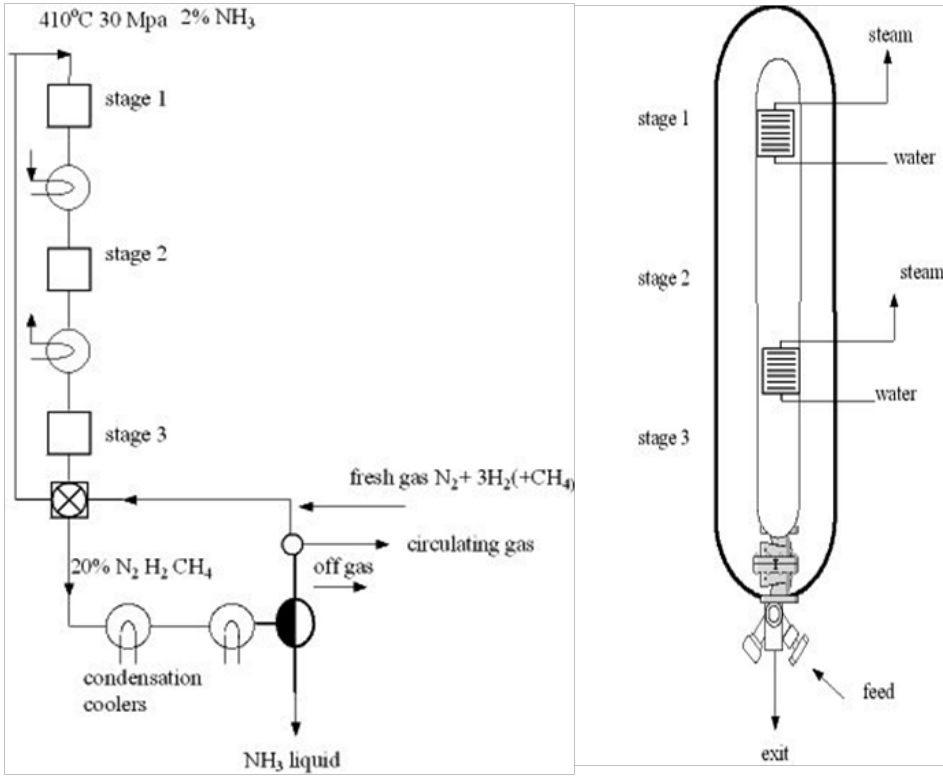

Fig. 68 & Fig. 68A: Showing the diagram of multistage Ammonia reactor

2. If a catalyst must be replaced in individual stages at different times on account of different catalyst compositions and/or aging
3. If a gradual addition of a reactant has kinetic advantages compared to the total addition to the feed (here a suitably designed intermediate heat exchanger ensures a uniform distribution and mixing with the reaction gas stream)
4. If the intermediate stages are used to extract a limiting product in the case of equilibrium limited reactions; an example is the intermediate absorption of SO_3 before the last stage of the SO_3 synthesis
5. With reaction temperatures above 300°C intermediate cooling can be performed directly with boiling water, whereas in a fixed bed a high-temperature heat-transfer medium must be used as coolant.

Integrated Heat Exchangein Fixed Bed Reactors

The aim of reaction control with heat exchange integrated in the fixed bed using a circulating heat-transfer medium is to maintain the catalyst temperature in a narrow optimum range under all operating conditions. With strongly exothermic successive reactions, such as partial oxidation, and partial hydrogenations, on account of the danger of a runaway reaction this requirement can be met only if:

1. The temperature of the heat-transfer medium close to the desired catalyst temperature
2. Large heat-exchange surfaces are available per unit catalyst volume
3. A sufficiently large mass flow velocity of the reaction gases ensures good heat transport from the packing to the heat-exchange surface

With exothermic equilibrium reactions and endothermic reactions these requirements are less stringent since these reactions cannot runaway, although here too it is beginning to be recognized that a tight and uniform temperature control over the reactor cross section is advantageous.

Heat Transfer Media for Fixed-Bed Reactors

The first of the above requirements presupposes an assortment of heat-transfer media that covers the whole temperature range of interest for gas-phase reactions in fixed-bed reactors. It is convenient to distinguish between gaseous,

liquid and vaporizing heat-transfer media. Gaseous heat-transfer media in the form of hot flue gases are used in the temperature range above 500°C exclusively to supply heat for endothermic reactions. Conversely, vaporizing heat-transfer media are used exclusively to remove heat from exothermic reactions. Whereas formerly petroleum fractions such as kerosene (*e.g.*, in ethylene oxide synthesis) were more widely used they have now been largely replaced by boiling water on account of their flammability, lower heat of vaporization and the need to produce steam in a downstream condenser/heat exchanger. Depending on the saturated vapor pressure the temperature range from 100 to 310°C (100 bar) can be covered with boiling water. In this range it is the preferred heat-transfer medium for evaporative cooling if an isothermal cooling temperature is required. Locally variable cooling temperature profiles can be established most easily with liquid heat transfer media that do not vaporize in the intended operating range. In order to avoid cavitation, pressurized water should be used only up to ca. 220°C; heat-transfer oils cover the temperature range up to 300°C, while above this temperature salt melts are now used exclusively in reaction technology. Compared to heat-transfer oils they have the advantage that they are incombustible and stable, although they have the disadvantage that they solidify at about 200°C (nitrate melts) or 400°C (carbonate melts). The temperature ranges of possible heat-transfer media are compared in Figure 69 In addition to the thermal stability, the energy $\dot{N}$ per unit amount of transported

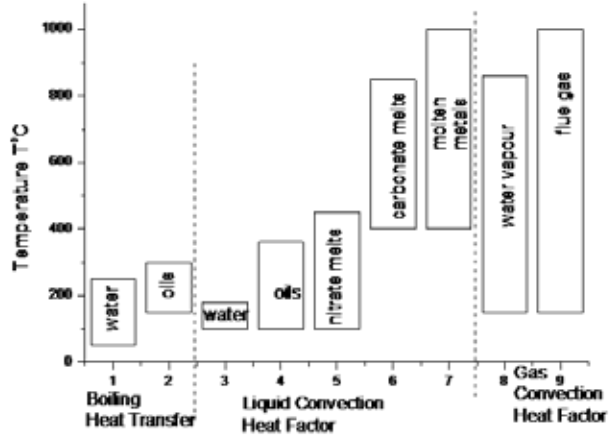

Fig. 69: Application ranges for common heat-transfer media.

heat $\dot{Q}$ required to circulate a heat-transfer medium is an Important criterion of choice.

The following equation has been derived for the evaluation of heat-transfer media without phase change.

$$\frac{\frac{\dot{Q}}{\Delta T_c}}{\dot{N}^{0.36}} \sim \frac{\varrho^{0.73} \cdot c_p}{\eta^{0.09}}$$

where $\dot{Q}$ is the heat flow transferred by the heat transfer medium while its temperature increases by exactly ΔT_c, $\dot{N}$ is the required pump power, and $\dot{Q}$, C_p, and η are the density, specific heat capacity, and viscosity of the heat-transfer medium. For liquid heat-transfer media, the equation is derived from the pressure drop in a turbulently traversed, hydraulically smooth pipe. It is practical to solve Equation for the pump power:

$$\dot{N} \sim \left[\frac{\dot{Q}}{\Delta T_c}\right]^{2.75} \cdot \frac{\eta^{0.25}}{c_p^{2.75} \cdot \varrho^2}$$

Thus the required power varies as almost the third power of $\dot{Q}/\Delta T_c$. The component $\eta^{0.25}/c_p^{2.75} \cdot \varrho^2$, which depend only on the physical properties of the heat-transfer medium, is plotted as a function of temperature in Figure 70. This shows the exceptional heat-transfer properties of water that result from its density and, in particular, its high specific heat, as well as the properties of gases (air) and vapors (water vapor), which are about seven orders of magnitude worse. Common heat-transfer oils and salt melts (sodium nitrate) lie close together, but about an order of magnitude above water. The poor performance of molten sodium compared to heat transfer oils and salt melts is noteworthy.

To test Equation on a more realistic example of the cooling of a multitubular reactor, a quadratic tube bundle (cross section 1.5 × 1.5 m) with fourfold passage of the coolant was designed by using detailed equations for pressure drop and heat transfer for various heat transfer media. The heat release of 1650 kW in 1591 (37 × 43) tubes of 30 mm external diameter and 4 m length corresponds to the conditions in a partial oxidation reaction. A temperature rise between feed and outlet of ΔT_c = 5K was assumed for the heat-transfer medium (additionally 150K for air and water vapor). Table lists as results the required pump power $\dot{N}$, the pressure drop in the cooling circuit Δ_p (whereby p = 1 bar exit pressure

was assumed for water vapor and air), and the excess temperature of the reactor wall above the heat-transfer medium temperature ΔT_w, assuming constant wall temperature along the length of the tube. It was shown that the results of this more precise design equation for the liquid heat-transfer media can be correlated with the equation

$$\dot{N} = 7800 \left[\frac{\dot{Q}}{\Delta T_c}\right]^{2.73} \frac{\eta^{0.27}}{c_p^{2.73} \cdot \varrho^2}$$

Water is thus the ideal heat-transfer medium within its temperature range. For higher temperatures molten salts have increasingly replaced the previously more commonly used heat-transfer oils. Salt melts cover a larger temperature range and have the particular advantage over oils that they are incombustible. The potential danger of a relatively large amount of hot salt melt obviously exists but it reliably dealt with by experienced reactor construction companies. Special nitrate melts (HITEC) can be used in the temperature range 200 - 500°C. Gradual decomposition begins above this temperature which can accelerate violently above 600°C. Access of organic components to the melt (nitrate decomposition) and of water (steam explosion) must be excluded. New salt melts, for example,

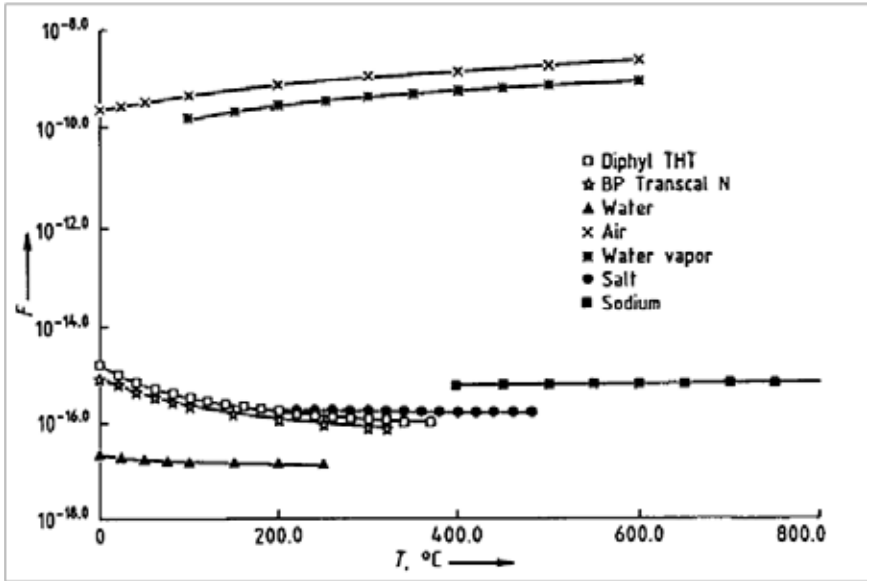

Fig. 70: The material-specific factor $F = \eta^{0.25}/c_p^{2.75} \cdot \rho^2$ for various heat-transfer media as a function of temperature

Table: Results of the example calculation

Heat-transfer medium	Producer	Pump power N, kW	Pressure drop Δp, bar	Mean temperature difference ΔT_m, K	Permitted cooling temperature increase ΔT_c, K
Water		0.060	0.008	0.75	5
Transcal N	BP	0.629	0.042	2.32	5
Diphyl THT	Bayer	0.862	0.054	2.35	5
Sodium		4.54	0.150	0.04	5
HT salt		1.31	0.105	1.45	5
Water vapor		0.119×10^{6}	8.759	1.30	5
Water vapor		0.254×10^{3}	0.175	14.22	150
Air		0.229×10^{6}	18.001	1.08	5
Air		0.456×10^{3}	0.341	12.29	150

based on carbonates are being developed for the temperature range 400 – 800°C. In this case it is not so much the thermal stability of the molten salt but rather the corrosion of the reactor materials that presents problems. Gases are the only heat transfer media usable over the entire temperature range, but because of their low density they have an unfavorable heat transport behavior (Fig. 70). They are therefore used exclusively as flue gases to supply heat at high temperatures. However large temperature differences between the heat-transfer medium and the reactor wall with possible adverse effects on the uniformity of the heat supply must then be accepted.

CONTINUOUS STIRRED-TANK REACTOR (CSTR)

The continuous stirred-tank reactor (CSTR), also known as vat- or back-mix reactor, is a common ideal reactor type in chemical engineering. A CSTR often refers to a model used to estimate the key unit operation variables when using a continuous agitated-tank reactor to reach a specified output. The mathematical model works for all fluids: liquids, gases, and slurries.

The behavior of a CSTR is often approximated or modeled by that of a Continuous Ideally Stirred-Tank Reactor (CISTR). All calculations performed with CISTRs assume perfect mixing. In a perfectly mixed reactor, the output composition is identical to composition of the material inside the reactor, which is a function of residence time and rate of reaction. If the residence time is 5-10 times the mixing time, this approximation is valid for engineering purposes. The CISTR model is often used to simplify engineering calculations and can be used to describe research reactors. In practice it can only be approached, in particular in industrial size reactors.

Assume:

—perfect or ideal mixing, as stated above

Integral mass balance on number of moles Ni of species i in a reactor of volume V. $[accumulation] = [in] - [out] + [generation]$.

1. $$\frac{dN_i}{dt} = F_{io} - F_i + V\nu_i r_i$$

where F_{io} is the molar flow rate inlet of species *i*, F_i the molar flow rate outlet, and V_i stoichiometric coefficient. The reaction rate, *r*, is generally dependent on the reactant concentration and the rate constant (k). The rate constant can be determined by using a known empirical reaction rates that is adjusted for temperature using the Arrhenius temperature dependence. Generally, as the temperature increases so does the rate at which the reaction occurs. Residence time, τ, is the average amount of time a discrete quantity of reagent spends inside the tank.

Assume:

- constant density (valid for most liquids; valid for gases only if there is no net change in the number of moles or drastic temperature change)
- isothermal conditions, or constant temperature (*k* is constant)
- steady state
- single, irreversible reaction ($\nu_A = -1$)
- first-order reaction ($r = kC_A$)

$A \rightarrow$ products

$N_A = C_A V$ (where C_A is the concentration of species A, V is the volume of the reactor, N_A is the number of moles of species A)

2. $$C_A = \frac{C_{Ao}}{1 + k\tau}$$

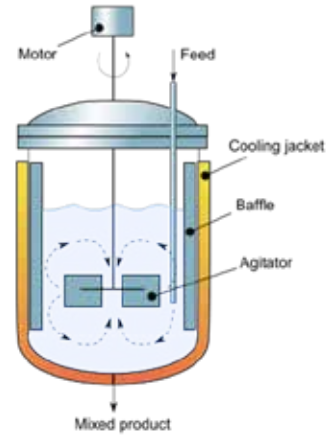

Fig. 71: Cross-sectional diagram of Continuous stirred-tank reactor

Fig. 71A: The picture of a CSTR

The values of the variables, outlet concentration and residence time, in Equation are major design criteria.

To model systems that do not obey the assumptions of constant temperature and a single reaction, additional dependent variables must be considered. If the system is considered to be in unsteady-state, a differential equation or a system of coupled differential equations must be solved.

CSTR's are known to be one of the systems which exhibit complex behavior such as steady-state multiplicity, limit cycles and chaos.

3. *Non-ideal CSTR*

The actual reaction volume will be affected by the non-uniform mixing (short-circuiting) or existence of dead zone areas. Temperature effect will also cause significant effect on the reaction rate.

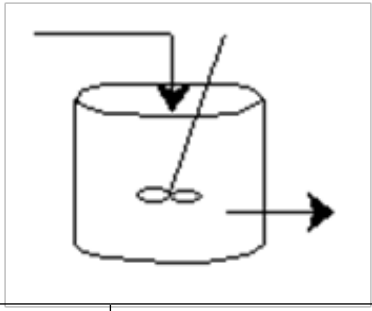

Type of Reactor	Characteristics
Continuously Stirred Tank Reactor (CSTR)	Run at steady state with continuous flow of reactants and products; the feed assumes a uniform composition throughout the reactor, exit stream has the same composition as in the tank

Kinds of Phases Present	Usage	Advantages	Disadvantages
1. Liquid phase 2 Gas-liquid phases 3. Solid-liquid phases	1. When agitation is required 2. Series configurations for different concentration streams	1. Continuous operation 2. Good temperature control 3. Easily adapts to two phase runs 4. Good control 5. Simplicity of construction 6. Low operating (labor) cost 7. Easy to clean	1. Lowest conversion per unit volume 2. By-passing and channeling possible with poor agitation

General Mole Balance Equation

$$F_{A0} - F_A + \int_0^V r_A \, dV = \frac{dN_A}{dt}$$

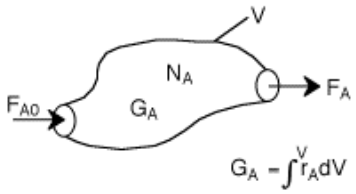

Assumptions

1. Steady state therefore

$$\frac{dN_A}{dt} = 0$$

2. Well mixed therefore r_A is the same throughout the reactor

$$\int_0^V r_A dV = r_A \int_0^V dV = r_A V$$

Rearranging the generation

$$V = \frac{F_{A0} - F_A}{-r_A}$$

In terms of conversion

$$X = \frac{F_{A0} - F_A}{F_{A0}}$$

$$V = \frac{F_{A0} X}{-r_A}$$

Reactor Sizing

Given $-r_A$ as a function of conversion, $-r_A = f(X)$, one can size any type of reactor. The volume of a CSTR can be represented as the shaded areas in the Levenspiel Plot shown below:

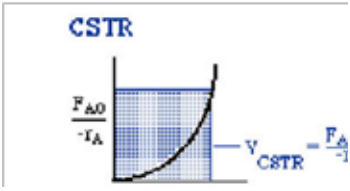

Reactors in Series

Given $-r_A$ as a function of conversion, $-r_A = f(X)$, one can also design any sequence of reactors in series provided there are no side streams by defining the overall conversion at any point.

$$X_i = \frac{\text{moles of A reacted up to point i}}{\text{moles of A fed to first reactor}}$$

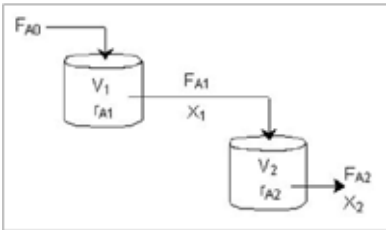

Mole Balance on Reactor 1

$$\text{In} - \text{Out} + \text{Generation} = 0$$

$$F_{A0} - F_{A1} + r_{A1}V_1 = 0$$

$$X_1 = \frac{F_{A0} - F_{A1}}{F_{A0}}$$

$$F_{A1} = F_{A0} - F_{A0}X_1$$

$$V_1 = \frac{F_{A0}X_1}{-r_{A1}}$$

Mole Balance on Reactor 2

$$\text{In} - \text{Out} + \text{Generation} = 0$$

$$F_{A1} - F_{A2} + r_{A2}V_2 = 0$$

$$X_2 = \frac{F_{A0} - F_{A2}}{F_{A0}}$$

$$F_{A2} = F_{A0} - F_{A0}X_2$$

$$V_2 = \frac{F_{A0}(X_2 - X_1)}{-r_{A2}}$$

Given $-r_A$ = f(X) the Levenspiel Plot can be used to find the reactor volume

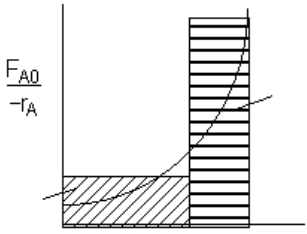

For a PFR between two CSTRs

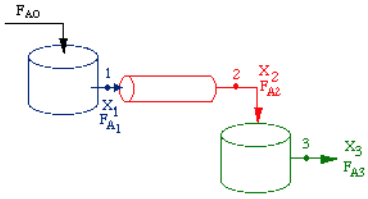

CONTINUOUS FLOW STIRRED TANK REACTOR (CFSTR)

A Continuous Flow Stirred Tank Reactor (CFSTR) is one in which the contents are stirred so uniformly that it is assumed that no variation or concentration gradients exist within the vessel. In theory, any sample taken from the overflow of the reactor will be identical with any sample taken from within the vessel. In this reactor there is an in-flow of nutrient and an equal out-flow of nutrient, plus microbial waste products and microbial cells.

In order to describe the nature of a CFSTR one should understand three parameters affecting reactor dynamics, these are (1) flow rate, (2) residence time and (3) dilution time.

(1) Flow rate Q=V/RT

That is Flow rate (Q) in ml/min is equal to the reactor volume (V) in ml, divided by the Residence Time (RT) in minutes. It can be measured empirically in a reactor in steady state, as the volume of effluent from the reactor per unit of time. In steady state the inflow and outflow of the reactor are equal and the culture volume of the reactor does not change.

(2) Retention time RT = V/Q

The residence time (RT) in minutes is the time it takes to entirely exchange the volume of the reactor and is expressed as shown above, where V = the volume of the reactor and Q is the flow rate of the effluent leaving the system.

(3) Flow Rate Q = V/RT

The flow rate (Q) (in ml/min) then is expressed as shown above, where V is the reactor volume and RT is the residence time. If for example the volume of the reactor is 400 ml and the flow rate is 40ml/min. then the Residence time R is 10 minutes.

(4) Dilution Rate D = Q/V

The dilution rate equals the flow rate divided by the reactor volume.

In the example above, the dilution rate is:

$$D = \frac{40 \text{ ml/min}}{400 \text{ ml}} = 0.1/\text{min}$$

That is 0.1 or 10% of the volume of the vessel is changed every minute.

In microbiology classes a CFSTR is called a chemostat. Adjusting the flow rate can alter the rate of growth of the culture therein. Reducing the flow rate permits the exhaustion of some nutrients and the accumulation of wastes slowing growth as the culture approaches stationary phase. Increasing the flow rate increases the nutrient concentration and reduces wastes bringing the culture closer to exponential phase. In a chemostat at steady state u (the instantaneous growth rate of the culture is equal to D (the dilution rate). If one increases the flow rate such that D > u then the planktonic culture is flushed from the system leaving only attached cells within the reactor. At this point the reactor is operating as a biofilm reactor. Of course planktonic cells are constantly being released from the biofilm by erosion or scheduled release but these cells are rapidly washed from the reactor.

Typically in setting up a reactor, the vessel is filled to capacity with nutrient medium, coupons are inserted and the reactor is seeded (inoculated) with the organism or combination of organisms desired. A time interval with the nutrient inflow closed is permitted in order for cells to attach to the coupons and then the influent is adjusted to a level which will rapidly clear the planktonic population (*i.e.* growth rate > residence time).

***Exercise*:** Building and Using a Biofilm Continuous Flow Stirred Reactor, a part of the Hypertext biofilm laboratory exercise collection describes the construction of a CFSTR.

This reactor may be fed either by gravity or by a pump from a nutrient medium reservoir. The waste medium is collected in a container and disinfected or autoclaved prior to disposal. The waste medium container should be placed in a tray or basin with sufficient capacity to hold the entire contents of the system in the unlikely event of a catastrophic failure. Here again the coupons used are typically glass microscope slides. The preprinted slides distributed by various companies are ideal for this purpose since they have printed on them slightly raised circles of uniform dimension so that, if one wishes to harvest cells from a known surface area, this can be readily done using the expression (Area = πr^2).

FLUIDIZED BED REACTOR

A fluidized bed reactor (FBR) is a type of reactor device that can be used to carry out a variety of multiphase chemical reactions. In this type of reactor,

a fluid (gas or liquid) is passed through a granular solid material (usually a catalyst possibly shaped as tiny spheres) at high enough velocities to suspend the solid and cause it to behave as though it were a fluid. This process, known as fluidization, imparts many important advantages to the FBR. As a result, the fluidized bed reactor is now used in many industrial applications.

Basic Principles

The solid substrate (the catalytic material upon which chemical species react) material in the fluidized bed reactor is typically supported by a porous plate, known as a distributor. The fluid is then forced through the distributor up through the solid material. At lower fluid velocities, the solids remain in place as the fluid passes through the voids in the material. This is known as a packed bed reactor. As the fluid velocity is increased, the reactor will reach a stage where the force of the fluid on the solids is enough to balance the weight of the solid material. This stage is known as incipient fluidization and occurs at this minimum fluidization velocity. Once this minimum velocity is surpassed, the contents of the reactor bed begin to expand and swirl around much like an agitated tank or boiling pot of water. The reactor is now a fluidized bed. Depending on the operating conditions and properties of solid phase various flow regimes can be observed in this reactor.

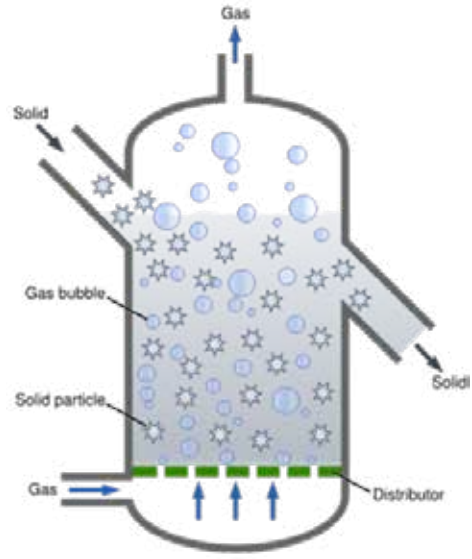

Fig. 72: A fluidized bed reactor

History and Current Uses

Fluidized bed reactors are a relatively new tool in the chemical engineering field. The first fluidized bed gas generator was developed by Fritz Winkler in Germany in the 1920s. One of the first United States fluidized bed reactors used in the petroleum industry was the Catalytic Cracking Unit, created in

Baton Rouge, LA in 1942 by the Standard Oil Company of New Jersey (now Exxon Mobil). This FBR and the many to follow were developed for the oil and petrochemical industries. Here catalysts were used to reduce petroleum to simpler compounds through a process known as cracking. The invention of this technology made it possible to significantly increase the production of various fuels in the United States. In the late 1980's, the work of Gordana V. Novakovic, Robert S. Langer, V.A. Shiva Ayyadurai and others began the use of fluidized bed reactors in biological sciences for understanding and visualizing the fluid dynamics of blood deheparinization. Today fluidized bed reactors are still used to produce gasoline and other fuels, along with many other chemicals. Many industrially produced polymers are made using FBR technology, such as rubber, vinyl chloride, polyethylene, styrenes, and polypropylene. Various utilities also use FBR's for coal gasification, nuclear power plants, and water and waste treatment settings. Used in these applications, fluidized bed reactors allow for a cleaner, more efficient process than previous standard reactor technologies.

Advantages

The increase in fluidized bed reactor use in today's industrial world is largely due to the inherent advantages of the technology.

—**Uniform Particle Mixing**: Due to the intrinsic fluid-like behavior of the solid material, fluidized beds do not experience poor mixing as in packed beds. This complete mixing allows for a uniform product that can often be hard to achieve in other reactor designs. The elimination of radial and axial concentration gradients also allows for better fluid-solid contact, which is essential for reaction efficiency and quality.

—**Uniform Temperature Gradients**: Many chemical reactions require the addition or removal of heat. Local hot or cold spots within the reaction bed, often a problem in packed beds, are avoided in a fluidized situation such as an FBR. In other reactor types, these local temperature differences, especially hotspots, can result in product degradation. Thus FBRs are well suited to exothermic reactions. Researchers have also learned that the bed-to-surface heat transfer coefficients for FBRs are high.

—**Ability to Operate Reactor in Continuous State**: The fluidized bed nature of these reactors allows for the ability to continuously

withdraw product and introduce new reactants into the reaction vessel. Operating at a continuous process state allows manufacturers to produce their various products more efficiently due to the removal of startup conditions in batch processes.

Disadvantages

As in any design, the fluidized bed reactor does have it draw-backs, which any reactor designer must take into consideration.

—**Increased Reactor Vessel Size**: Because of the expansion of the bed materials in the reactor, a larger vessel is often required than that for a packed bed reactor. This larger vessel means that more must be spent on initial capital costs.

—**Pumping Requirements and Pressure Drop**: The requirement for the fluid to suspend the solid material necessitates that a higher fluid velocity is attained in the reactor. In order to achieve this, more pumping power and thus higher energy costs are needed. In addition, the pressure drop associated with deep beds also requires additional pumping power.

—**Particle Entrainment**: The high gas velocities present in this style of reactor often result in fine particles becoming entrained in the fluid. These captured particles are then carried out of the reactor with the fluid, where they must be separated. This can be a very difficult and expensive problem to address depending on the design and function of the reactor. This may often continue to be a problem even with other entrainment reducing technologies.

—**Lack of Current Understanding**: Current understanding of the actual behavior of the materials in a fluidized bed is rather limited. It is very difficult to predict and calculate the complex mass and heat flows within the bed. Due to this lack of understanding, a pilot plant for new processes is required. Even with pilot plants, the scale-up can be very difficult and may not reflect what was experienced in the pilot trial.

—**Erosion of Internal Components**: The fluid-like behavior of the fine solid particles within the bed eventually results in the wear of the reactor vessel. This can require expensive maintenance and upkeep for the reaction vessel and pipes.

—**Pressure Loss Scenarios**: If fluidization pressure is suddenly lost, the surface area of the bed may be suddenly reduced. This can either be an inconvenience (*e.g.* making bed restart difficult), or may have more serious implications, such as runaway reactions (*e.g.* for exothermic reactions in which heat transfer is suddenly restricted).

Current Research and Trends

Due to the advantages of fluidized bed reactors, a large amount of research is devoted to this technology. Most current research aims to quantify and explain the behavior of the phase interactions in the bed. Specific research topics include particle size distributions, various transfer coefficients, phase interactions, velocity and pressure effects, and computer modeling. The aim of this research is to produce more accurate models of the inner movements and phenomena of the bed. This will enable chemical engineers to design better, more efficient reactors that may effectively deal with the current disadvantages of the technology and expand the range of FBR use.

BATCH REACTORS

Batch reactors are examples of "closed reactors" that is ones that, once seeded or inoculated, receive no further inputs of mass or energy and permit no outputs of waste materials. Batch reactors may be stirred or not stirred but in any case, conditions in the reactor are constantly changing. Nutrients and other materials like oxygen are declining and metabolic waste products are

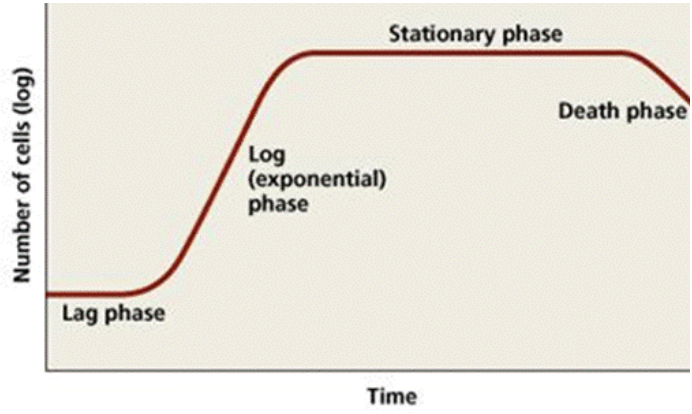

Fig. 73: Standard Growth Curve of a batch Reactor

increasing. Perhaps the simplest example of a batch "reactor" is a nutrient broth culture tube, although microbial colonies growing on slants or plates are also examples of batch processes.

The earliest "Mason Jar Reactors" mentioned above, were also batch reactors in which glass microscope slides were suspended as coupons (Glossary) in the reactor medium. In this reactor type cells will typically form biofilm on the coupons and on the walls of the reactor vessel but a large planktonic population will also co-exist in the reactor. Characklis and Marshall maintain that "a stable biofilm cannot be maintained in a batch or closed system".

The microbial growth pattern in a batch reactor is the well recognized growth curve memorized by every introductory microbiology student, consisting of a lag, an exponential, a stationary and, if the culture persists long enough, a death phase.

These conditions created in a batch reactor are not commonly found in nature. Nutrient and waste exchange almost always occur in natural systems although not in many industrial (and pre-industrial) processes. Sauerkraut, pickle, and kimchee production as well as the fermentation of beer, wine, and soy sauce are all carried out in batch culture.

Exercise 1, Making and using a *Batch Biofilm Reactor* gives detailed instructions on making inexpensive biofilm reactors not so different from those original "Mason Jar Reactors" used by investigators at the Center for Biofilm Engineering early in their work.

Fig. 74: A photograph showing exhaustion of nutrients and accumulation of waste products in a batch reactor.

Exercise 13, the Static Coupon Reactor. In this exercise, a piece of sterile filter paper is placed on the surface of a Tryptic Soy Agar plate. The filter paper is saturated with dilute medium such as 1/10 Tryptic Soy Broth. The filter paper is inoculated with the organisms of interest and a sterile microscope slide is placed on the filter paper. A thin layer of cells forms on the glass slide with no further input of nutrient and, of course waste products accumulate within the system. Although this is not a fluid system, it has some of the characteristics of a batch reactor as does any culture growing on a solid agar surface. This protocol was devised by scientists at the S.C. Johnson Corporation in order to produce consistent biofilms for testing their line of cleansing and disinfectant products.

MEMBRANE BIOREACTOR

Membrane Bioreactors combine conventional biological treatment processes with membrane filtration to provide an advanced level of organic and suspended solids removal. When designed accordingly, these systems can also provide an advanced level of nutrient removal. In an MBR system, the membranes are submerged in an aerated biological reactor. The membranes have porosities ranging from 0.035 microns to 0.4 microns (depending on the manufacturer), which is considered between micro and ultra filtration.

This level of filtration allows high quality effluent to be drawn through the membranes and eliminates the sedimentation and filtration processes typically used for wastewater treatment. Because the need for sedimentation is eliminated, the biological process can operate at a much higher mixed liquor concentration. This dramatically reduces the process tankage required and allows many existing plants to be upgraded without adding new tanks. To provide optimal aeration and scour around the membranes, the mixed liquor is typically kept in the 1.0-1.2% solids range, which is 4 times that of a conventional plant.

The membrane bioreactor has several distinct advantages over the Extended Aeration (EA) and Sequencing Batch Reactor (SBR) systems that make most regulatory agencies look favorably on MBRs, especially for small plants in environmentally sensitive areas. However, since the equipment is more costly than conventional plants, it is not the appropriate technology for every application. The key advantages of MBRs are that they provide a higher level of treatment and are much more resistant to upsets due to fluctuating influent

flows. In addition, if land is at a premium, the MBR system can be designed to have a much smaller footprint.

Some of the other benefits of MBRs include:

—Hydraulic Retention Time (HRT) of 4-8 hours *vs* 16-24 hours

—Solids Retention Time (SRT) of 15-365 days, can vary based on flow without negative process impact

—MLSS of 10-15,000 mg/L

—Sludge Yield of 20-40% less than conventional

—Footprint of 25% Conventional Plant

—Modular expand ability

—Highest quality effluent

—Capable of meeting AWT standards for nutrient removal

—Barrier to Giardia/Crypto

—Less susceptible to upsets due to flow variations

—Less odor

—Simple, yet sophisticated

To better explain the process, a schematic of a membrane system is provided below.

As noted, the membrane manufacturers that we are currently working with are Zenon and Kubota. Process-wise, these two systems are very similar and both will provide high quality effluent. However, there are several differences in how the membranes themselves are configured and, in turn, how the ancillary

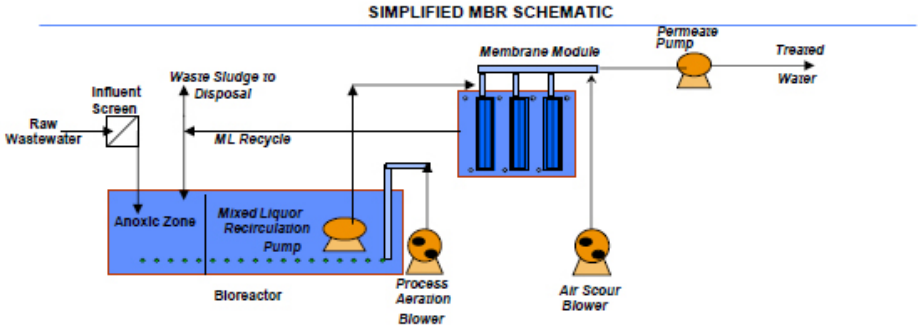

Fig. 75: Showing the Schematic diagram of Membrane Bioreactor (MBR)

Fig. 76: Showing the different types of Membrane Bioreactors

equipment (pumps, cleaning systems, valves) is configured to support each type of membrane.

Kubota is a plate membrane where the Zenon's ZeeWeed® is a hollow fiber membrane. The Kubota plate membrane is a slightly looser membrane. ZeeWeed®'s pore size is 0.1 micron (0.035 micron effective); Kubota's is 0.4 micron (0.1 micron effective). As such, in theory, Kubota's removal efficiency will not be as good as the Zenon hollow fiber system. However, it has proven it can meet all USEPA standards for public access reuse, it is has an order of magnitude better removal than a conventional sand or fabric filter and it will provide bacterial level removal.

In addition, as a hollow fiber, the Zenon system can operate at a higher suction pressure than the Kubota plate system. This differential does allow operators to "push" the Zenon system harder than the Kubota system when it is fouled. However, the looser Kubota membrane does allow a higher "flux rate", or gallons per day per square foot of membrane.

Though the tighter porosity of the Zenon membrane results in higher rates of particle rejection, it createsa more complex plant since Zenon requires an automatic backpulse system and Kubota does not. The Zenon backpulse system is used to force flow back through the fibers every 10-15 minutes to prevent plugging. This system is integrated into the permeate pump skid and requires up to 10 automatic valves.

Since the Kubota system does not use a back pulse system, the mechanics are much simpler. The process schematics provided below illustrate the differences between the permeate valving for these two systems.

Another key difference is how the membranes are cleaned. Both systems occasionally require an intense cleaning to remove excessive biogrowth and grease that can foul the membranes. The frequency of cleaning is a site-specific factor but for most plants, cleaning is required every three to six months. For this type of cleaning, the membranes soak in a dilute solution of sodium hypochlorite for a period of time before being returned to service. In certain cases, a mild acid or caustic solution may also be required.

For the Zenon system design, individual membrane chambers are provided to allow in situ cleaning of the membrane banks. Zenon membranes are taken

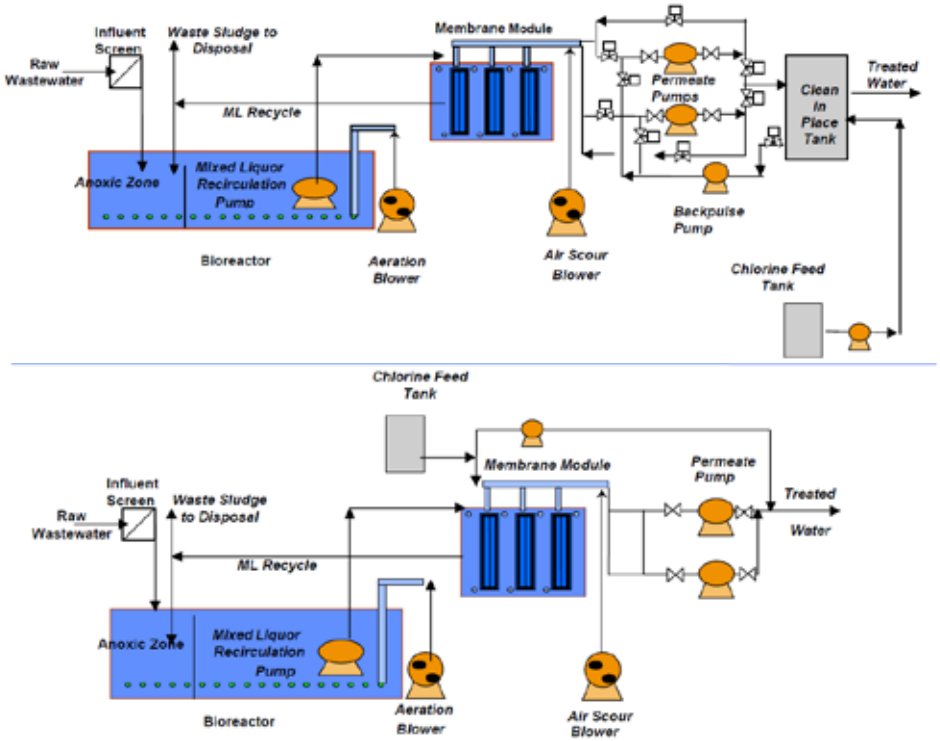

Fig. 77: Showing the schematic diagrams of Zenon ZeeWeed® and Kubota Mbrs

out of service, the chambers drained and the membranes are soaked for 24-48 hours in 200 to 1000 mg/L of bleach. Once clean, the chlorine remaining in the chamber can be readily deactivated by the addition of a dechlorination chemical such as dry sodium sulfite.

Unlike the Zenon system, the Kubota cleaning cycle can be done in the mixed liquor WITHOUT draining the tank. A dilute solution of bleach is allowed to flow by gravity back through the permeate lines. The solution soaks in the membranes for 1-2 hours, and then the plant is brought back on-line. Only a negligible fraction of the total biomass (*i.e.* that which is growing on each membrane plate) is killed off during this process due to the minimal amount of 0.5% to 1.0% bleach solution used. As a result, you still have an active biomass in the MBR upon startup after cleaning, resulting in a simplified cleaning process that minimizes downtime. If effluent requirements dictate, the "first flush" of the effluent after cleaning can be recycled to the head of the plant to minimize particulate release. However, very few plants will have this stringent an effluent requirement.

In addition to cleaning the membranes themselves, rags and stringy material can catch on the membranes fibers and casing and interfere with proper air scour. The Zenon membrane fibers are in cassettes and the entire

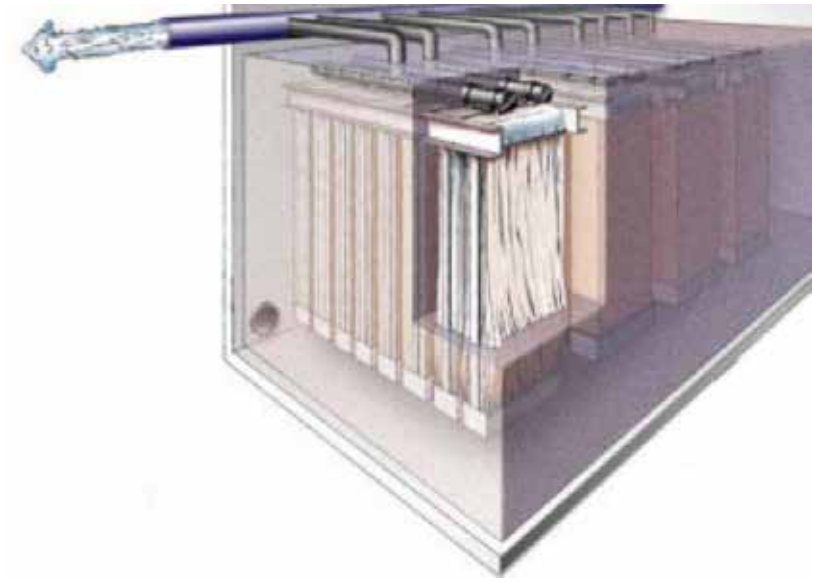

Fig. 79: Showing the Zenon Membrane and Membrane Bioreactor

cassette must be lifted out of the tank. Our experience is that this de-ragging is needed at least as frequently as the chlorine cleaning and therefore recommend installing a hoist and monorail or bridge crane with the Zenon systems.

Kubota has 50 to 400 membrane plates in each cassette and, if desired, the entire case can be lifted for maintenance. However, since individual plates can be pulled up by hand and de-ragged, the need for a permanent hoist is eliminated for smaller facilities.

When comparing MBRs to other processes, the issue of energy efficiency is often brought up. MBRs utilize aeration for membrane scour and require permeate pumping systems. At full design flow, MBRs typically use more power. However, few plants operate at full design flow, especially those in seasonal resorts. By properly designing the MBRs, portions of an MBR plant can be taken out of service and the cassettes can be cycled during low flow periods to provide a lower net energy cost.

In addition, because they do not need separate cleaning chambers, and because they are provided with a "box" to control the air scour, the Kubota flat plate membranes can be arranged in the final aeration chamber and the scour aeration can also provide process aeration. This can virtually eliminate the extra power due to scour aeration for this style of MBR. In summary, TSG has designed numerous MBR systems including 7 systems we have built and/or operated in the Caribbean. When considering whether to use this technology or not, the above listed advantages need to be weighed against the potential additional capital cost.

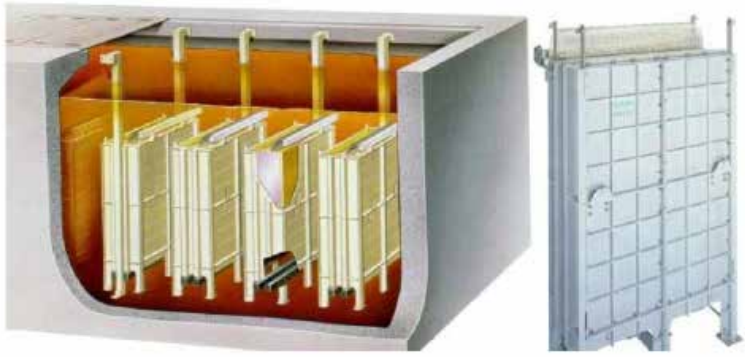

Fig. 78: Showing the Kubota Membrane and Membrane Bioreactor

When used with domestic wastewater, MBR processes could produce effluent of high quality enough to be discharged to coastal, surface or brackish waterways or to be reclaimed for urban irrigation. Other advantages of MBRs over conventional processes include small footprint, easy retrofit and upgrade of old wastewater treatment plants.

Fig. 80: The Operation of an Membrane Bioreactor

It is possible to operate MBR processes at higher mixed liquor suspended solids (MLSS) concentrations compared to conventional settlement separation systems, thus reducing the reactor volume to achieve the same loading rate.

Two MBR configurations exist: internal/submerged, where the membranes are immersed in and integral to the biological reactor; and external/sidestream, where membranes are a separate unit process requiring an intermediate pumping step.

Major Considerations in MBR

Fouling and Fouling Control

The MBR filtration performance inevitably decreases with filtration time. This is due to the deposition of soluble and particulate materials onto and into the membrane, attributed to the interactions between activated sludge components and the membrane. This major drawback and process limitation has been under investigation since the early MBRs, and remains one of the most challenging issues facing further MBR development.

In recent reviews covering membrane applications to bioreactors, it has been shown that, as with other membrane separation processes, membrane fouling is the most serious problem affecting system performance. Fouling leads to a significant increase in hydraulic resistance, manifested as permeate flux decline or transmembrane pressure (TMP) increase when the process is operated under constant-TMP or constant-flux conditions respectively. In systems where flux is maintained by increasing TMP, the energy required to achieve filtration increases. Alternatively frequent membrane cleaning is therefore required,

increasing significantly the operating costs as a result of cleaning agents and production downtime. More frequent membrane replacement is also expected.

Membrane fouling results from interaction between the membrane material and the components of the activated sludge liquor, which include biological flocs formed by a large range of living or dead microorganisms along with soluble and colloidal compounds. The suspended biomass has no fixed composition and varies both with feed water composition and MBR operating conditions employed. Thus though many investigations of membrane fouling have been published, the diverse range of operating conditions and feedwater matrices employed, the different analytical methods used and the limited information reported in most studies on the suspended biomass composition, has made it difficult to establish any generic behaviour pertaining to membrane fouling in MBRs specifically.

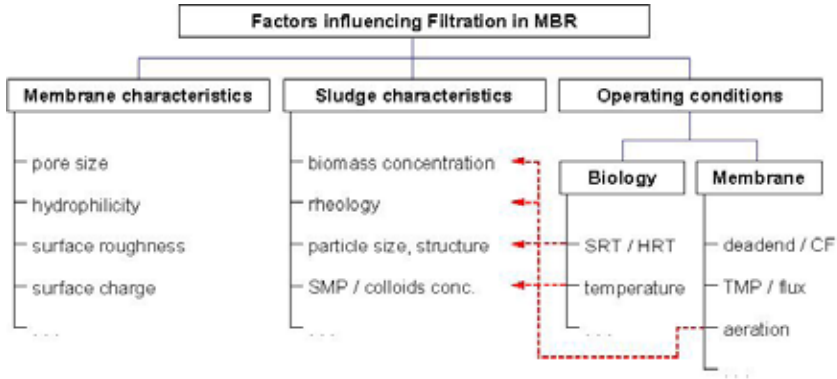

The air-induced cross flow obtained in submerged MBR can efficiently remove or at least reduce the fouling layer on the membrane surface. A recent review reports the latest findings on applications of aeration in submerged membrane configuration and describes the enhancement of performances offered by gas bubbling. As an optimal air flow-rate has been identified behind which further increases in aeration have no effect on fouling removal, the choice of aeration rate is a key parameter in MBR design.

Many other anti-fouling strategies can be applied to MBR applications. They comprise, for example:

—Intermittent permeation, where the filtration is stopped at regular time interval for a couple of minutes before being resumed. Particles

deposited on the membrane surface tend to diffuse back to the reactor; this phenomenon being increased by the continuous aeration applied during this resting period.

—Membrane backwashing, where permeate water is pumped back to the membrane, and flow through the pores to the feed channel, dislodging internal and external foulants.

—Air backwashing, where pressurized air in the permeate side of the membrane build up and release a significant pressure within a very short period of time. Membrane modules therefore need to be in a pressurised vessel coupled to a vent system. Air usually does not go through the membrane. If it did, the air would dry the membrane and a rewet step would be necessary, by pressurizing the feed side of the membrane.

—Proprietary anti-fouling products, such as Nalco's Membrane Performance Enhancer Technology.

In addition, different types/intensities of chemical cleaning may also be recommended:

—Chemically enhanced backwash (daily);

—Maintenance cleaning with higher chemical concentration (weekly);

—Intensive chemical cleaning (once or twice a year).

Intensive cleaning is also carried out when further filtration cannot be sustained because of an elevated transmembrane pressure (TMP). Each of the four main MBR suppliers (Kubota, Memcor, Mitsubishi and Zenon) have their own chemical cleaning recipes, which differ mainly in terms of

	Type	Chemical	Conc. (%)	Protocols
Mitsubishi	CIL	NaOCl	0.3	Backflow through membrane
		Citric acid	0.2	(2 hr) + soaking (2 hr)
Zenon	CIP	NaOCl	0.2	Backpulse and recirculate
		Citric acid	0.2-0.3	
Memcor	CIP	NaOCl	0.01	Recirculate through lumens,
		Citric acid	0.2	mixed liquors and in-tank air manifolds
Kubota	CIL	NaOCl	0.5	Backflow and soaking (2 hr)
CIL: Cleaning in line where chemical solutions are generally backflow (under gravity) inside the membrane.				
CIP: Cleaning in place where membrane tank is isolated and drained; the module is rinsed before being soaked in the cleaning solution and rinsed to remove excess of chlorine.				

concentration and methods. Under normal conditions, the prevalent cleaning agents remain NaOCl (Sodium Hypochlorite) and citric acid. It is common for MBR suppliers to adapt specific protocols for chemical cleanings (*i.e.* chemical concentrations and cleaning frequencies) for individual facilities.

Biological Performances/Kinetics

COD Removal and Sludge Yield

Simply due to the high number of microorganism in MBRs, the pollutants uptake rate can be increased. This leads to better degradation in a given time span or to smaller required reactor volumes. In comparison to the conventional activated sludge process (ASP) which typically achieves 95%, COD removal can be increased to 96-99% in MBRs. COD and BOD_5 removal are found to increase with MLSS concentration. Above 15g/L COD removal becomes almost independent of biomass concentration at >96%. Arbitrary high MLSS concentrations are not employed, however, as oxygen transfer is impeded due to higher and Non-Newtonian fluid viscosity. Kinetics may also differ due to easier substrate access. In ASP, flocs may reach several 100 μm in size. This means that the substrate can reach the active sites only by diffusion which causes an additional resistance and limits the overall reaction rate (diffusion controlled). Hydrodynamic stress in MBRs reduces floc size (to 3.5 μm in sidestream MBRs) and thereby increases the apparent reaction rate. Like in the conventional ASP, sludge yield is decreased at higher SRT or biomass concentration. Little or no sludge is produced at sludge loading rates of 0.01 kgCOD/(kgMLSS d). Due to the biomass concentration limit imposed, such low loading rates would result in enormous tank sizes or long HRTs in conventional ASP.

Nutrient Removal

Nutrient removal is one of the main concerns in modern wastewater treatment especially in areas that are sensitive to eutrophication. Like in the conventional ASP, currently, the most widely applied technology for N-removal from municipal wastewater is nitrification combined with denitrification. Besides phosphorus precipitation, enhanced biological phosphorus removal (EBPR) can be implemented which requires an additional anaerobic process step. Some characteristics of MBR technology render EBPR in combination with post-denitrification an attractive alternative that achieves very low nutrient effluent concentrations.

Anaerobic MBRs

Anaerobic MBRs were introduced in the 1980s in South Africa and currently see a renaissance in research. However, anaerobic processes are normally used when a low cost treatment is required that enables energy recovery but does not achieve advanced treatment (low carbon removal, no nutrients removal). In contrast, membrane-based technologies enable advanced treatment (disinfection), but at high energy cost. Therefore, the combination of both can only be economically viable if a compact process for energy recovery is desired, or when disinfection is required after anaerobic treatment (cases of water reuse with nutrients). If maximal energy recovery is desired, a single anaerobic process will be always superior to a combination with a membrane process.

Table 3: Process conditions and degrees of removal in typical conventional ASP and selected MBR plants for municipal wastewater treatment ([a] Mudrack and Kunst, 1985, [b] MUNLV, 2003, [c] Cicek et al., 1999, [d] Hotchkies, [e] Kraume and Bracklow, 2003, [f] Tazi-Pain et al., 2002, [g] de Haas et al., 2004, [h] Mallia et al., 2001, [i] Gander et al., 2000).

	Unit	Conventional ASP[a,b,c]	MBR[b]	MBR[c]	ZenoGem Milton, (USA)[d]	6 German 750-12,000 EP plants[e]	BIOSEP (France)[f]	Magnetic Island (Australia)[g]
SRT	d	10-25	< 30	30	> 15[h]	25-28	> 20	30
HRT	h	4-8[i]	> 6	8[i]	3	< 10		
MLSS	kg m^{-3}	5	12-16		15-20[h]	8-16, mainly 12	15	15
BOD_5 loading rate	kg m^{-3} d^{-1}	0.25 0.32-0.64[i]		0.4-0.7	2.5	0.32-0.79		
BOD_5 (F:M)	kg kg^{-1} d^{-1}	0.05	< 0.08		< 0.2	0.02-0.066		
BOD_5 removal effluent conc.	% mg L^{-1}	85-95[i] 15		98-99[i]	> 99 < 2	98 < 5	> 97.5	 < 3
COD removal effluent conc.	% mg L^{-1}	94.5	< 30	99		96.1 < 25	97	
TSS removal TSS turbidity	% mg L^{-1} NTU	60.9 10-15	0	99.9	> 99 < 2 < 0.1	0	99.8	 0.6
N_{total} removal effluent conc. NH_4^+ removal	% mg L^{-1} %	 < 13 98.9	< 13	 99.2	> 96 (TKN) < 2 (TKN) < 0.5 mg L^{-1}	92 < 10 < 1 mg L^{-1}	98.6 (TKN) 0.4 (TKN)	 < 2 (with sugar dosing)
P_{total} removal effluent conc.	% mg L^{-1}	88.5 0.8-1	< 0.3	96.6	> 99 < 0.1	86.5 1		 < 0.3

Mixing/Hydrodynamics

Like in any other reactors, the hydrodynamics (or mixing) within an MBR plays an important role in determining the pollutant removal and fouling control within an MBR. It has a substantial effect on the energy usage and size requirements of an MBR, therefore the whole life cost of an MBR is high. The removal of pollutants is greatly influenced by the length of time fluid elements

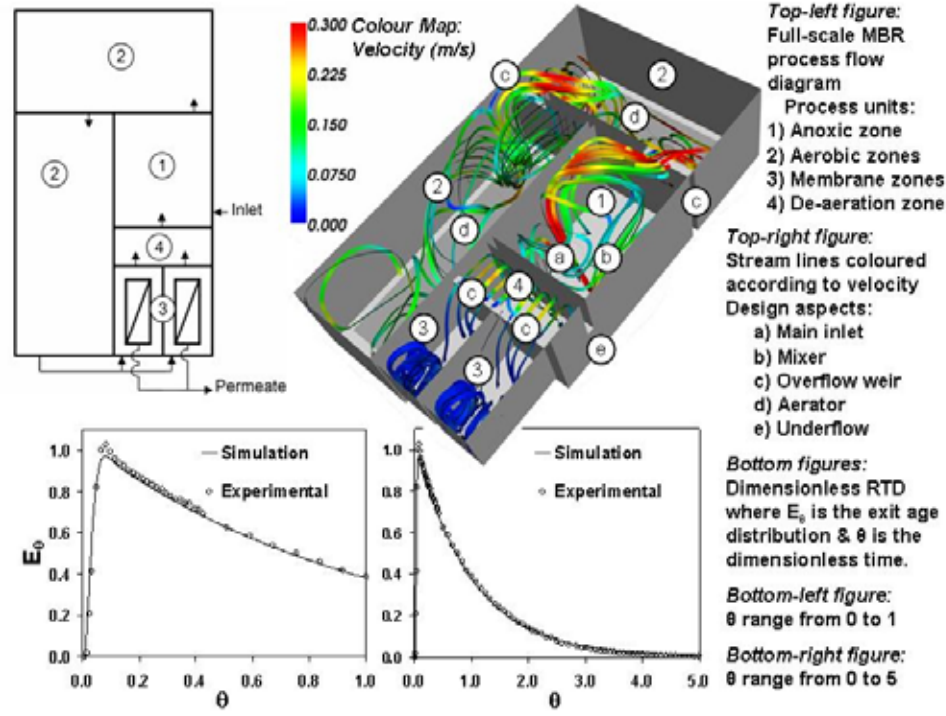

Fig. 81: Example of computational fluid dynamic (CFD) modelling results (streamlines) for a full scale MBR (Adapted from the Project AMEDEUS – Australian Node Newsletter August 2007

spend in the MBR (*i.e.* the residence time distribution or RTD). The residence time distribution is a description of the hydrodynamics/mixing in the system and is determined by the design of the MBR (*e.g.* MBR size, inlet/recycle flowrates, wall/baffle/mixer/aerator positioning, mixing energy input). An example of the effect of mixing is that a continuous stirred-tank reactor will not have as high pollutant conversion per unit volume of reactor as a plug flow reactor. The control of fouling, as previously mentioned, is primarily undertaken using coarse bubble aeration. The distribution of bubbles around the membranes, the shear at the membrane surface for cake removal and the size of the bubble are greatly influenced by the mixing/hydrodynamics of the system. The mixing within the system can also influence the production of possible foulants. For example, vessels not completely mixed (*i.e.* plug flow reactors) are more susceptible to the effects of shock loads which may cause cell lysis and release of soluble microbial products.

Many factors affect the hydrodynamics of wastewater processes and hence MBRs. These range from physical properties (*e.g.* mixture rheology and gas/liquid/solid density etc.) to the fluid boundary conditions (*e.g.* inlet/outlet/recycle flowrates, baffle/mixer position etc.). However, many factors are peculiar to MBRs, these cover the filtration tank design (*e.g.* membrane type, multiple outlets attributed to membranes, membrane packing density, membrane orientation etc.) and its operation (e.g. membrane relaxation, membrane back flush etc.).The mixing modelling and design techniques applied to MBRs are very similar to those used for conventional activated sludge systems. They include the relatively quick and easy compartmental modelling technique which will only derive the RTD of a process (*e.g.* the MBR) or the process unit (*e.g.* membrane filtration vessel) and relies on broad assumptions of the mixing properties of each sub unit. Computational fluid dynamics modelling (CFD) on the other hand does not rely on broad assumptions of the mixing characteristics and attempts to predict the hydrodynamics from a fundamental level. It is applicable to all scales of fluid flow and can reveal much information about the mixing in a process, ranging from the RTD to the shear profile on a membrane surface. Investigations of MBR hydrodynamics have occurred at many different scales, ranging from examination of shear stress at the membrane surface to RTD analysis of the whole MBR. Cui *et al.* (2003) investigated the movement of Taylor bubbles through tubular membranes, Khosravi, M. (2007) examined the entire membrane filtration vessel using CFD and velocity measurements, while Brannock *et al.* (2007) examined the entire MBR using tracer study experiments and RTD analysis.

PLUG FLOW REACTORS

The plug flow reactor (PFR, sometimes called continuous tubular reactor, CTR, or piston flow reactors) is a model used to describe chemical reactions in continuous, flowing systems of cylindrical geometry (see the drawing). The PFR model is used to predict the behaviour of chemical reactors of such design, so that key reactor variables, such as the dimensions of the reactor, can be estimated.

Fluid going through a PFR may be modeled as flowing through the reactor as a series of infinitely thin coherent "plugs", each with a uniform composition, traveling in the axial direction of the reactor, with each plug having a different

composition from the ones before and after it. The key assumption is that as a plug flows through a PFR, the fluid is perfectly mixed in the radial direction but not in the axial direction (forwards or backwards). Each plug of differential volume is considered as a separate entity, effectively an infinitesimally small continuous stirred tank reactor, limiting to zero volume. As it flows down the tubular PFR, the residence time (τ) of the plug is a function of its position in the reactor. In the ideal PFR, the residence time distribution is therefore a Dirac delta function with a value equal to τ.

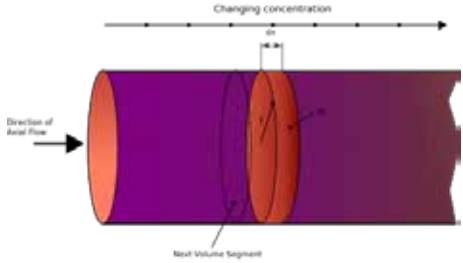

Fig. 82: Schematic diagram of a Plug Flow Reactor (PFR)

PFR modeling

The PFR is governed by ordinary differential equations, the solution for which can be calculated providing that appropriate boundary conditions are known. The PFR model works well for many fluids: liquids, gases, and slurries. Although turbulent flow and axial diffusion cause a degree of mixing in the axial direction in real reactors, the PFR model is appropriate when these effects are sufficiently small that they can be ignored. In the simplest case of a PFR model, several key assumptions must be made in order to simplify the problem, some of which are outlined below. Note that not all of these assumptions are necessary, however the removal of these assumptions does increase the complexity of the problem. The PFR model can be used to model multiple reactions as well as reactions involving changing temperatures, pressures and densities of the flow. Although these complications are ignored in what follows, they are often relevant to industrial processes.

Assumptions:

- plug flow
- steady state
- constant density (reasonable for some liquids but a 20% error for polymerizations; valid for gases only if there is no pressure drop, no net change in the number of moles, nor any large temperature change)
- single reaction occurring in the bulk of the fluid (homogeneously).

A material balance on the differential volume of a fluid element, or plug, on species i of axial length dx between x and x + dx gives:

[accumulation] = [in] - [out] + [generation] - [consumption]

Accumulation is 0 under steady state; therefore, the above mass balance can be re-written as follows:

1. $F_i(x) - F_i(x + dx) + A_t dx \nu_i r = 0.$

where:

- x is the reactor tube axial position, m
- dx the differential thickness of fluid plug
- the index i refers to the species i
- $F_i(x)$ is the molar flow rate of species i at the position x, mol/s
- D is the tube diameter, m
- A_t is the tube transverse cross sectional area, m^2
- ν is the stoichiometric coefficient, dimensionless
- r is the volumetric source/sink term (the reaction rate), mol/m^3s.

The flow linear velocity, u (m/s) and the concentration of species i, C_i (mol/m^3) can be introduced as:

$$u = \frac{\dot{v}}{A_t} = \frac{4\dot{v}}{\pi D^2} \quad \text{and} \quad F_i = A_t u C_i$$

On application of the above to Equation 1, the mass balance on i becomes:

2. $A_t u[C_i(x) - C_i(x + dx)] + A_t dx \nu_i r = 0.$

When like terms are cancelled and the limit $d_x \rightarrow 0$ is applied to Equation 2 the mass balance on species i becomes

3. $u\frac{dC_i}{dx} = \nu_i r.$

The temperature dependence of the reaction rate, r, can be estimated using the Arrhenius equation. Generally, as the temperature increases so does the rate at which the reaction occurs. Residence time, , is the average amount of time a discrete quantity of reagent spends inside the tank.

Assume:

- isothermal conditions, or constant temperature (k is constant)
- single, irreversible reaction ($\nu_A = -1$)
- first-order reaction ($r = k C_A$)

After integration of Equation 3 using the above assumptions, solving for $C_A(x)$ we get an explicit equation for the concentration of species A as a function of position:

4. $C_A(x) = C_{A0}e^{-k\tau}$,

where C_{A0} is the concentration of species A at the inlet to the reactor, appearing from the integration boundary condition.

Operation and Uses

PFRs are used to model the chemical transformation of compounds as they are transported in systems resembling "pipes". The "pipe" can represent a variety of engineered or natural conduits through which liquids or gases flow. (*e.g.* rivers, pipelines, regions between two mountains, etc.) An ideal plug flow reactor has a fixed residence time: Any fluid (plug) that enters the reactor at time will exit the reactor at time, where τ is the residence time of the reactor. The residence time distribution function is therefore a dirac delta function at. A real plug flow reactor has a residence time distribution that is a narrow pulse around the mean residence time distribution. A typical plug flow reactor could be a tube packed with some solid material (frequently a catalyst). Typically these types of reactors are called packed bed reactors or PBR's. Sometimes the tube will be a tube in a shell and tube heat exchanger.

Advantages and Disadvantages

CSTRs (Continuous Stirred Tank Reactor) and PFRs have fundamentally different equations, so the kinetics of the reaction being undertaken will to some extent determine which system should be used. However there are a few general comments that can be made with regards to PFRs compared to other reactor types. Plug flow reactors have a high volumetric unit conversion, run for long periods of time without maintenance, and the heat transfer rate can be optimized by using more, thinner tubes or fewer, thicker tubes in parallel. Disadvantages of plug flow reactors are that temperatures are hard to control and can result in undesirable temperature gradients. PFR maintenance is also more expensive than CSTR maintenance. Through a recycle loop a PFR is able to approximate a CSTR in operation. This occurs due to a decrease in the concentration change due to the smaller fraction of the flow determined by the feed; in the limiting case of total recycling, infinite recycle ratio, the PFR perfectly mimics a CSTR.

Applications

Plug flow reactors are used for some of the following applications:

- Large-scale reactions
- Fast reactions
- Homogeneous or heterogeneous reactions
- Continuous production
- High-temperature reactions

SOLID STATE FERMENTATION BIOREACTOR

Introduction

Solid state fermentation (SSF) involves the growth of microorganisms on moist solid substrates in the absence of visible water between the substrate particles (Pandey *et al.*, 2001). Compared to submerged fermentation, the solid media used in SSF contain less water but an important gas phase exists between the particles (Durand, 2003). This feature is of great importance because of the poor thermal conductivity of the air compared to the water. As a result of the low Aw in SSF bioreactors, smaller fermenters are required and more concentrated products are produced, simultaneously reducing energy requirements for downstream processing (Robinson *et al.*, 2001; Robinson and Nigam, 2003). However, this technique shows several disadvantages over submerged fermentation (SmF), which have discouraged its use for industrial production (Hölker *et al.*, 2004). One of the major obstacles is the limited knowledge related to the design and operation of large-scale bioreactors (Ashley *et al.*, 1999; Durand and Chereau, 1987).

Difficulties in controlling important culture parameters, such as mass transfer and heat removal, have not been overcome completely (Fujian *et al.* 2002). The low moisture and poor thermal conductivity of the substrate make heat transfer and temperature control difficult in SSF (Bhargav *et al.* 2008). Many bioreactors have been traditionally used in SSF processes. These can be mainly classified in two groups: the ones which show an agitation system and the ones which work in static conditions. The first category comprises rotating drums, gas-solid fluidized beds, rocking drums, horizontal paddle mixer, etc, while the second one includes the packed-bed and the trays bioreactor. Static beds are required when the substrate bed must remain static throughout the

growth phase or when the substrate particles have to be knitted together by the fungal mycelium, such as in the production of fermented foods like Tempe (Mitchell and von Meien, 2000). On the other hand, the use of mixed bioreactors improves the homogeneity of the bed and ensures an effective heat and mass transfer (Bhargav *et al.* 2008). However, the shear forces caused by rotation and agitation damage or disrupt fungal mycelia and reduce the porosity of the substrates (Fujian *et al.*, 2002; Ramesh and Lonsane, 1990; Fernandez *et al.*, 1996). It has been demonstrated that enzymatic extracts obtained from the fungus *Aspergillus awamori* grown on grape pomace as the sole solid substrate produces pectinases, xylanases and cellulases by SSF. We are now interested in the study of the mentioned enzymes in a laboratory scale bioreactor, using a rotating drum with this purpose. In spite of this configuration is considered to be better and more uniform than other fermenters, fungal cultures can be damaged as a consequence of the shear forces during mixing (Pandey *et al.*, 2001). For this reason, the effect of the type of agitation on the enzyme production at different air-flow rates was evaluated.

Materials and Methods

Spore Production

Aspergillus awamori 2B.361 U2/1, classified by the Commonwealth Mycological Institute as *Aspergillus niger* complex, was propagated and stored on slants which contained a synthetic medium for fungal growth composed of (g/L): 1 peptone, 0.5 yeast extract, 15 agar, 6 xylan and 1 pectin. This medium contains xylan and pectin as sole carbon sources to induce the production of xylanase and exo-polygalacturonase. Spores stored on synthetic medium slants were washed with 10 ml of 0.9% NaCl. The spore solution (0.5 ml) was spread on the surface of 100 ml synthetic medium in Erlenmeyer flasks (500 ml), and incubated at 30°C for 5 days. After the incubation period, 10 ml of 0.9% NaCl solution was added to the flasks and the spores were suspended by gentle shaking. The number of spores was counted in an Improved Neubauer Counting Chamber. Inoculums concentrations were adjusted to 4.5×10^8 spores/g solid substrate.

Solid Substrate for Fermentations

White grape pomace from the Xerez-Sheres-Sherry area in Spain (*Palomino Fino* variety) was used as natural substrate for the SSF experiments. Different samples of white virgin pomace were collected. The pomace was obtained from

a local wine cellar after pressing the above mentioned variety of grape and stored at –24°C until use. For any given series of experiments, sub-samples (250 g) were taken and defrosted to ambient temperature. The solid was then washed several times with distilled water to reduce its high reducing sugars content. After this, it was dried in an oven (60°C for 48h), milled and sieved (56.3% of the total weight of particles was over 1 mm in diameter). Finally, the solid was sterilized in an autoclave for 20 min at 120°C and 1.2 atm. Orange peels (Washington Navel variety) were obtained after juice extraction from oranges collected at a local market. Samples were stored at -24°C. Before their use in SSF experiments, orange peels were defrosted and extensively washed in order to remove all water soluble compounds. Solid was dried at 60°C for 48 h., then milled (62.8% of its weight was constituted of particles over 1 mm in diameter) and finally sterilized in an autoclave (20 min, 120°C, 1.2 atm). When mixtures of grape pomace and orange peels were used, both residues were conditioned separately as it has been previously described, mixed in a 1:1 proportion and sterilized in an autoclave.

Rotating Drum

The fermentor consists of a 250 mL glass roller bottle (Ø 7 cm) connected to a filtered-air supply (Figure 83). Air flow is measured by a rotameter and then is sterilized by passing through a 0.45 μm cellulose filter. The humidifier system is based on a glass column filled with glass beads (3mm) and sterilized distilled water. The air is introduced in the roller bottle through a syringe, which is assembled to a barbed wire to remove the solid stuck in the bottle.

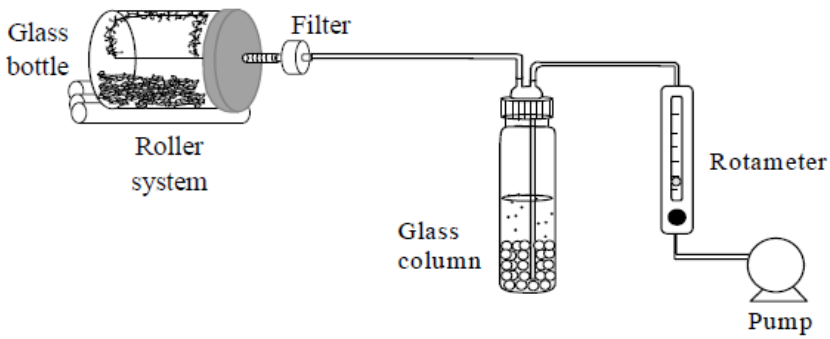

Fig. 83: The diagram of the Laboratory rotatory drum bioreactor

For the experiments carried out in agitation, the bottle is placed in a roller system composed of 5 cylinders which rotate continuously. In this way, the mixture of the media of fermentation is produced as consequence of the movement of the bottle. For the fermentations, 10 g of pre-inoculated solid substrate with 4.5×10^8 spores/g were added to the bottle. The bed reached a length of 2.5 cm leaving enough space to obtain good agitation. The system was incubated at 27°C for 5 days. The effects of aeration and agitation in the production of xylanase, exo-PG and CMCase were evaluated in the rotating drum. For this purpose, the air flow rates of 0, 9, 120 and 200 mL/min in static were tested, studying different kind of agitation: constant and intermittent (one agitation of 1 min/day and 2 agitations of 10 min/day).

Extraction Conditions

After the fermentation, the media was spilled in Erlenmeyer flasks containing 70 mL of Tween 80 (0.01%) and then stirred in a rotary shaker (150 rpm, 30 min, 4°C). These conditions of extraction were optimized in a previous work (Diaz *et al.*, 2007). The suspension resulting after the extraction was centrifuged at 10000 rpm for 10 minutes at 4°C. The supernatant obtained—the enzymatic extract—was stored at -20°C until required for analysis.

In each sample, the concentration of reducing sugar, the pH and xylanase, exo-PG and CMC-ase activities were evaluated.

Enzyme Assay

The enzymatic activities of xylanase (EC 3.2.1.8), exo-polygalacturonase (EC 3.2.1.67) and CMC-ase (EC 3.2.1.4) in the different extracts obtained were assayed. For the xylanase, the reaction mixture containing 0.1 mL of enzymatic extract and 0.9 mL of xylan suspension (0.5%w/w Birchwood xylan in 0.05M citrate buffer, pH 5.4) was incubated at 50°C for 10 min. The reducing sugars produced were measured by a modification of the dinitrosalicylic acid method (DNS) using D-xylose as the standard (Miller, 1959). They are given in mmol per gram of dried solid (mmol/gds). CMC-ase activity was determined by the same procedure described for xylanase, but carboxymethyl-cellulose (Panreac) was used as substrate. Exo-polygalacturonase (Exo-PG) activity was evaluated by adding 0.2 mL of enzymatic extract to 0.8 mL of pectin solution (0.5% pectin in 0.1M acetate buffer, pH 5.0). Samples were incubated at 45°C for 10 min and the reducing groups in the enzymatic extract were determined by the DNS method.

All the measurements were made in duplicate and the results are expressed as reducing sugars using a calibration curve. A unit of enzyme activity (IU) was defined as the amount of enzyme producing 1 μmol of reducing sugars per minute at the specified conditions.

Results and Discussion

The concentration of reducing sugar, pH and xylanase, exo-PG and CMC-ase activities were assayed in the extracts obtained from the bioreactor in the different conditions tested. As every experiment was made in duplicate, the average values and the confidence limits for a probability of 95% are also shown.

Different air flow rates were evaluated in order to identity the best aeration for the production of the highest enzyme activities. The effect of the type of agitation was also tested. The concentration of reducing sugars analysed in all the extracts was very low, around 0.020 mmol/gds, with the exception of

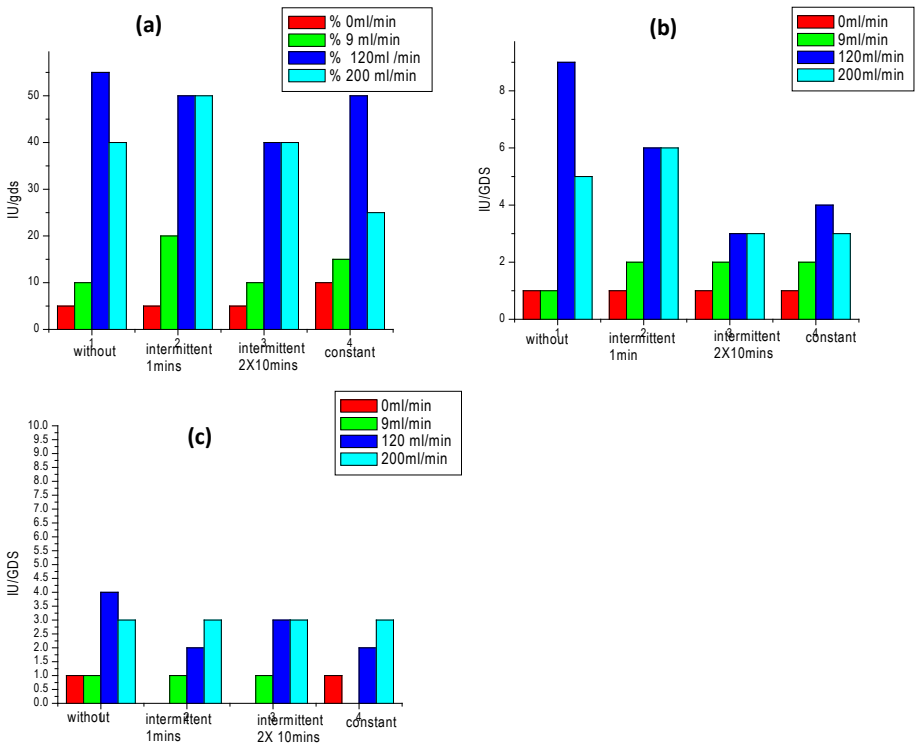

Fig. 84: Effect of the type of agitation at different air flow rates in enzyme production (a. xylanase, b. exo-PG and c. CMC-ase) using the rotating drum.

the experiments carried out without force aeration in static and with constant agitation (data not shown). In these situations, the reducing sugars were not consumed because the fungus didn't grow properly. When the media was not agitated neither aerated it could be explained considering that there wasn't enough oxygen to obtain good growth. In relation to the experiment carried out without aeration in constant agitation, the mycelium and the substrate particles were agglomerated. In these conditions, the heat, mass and oxygen transfers were greatly reduced, affecting the fungus growth. The pH values of the extracts agreed with the results of the reducing sugars (data not shown). The experiments carried out without force aeration, in static and with constant agitation, showed a pH of 3.5, which is the typical value of the substrate before the fermentation. This fact confirms that good growth had not been produced in these conditions. Enzyme activities measured for the studied enzymes are shown in Figure 84.

It can be observed that the air flow rate influenced in xylanase production, analysing the highest activities with 120 and 200 mL/min. On the other hand, the effect of agitation depended on the air flow rate used. When force aeration wasn't applied, the xylanase activities measured were very low and practically the same with all the types of agitation used. In these conditions the fungus didn't possessed enough oxygen to grow properly and produce enzymes. The maximum xylanase activity obtained with 9 mL/min (19.52 ± 6.39 IU/gds) was attained with an intermittent agitation of 1 min/day. At low flow rates, a soft aeration could improve O_2 and CO_2 transfer; however, a more frequent agitation could damage fungal cultures as a consequence of the shear forces during mixing. A similar effect was observed with 120 mL/min, analysing the lowest xylanase activity when the system was agitated twice a day and continuously. However, this flow rate provided enough oxygen for the metabolism of the fungus and, in consequence, for xylanase production because it wasn't necessary to agitate the system to attain the maximum activity of 54.42 ± 2.88 IU/gds. This value is 10 times higher than the one obtained in the same conditions without force aeration. Moreover, it was of the same order of magnitude as the maximum attained with the flow rate of 200 mL/min. Thus, a flow rate of 120 mL/min was enough to produce the highest xylanase activity. The type of agitation didn't show an important effect in exo-PG and CMC-ase production with 0 and 9 mL/min, moreover, low activities were measured under these conditions

of aeration. As it happened with xylanase, the maximum exo-PG and CMC-ase activities (8.77 ± 0.88 and 3.69 ± 0.05 IU/gds, respectively) were reached using a flow rate of 120 mL/min. This aeration provided enough oxygen for the metabolism of the fungus and, in consequence, for the enzyme production being unnecessary the agitation of the system. The application of a higher flow rate didn't increase exo-PG and CMC-ase production. The highest exo-PG and CMC-ase activities, obtained with 200 mL/min were assayed when the system was not agitated or it was done 1 min/day. A more frequent agitation could damage fungal cultures as a consequence of the shear forces during mixing. The production of enzymes using a rotating drum has been reported for other authors. For example, Kalogeris *et al.* used a laboratory-scale rotating drum to study the effect of the air flow in the production of cellulases and hemicellulases (Kalogeris *et al.*, 1999; Kalogeris *et al.*, 2003). The results revealed that high aeration favoured both biomass and enzyme production. However, there was a maximum air flow rate above which the enzyme recovery didn't enhance.

Conclusions

A laboratory rotating drum bioreactor was designed and operated for the production of hydrolytic enzymes by solid state fermentation on a mixture 1:1 (w/w) of grape pomace and orange peels. In this reactor, the air flow rate shows a significant effect on enzyme activity, which increases when aeration is used rather than a static environment. The maximum enzyme activities were attained in static conditions using an air flow rate of 120 mL/min. Although this reactor was designed to work in agitation, the best results were reached in static or with low agitation (1min/day).

ALGAE BIOREACTOR

Historical Background

The first experiments with the aim of cultivating algae were conducted in 1957 by the "Carnegie Institution" in Washington. In these experiments, the mono-cellular Chlorella were cultivated by adding CO_2 and some minerals. In the early days, bioreactors were used which were made of glass and later changed to a kind of plastic bag. The goal of all this research has been the cultivation of algae to produce a cheap animal feed.

Introduction

An algae bioreactor or photo bioreactor is used for cultivating algae on purpose to fix CO_2 or produce biomass. Specifically, algae bioreactors can be used to produce fuels such as biodiesel and bioethanol, to generate animal feed, or to reduce pollutants such as NOx and CO_2 in flue gases of power plants. Fundamentally, this kind of bioreactor is based on the photosynthetic reaction which is performed by the chlorophyll-containing algae itself using dissolved carbon dioxide and sunlight energy. The carbon dioxide is dispersed into the reactor fluid to make it accessible for the algae. The bioreactor has to be made out of transparent material. The algae are photoautotroph organisms which perform oxygenetic photosynthesis.

Frequently Used Photo Reactor Types

Nowadays 3 basic types of algae photobioreactors have to be differentiated, but the determining factor is the unifying parameter—the available intensity of sunlight energy.

Plate Photobioreactor

A plate reactor simply consists of vertically arranged or inclined rectangular boxes which are often divided in two parts to effect an agitation of the reactor fluid. Generally these boxes are arranged to a system by linking them. Those connections are also used for making the process of filling/emptying, introduction of gas and transport of nutritive substances, easier. The introduction of the flue gas mostly occurs at the bottom of the box to ensure that the carbon dioxide has enough time to interact with algae in the reactor fluid.

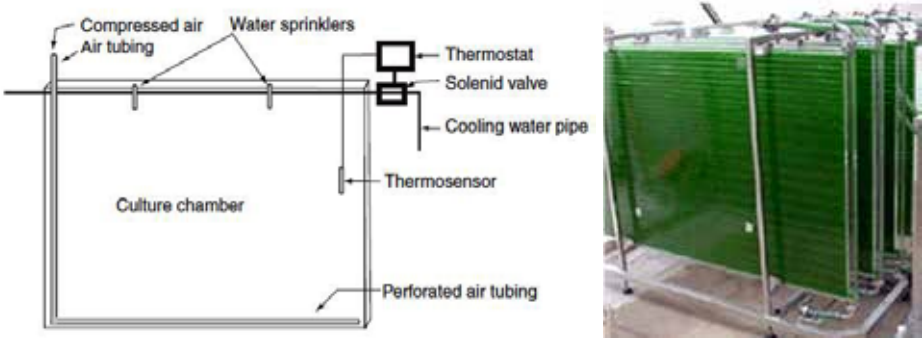

Fig. 85: Showing the Diagram and the photograph of Plate Photobioreactor

Tubular Photobioreactor

A tubular reactor consists of vertical or horizontal arranged tubes, connected together to a pipe system. The algae-suspended fluid is able to circulate in this tubing. The tubes are generally made out of transparent plastics or borosilicate glass and the constant circulation is kept up by a pump at the end of the system. The introduction of gas takes place at the end/beginning of the tube system. This way of introducing gas causes the problem of deficiency of carbon dioxide, high concentration of oxygen at the end of the unit during the circulation, and bad efficiency.

Fig. 86: Showing the tubular Photobioeractor

Bubble Column Photobioreactor

A bubble column photo reactor consists of vertical arranged cylindrical column, made out of transparent material. The introduction of gas takes place at the bottom of the column and causes a turbulent stream to enable an optimum gas exchange. At present these types of reactors are built with a maximum diameter of 20 cm to 30 cm in order to ensure the required supply of sunlight energy. This type allows for a reduction of the harmful shear forces. The biggest problem with the sunlight determined construction is the limited size of the diameter. Feuermann *et al.* invented a method to collect sunlight with a cone shaped collector and transfer it with some fiberglass cables which are adapted

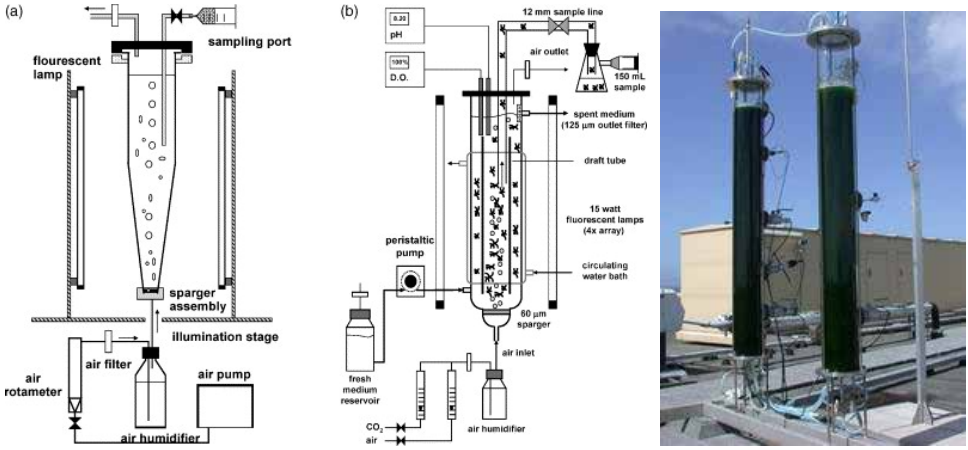

Fig. 87: Showing the Bubble Column Photobioreactor

to the reactor in order to enable constructions of a column reactor with wider diameters. - on this scale the energy consumption due to pumps etc. and the CO_2 cost of manufacture may outweigh the CO_2 captured by the reactor.

Industrial Usage

The cultivation of algae in a photobioreactor creates a narrow range of industrial application possibilities. Some power companies already established research facilities with algae photobioreactors to find out how efficient they could be in reducing CO_2 emissions, which are contained in flue gas, and how much biomass will be produced. Algae biomass has many uses and can be sold to generate additional income. The saved emission volume can bring an income too, by selling emission credits to other power companies. The utilisation of algae as food is very common in East Asian regions. Most of the species contain only a fraction of usable proteins and carbohydrates, and a lot of minerals and trace elements. Generally, the consumption of algae should be minimal because of the high iodine content. For example, if someone has hyperthyroidism it could be very dangerous for their health. Likewise, many species of diatomaceous algae produce compounds unsafe for humans. The algae, especially some species which contain over 50 percent oil and a lot of carbohydrates, can be used for producing biodiesel and bioethanol by extracting and refining the fractions. This point is very interesting, because the algae biomass is generated 30 times faster than some agricultural biomass, which is commonly used for producing biodiesel.

MICROBIOREACTORS

As a step toward high-throughput bioprocess development, we present design, fabrication, and characterization of polymer based micro-bioreactors integrated with automated sensors and actuators. The devices are realized, in increasing levels of complexity, in poly(dimethylsiloxane) and poly(methyl methacrylate) by micromachining and multilayer thermal compression bonding procedures. Online optical measurements for optical density, pH, and dissolved oxygen are integrated. Active mixing is made possible by a miniature magnetic stir bar. Plug-in-and-flow microfluidic connectors and fabricated polymer micro-optical lenses/connectors are integrated in the micro-bioreactors for fast set up and easy operation. Application examples demonstrate the feasibility of culturing microbial cells, specifically *Escherichia coli*, in 150 mL-volume bioreactors in batch, continuous, and fed-batch operations.

Microbioreactor Configurations

The early generation of microbioreactor (Fig. 88A) was designed for batch cultivation of microbial cells. The reactor consisted of two PDMS layers (L2 and L3) sandwiched in between two PMMA layers (L1 and L4 in Fig. 88A). The bottom PMM layer, made by using a computer-numerical-controlled (CNC) milling machine with dimensional accuracy of 12 μm, included the microbioreactor chamber (150 μL volume) and three connecting channels (M), which are used for inoculation and replenishment of water. Two recesses (S, diameter 2 mm, depth 250 mm) at the bottom of the bioreactor chamber accommodated DO and pH fluorescence lifetime sensors (DO sensor foil PSt3, and pH sensor solution HP2A, Presens—Precision Sensing GmbH, Regensburg, Germany). Details of the fluorescence lifetime measurements are summarized elsewhere. In the center of the device, a reactor chamber was fabricated in layers L1 to have a cylindrical geometry with a diameter of 10 mm and a depth of 1 mm. A ring-shape magnetic stir bar (K) with 6 mm arm length and 0.5 mm thickness (custom-made by Engineered Concepts, Vestavia Hills, AL) was held by a PMMA post (T) and was used for active mixing in the reactor chamber. The mixing efficiency in the micro-bioreactor chamber was evaluated through experiments and computational fluid dynamic simulations. A thin layer (~100 μm in thickness) of spin-coated PDMS (L2; mixing ratio of silicone to curing agent was 10:1. Sylgard 184, Dow Corning Corp., Midland,

MI, USA) covered the reactor chamber and served as the aeration membrane. PDMS was spin-coated at a speed of 1200 rpm for 25 s and then baked at 70°C for 2 h for curing. The PDMS membrane bulged upward as a result of a positive pressure in the micro-bioreactor chamber to reach a reactor volume of 150 µL. To facilitate device assembly, hermetical sealing, and connection of microfluidic channels (M), this PDMS layer was held by a 5-mm thick PDMS gasket layer (L3). A top PMMA layer was used to provide a rigid support for the mechanical assembly. Three ports connected the microbioreactor chamber with external setup via microchannels (M) and served for the purposes of inoculation (P1), waste replenishment (P2), waste outflow (P3; used during inoculation). The microbioreactors were adapted to more complex fermentation processes, for example, chemostat and fed-batch, by adding additional features. The device in Figure 88B was used for pH control and fed-batch operations.

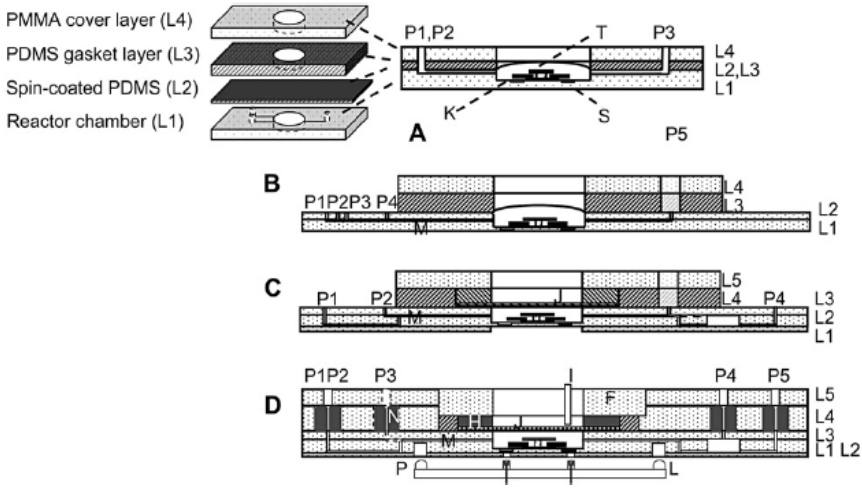

Fig. 88: (A) Microbioreactor device used in batch cell cultivation. (B) Device used in pH-control and fed-batch cell cultivation. Microchannel swere used for water- (P1), base- (P2), and acid-feeding (P3), inoculation (P4), and waste exit (P5) purposes, respectively. (C) Thermally bonded PMMA device used in continuous cell cultivation. Microfluidic channels allow for water-replenishment (P1), inoculation (P2), and waste exit (P3), and cell outflow (D) before and during chemostat experiments. (D) Cross-section of an integrated microbioreactor. L1-L5, thermally bonded PMMA layers; F PMMA cork used for mechanical assembly of the aeration membrane; H silicone O-ring for sealing; I optical fiber fixed by F; J grid for holding the PDMS membrane above the reactor chamber; K magnetic mixer in the center of reactor chamber; L recesses in PMMA for accommodating alignment pins P; M microfluidic channels; N small silicone O-rings for fluidic interconnections; O pH and DO fluorescent sensors; P PDMS alignment pins on optical plugs; S optical sensors.

The reactor chamber was made of two PMMA layers (L1 and L2 in Fig. 88B; Goodfellow Corp., PA) thermally bonded at a temperature of 140°C for 90 min in a homemade press. In this press, a pair of Belleville disc springs (diameter: 119.0 mm; thickness: 1.25 mm; height: 2.80 mm, MSC Industry Supply Co., Inc., New York) maintained a constant load of 0.12 MPa. The major feature for this microbioreactor is the ability of base-, acid-, and glucose-additions during fermentation, closed-loop controlled by external microvalves (INKX0514300A, The Lee Co., Westbrook, CT) and control circuits (IECX0501350A, The Lee Co.). Microfluidic channels (M), machined in layer L1 and sealed by layer L2, were used for water- (P1), base- (P2), and acid-feeding (P3), inoculation (P4), and waste outflow (P5; used during inoculation) purposes, respectively. Figure 88C was used for continuous culture of bacterial cells to obtain chemostat data (data shown in Fig. 88B). The microbioreactor chamber (10 mm in diameter and 2 mm in depth, with a total volume of 150 μL) and four connecting channels were fabricated in three thermally bonded bottom PMMA layers (layers L1 through L3; Goodfellow Corp.).

The thin PDMS aeration membrane was covered with an additional layer of stainless steel grid (B-PMX-062, Small Parts Inc., Miami, FL) fixed by a homemade PDMS O-ring to provide a perforated membrane structure and to avoid membrane bulging. Microfluidic channels (M) were machined in both sides of layer L2 and sealed by layers L1 and L3. These microfluidic channels allow for medium addition (P1), inoculation (P2), waste exit (P3, used during inoculation), and cell outflow (P4) before and during chemostat experiments. An external syringe pump (PhD2000, Harvard Apparatus, Holliston, MA)

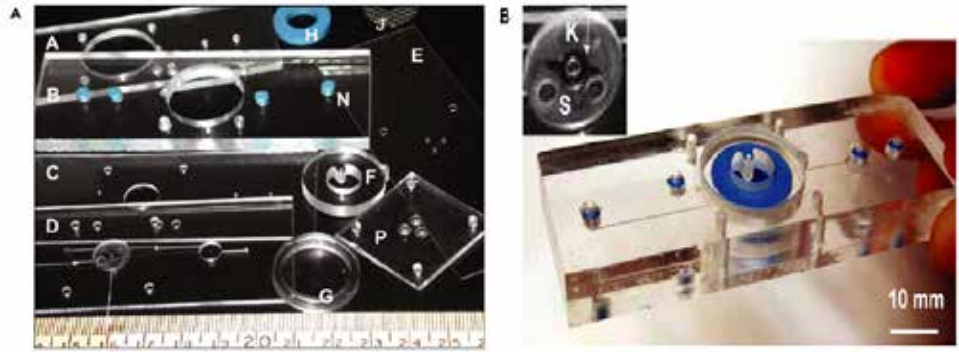

Fig. 89: (A) Overview of individual parts for the microbioreactor shown in Figure 88D. (B) Top view photograph of assembled and bonded microbioreactor.

connected to P1 provided a steady media feeding during continuous culture experiments. The latest microbioreactors (Figs. 88D and 89) improve interfacing of the microbioreactor to the external instruments (fluidic handling, optical monitoring, electronics, and computer control) without modifying the biological function of previous designs. The devices are made of five thermally bonded PMMA layers. Precise thermal bonding of PMMA layers with different glass transition (TG) temperatures was performed in a mechanical press in two steps. *First*, the three bottom layers (layers L1 through L3; Goodfellow Corp.) were bonded at a temperature of 140°C for 90 min. *Second*, the resulting composite was bonded with the top two layers (A and B; MSC Industrial Supply) at a lower temperature of 120°C for 60 min. The reactor chamber, fabricated in layers L2 and L3, had the same shape and size as in the previous designs. On the top of reactor chamber, the thin PDMS aeration layer was held by a 3-mm thick PDMS gasket layer (part G in Fig. 89, 20 mm inner diameter, 25 mm outer diameter, fabricated in a polycarbonate mold) to facilitate device assembly and sealing. A PMMA "cork" (Fig. 88D) (F) with an outer diameter slightly larger (13 μm arger in diameter) than the inner diameter of PMMA housing frame (machined in A and B) created a seal by compressing the PDMS (G) and a Sylastic RTV silicone elastomer (Dow Corning) O-ring (H, inner diameter of 10 mm, outer diameter of 20 mm, and height of 3 mm made with a polycarbonate mold). A small hole in the cork also aligned the optical fiber (I) for the OD transmission measurements. This cork allowed the microbioreactor to be cleaned and reused by replacing PDMS membranes after experiments, a useful feature in exploratory studies, but too labor intensive for parallel investigations. Therefore, in the disposable bioreactor version the PDMS membrane was permanently fixed between PMMA layers after thermal bonding and the stabilizing grid structure was molded in the PMMA layer B. Similar to previous microbioreactors (Fig. 88A°C), the fluorescence lifetime sensors are integrated at the bottom of device chamber (Fig. 88D) for pH and DO online measurements. Indentations beneath these sensors (L1 and L2) now couple optical fibers (O) to external fluorescence detectors and lifetime measurements for better alignment. The fluidic interface between a microbioreactor and external fluidic units was composed of custom-made elastomer O-rings (N) integrated in the PMMA device (Fig. 88D). They allowed aseptic self-sealing, "plug-in-and-run" functionality, between external fluid handling and internal microfluidic channels for inoculation, reagent feed, sampling, and waste outflow. The O-rings were cast in Sylastic RTV silicone

elastomer (Dow Corning) from stainless steel molds with an outer diameter of 4.2 mm, an inner diameter of 0.2 mm, and a depth of 4.6 mm. The stainless steel molds were fabricated by using a 2-mm diameter ball-head endmill (MSC Industrial Supply) Supply) at a high rotation speed of 8000 rpm and subsequent electro-polishing to obtain a smooth surface. The O-rings were cured at room temperature for more than 12 h to obtain a Young's modulus of 4.5 MPa. They were then embedded into housings machined in a thick PMMA layer (L4, Fig. 88B) and were fixed by a cover PMMA layer (A) when the two layers were thermally bonded. The housing for each O-ring had a slightly smaller diameter (4.1 mm) and depth (4.45 mm) so that the O-ring was compressed and the center hole sealed; 1.5-mm diameter through-holes in the covering PMMA layer corresponded to the center positions of the O-rings. When stainless steel tubes (12 mm long, 23 gages, Small Parts, Inc.) were inserted, the elastomer O-ring expanded and making a fluidic connection. The process was reversible and the seal leak tight up to pressures of ~0.6 MPa.